EUROPEAN Journal of Molecular Biotechnology

Has been issued since 2013.
E-ISSN 2409-1332
2018. 6(1). Issued 2 times a year

Journal is indexed by: **Chemical Abstracts Service** (USA), **CiteFactor** – Directory of International Reseach Journals (Canada), **Cross Ref** (UK), **EBSCOhost Electronic Journals Service** (USA), **Global Impact Factor** (Australia), **Journal Index** (USA), **Electronic scientific library** (Russian Federation), **Open Academic Journals Index** (Russian Federation), **Sherpa Romeo** (Spain), **ULRICH's WEB** (USA), **Universal Impact Factor** (Australia).

All manuscripts are peer reviewed by experts in the respective field. Authors of the manuscripts bear responsibility for their content, credibility and reliability.

Editorial board doesn't expect the manuscripts' authors to always agree with its opinion.

Postal Address: 1367/4, Stara Vajnorska str., Bratislava – Nove Mesto, Slovakia, 831 04

Website: http://ejournal8.com/
E-mail: aphr2010@mail.ru

Founder and Editor: Academic Publishing House Researcher s.r.o.

Release date 15.06.18.
Format 21 × 29,7/4.

Headset Georgia.

Order № 17.

European Journal of Molecular Biotechnology

2018

Is. 1

CONTENTS

Articles and Statements

An Investigation of the Reason of not Feasibility of Hetero-Diels-Alder Reaction of Isoselenazole with Unsymmetrical Acetylenic Dienophile: A Conceptual DFT Study and Topological Analysis of ELF Function
A. Benallou, H.E.A.E. Abdallaoui, H. Garmes 3

The Contribution to Bonding by Lone Pairs in the Hydrogen Transfer of Adenine Tautomerization (3H→9H) in the First Excited Electronic State: ELF Analysis
A. Benallou, H.E.A.E. Abdallaoui, H. Garmes 16

Rhodopsin. Bacteriorhodopsin in Biotechnology. Electromagnetic Conception for the Eyesight
I.Ignatov, Y. Pesheva 25

ZEOLITH Detox for Detoxification of Human Body. Proofs for Anti Inflammatory Effects of Zeolite and Detoxification
I. Ignatov, Y. Pesheva 41

Targered Changes in the Natural and Semi-Artificial Arid Phytocenoses in the Contact Zone with the Agrocenoses: A System Control Model-Based Approach
E.A. Ivantsova, N.V. Onistratenko, N.V. German, P.A. Krylov, A.A. Tikhonova, V.V. Novochadov 53

Bioactivity of Crude Extracts of Stem Bark of *Vetillaria Paradoxa*
I.A.A. Ibrahim, M.M. Mohammad, A. A. Faisal, H. Musa 61

Published in the Slovak Republic
European Journal of Molecular Biotechnology
Has been issued since 2013.
E-ISSN: 2409-1332
2018, 6(1): 3-15

DOI: 10.13187/ejmb.2018.1.3
www.ejournal8.com

Articles and Statements

An Investigation of the Reason of not Feasibility of Hetero-Diels-Alder Reaction of Isoselenazole with Unsymmetrical Acetylenic Dienophile: A Conceptual DFT Study and Topological Analysis of ELF Function

Abdelilah Benallou [a, *], Habib El Alaoui El Abdallaoui [a], Hocine Garmes [b]

[a] Team of Chemoinformatics Research and Spectroscopy and Quantum Chemistry, Physical and Chemistry Lab, Faculty of Science, University Chouaib Doukkali, El Jadida, Morocco
[b] Laboratory of Bio-organic Chemistry, Department of Chemistry, Faculty of Science, University Chouaib Doukkali, El Jadida, Morocco

Abstract

A detailed mechanistic study by molecular electron density of the Hetero-Diels-Alder (HDA) reaction of isoselenazole with unsymmetrical acetylenic dienophile is carried out. The high activation energy involved in the transition state of both Ortho and Meta cycloadduct implies that this reaction may not possible, even in the presence of solvent toluene. Besides, ELF shows that the not formation of the basin at the N2 nitrogen atom of isoselenazole moiety. Therefore, the negligible charge transfer between reagents and the large electron density attracted by the lone pair at the N2 atom, in addition to the C1SeN2 fragment distortion energy cost, they are not allowing the formation of the radicals (basins) necessary at the most significant atoms, these factors are probably responsible for the highest barrier activation.

Keywords: MED analysis, ELF, HDA, IRC, Conceptual DFT, TST.

1. Introduction

The Hetero-Diels-Alder (HDA) reactions are powerful tools in organic synthetic chemistry, they represent a significant importance, it have allow the construction of six-membered heterocycles with high stereo and regioselectivity of 1,3-butadiene and an ethylene dienophile (Soto-Delgado et al., 2010; Paton et al., 2011; Benallou et al., 2014; Benallou et al., 2014; Domingo, Saez, 2009). Furthermore, the synthetic utility of this reaction does not arise only from the substitution of both diene and dienophile, but also from the modification of one or more carbon atoms of the π systems by a heteroatom, such as Cl, N, O, S, ... etc. However, the substitution diversity of the dienophile or diene moiety breaks the symmetry and thus favors DA reactions by lowering the activation energy (Berski et al., 2006), which was related to the polar character. Interestingly, to analyze the changes in mechanical quantum observable on the reaction path, mainly the reorganization of the electron density throughout the reaction path, the theoretical model of the evolution of the bonding (Krokidis et al., 1998) and the topological analysis of the electrons localization (Krokidis et al., 1999) are combined during this last decade, because these

* Corresponding author
E-mail addresses: abdo_benallou@yahoo.fr (A. Benallou)

latter's are successively verified an appropriate tool for the studies of organic reactions (Mahdieh et al., 2017; Domingo et al., 2013; Mierzwa et al., 2015), that justify the development of the theoretical approach for the DA reactions implying a large number of dienes and dienophiles (Benallou et al., 2016; Benallou et al., 2016; Diels, Alder, 1928; Woodward et al., 1969; Winkler, 1996; Carruthers, 1990; Chen, Trudell, 1996; Finguelli, Tatichi, 2002). In this context, and to understand the reason of the not feasibility of the cycloaddition HDA reaction of isoselenazole 1 with acetylenic dienophile 2 to afford the intermediary cycloadducts and afterwards the subsequent removal of Selenium from this latter to yield the polysubstituted pyridine (Figure 1) (Shimada et al., 2009), a theoretical computational study has been established. However, this HDA reaction was performed in the presence of solvent toluene, although after 24h in reflux, this reaction does not take place (Shimada et al., 2009). Make a note of that, the polysubstituted and fused pyridine cores have been found in a wide variety of naturally occurring polycyclic alkaloid skeletons having biological, pharmaceutical, and agrochemical activities (Shimada et al., 2009).

In order to evaluate the factors responsible of not feasibility of HDA between isoselenazole with acetylenic dienophile, an analysis of the bonding formation along the reaction and a conceptual DFT (CDFT) indices have been performed and then a complete characterization to provide a new insight into the nature of the transition state (TS) and the mechanism processes, equally how do C-C and C-N bonds formation in this HDA reaction is carried out. Effectively, the combination of conceptual DFT, TST and ELF theories have been used to characterize the reaction pathway through optimized geometries for corresponding stationary points on the IRC path. Then the molecular mechanism study of the HDA reaction has been performed. However, ester groups ($COOCH_3$) as electron withdrawing group (EWG) is attached to acetylenic dienophile, so the asymmetric reaction will give two different region-isomers of ortho and meta intermediary poly-substituted pyridines product (Figure 1). The reaction pathway can be established using intrinsic reaction coordinate (IRC) procedure (Gonzalez, Schlegel, 1990) on the potential energy surface.

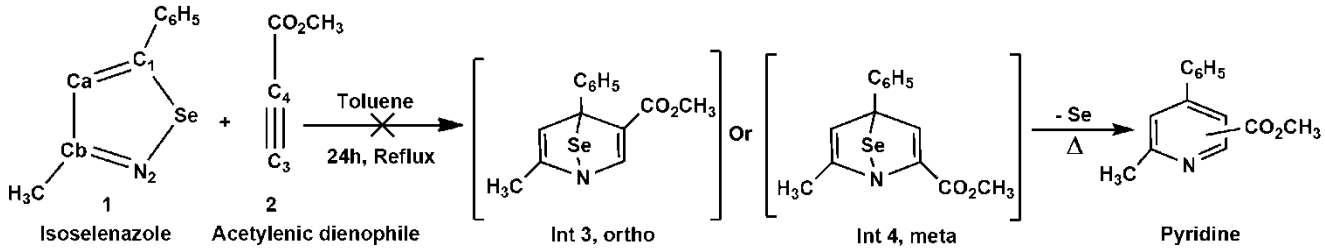

Fig. 1. Not-feasibility of the Hetero-Diels-Alder reactions of isoselenazole with acetylenic dienophile to yield poly-substituted pyridines

2. Computational methods

All DFT computations were carried out using the B3LYP (Lee et al., 1988) exchange–correlation functional, together with the standard 6-311++G(d,p) basis set (Hehre et al., 1986). The optimizations were carried out using the Berny analytical gradient optimization method (Schlegel, 1994). The stationary points were characterized by frequency computations in order to verify that the transition state structure (TS) has one and only one imaginary frequency. The IRC paths (Fukui, 1970) were traced in order to check the energy profiles connecting the TS to the two associated minima of the proposed mechanism using the second order Gonzalez–Schlegel integration method (Gonzalez, Schlegel, 1991). The electronic structures of stationary points were analyzed by the natural bond orbital (NBO) method (Reed et al., 1988) and by ELF topological analysis (Krokidis et al., 1999). The ELF study was performed with the Multiwfn program (Tian, Feiwu, 2012) using the corresponding mono determinantal wavefunctions of the selected structures of the IRC at the B3LYP/6-311++G(d,p)basis set. All computations were carried out with the Gaussian 09 suite of programs (Frisch et al., 2009). The global electrophilicity index (Parr et al., 1999), ω, is given by the following expression, $\omega = \mu^2/2\eta$, in terms of the electronic chemical potential μ and the chemical hardness η. Both quantities may be approached in terms of the one-electron energies of the frontier molecular orbital HOMO and LUMO, e_H and e_L, as $\mu=(e_H+e_L)/2$ and $\eta=(e_L-e_H)$, respectively (Parr, Yang, 1989) then the local electrophilicity for a site or an atom

(k) (Domingo et al., 2002) is given by the equation: $\omega_k=\omega f_k^+$. Domingo et al have proposed a new descriptor, the nucleophilicity index, N (Domingo, Pérez, 2011), based on the HOMO energies obtained within the Kohn–Sham scheme (Kohn et al., 1965), and defined as $N=E_{HOMO(Nu)}-E_{HOMO(TCE)}$. Similarly, the local nucleophilicity index N_k (Perez et al., 2009) defined as the product of global nucleophilic index N and the nucleophilic of the Fukui index $N_k=Nf_k^-$, while the nucleophilicity has referred to tetracyanoethylene (TCE) as a reference. Where f_k^- and f_k^+ are the Fukui functions for nucleophilic and electrophilic attacks, respectively (Contreras et al., 1999).

3. Results and discussion

In order to shed light the mainly factors responsible of the not feasibility of this HDA reactions between isoselenazole (1) and acetylenic dienophile (2), an analysis of the physicochemical parameter to choose the most favorable product based on the CDFT reactivity descriptors will be performed, followed by a potential energy surfaces (PES) study of the reaction to characterize the barrier activation of this reaction in gas phase and in presence of the solvent toluene. To conclude, an ELF bonding analysis along the new probably bond-formation pathway of this reaction will be carried out in order to study properties of electron localization in the processes of the bond formation/breaking.

3.1. Conceptual DFT (CDFT) indices of the reagents

In this paragraph, we will determine the physic-chemical characteristics of isoselenazole (1) and acetylenic dienophile (2) substrates, for this instance the distribution of the global and local electrophilicity and nucleophilicity indices of each molecule, as chemical potential μ and chemical hardness η in order to characterize the reactivity of these compounds, and thus, the CDFT indices of the isoselenazole and acetylenic dienophile are given in Table 1.

Table 1. HOMO and LUMO energies, chemical potential μ, chemical hardness η, global electrophilicity ω and global nucleophilicity N

Parameters	*Isoselenazole*	*Acetylenic dienophile*
HOMO (au)	- 0.23037	-0.24826
LUMO (au)	-0.05229	-0.03791
μ (au)	-0.141	-0.143
η (au)	0.178	0.210
ω (eV)	1.52	1.32
N (eV)	2.87	2.36

In Table 1, we have noted that the chemical potential of isoselenazole is slightly higher to compare with the acetylenic dienophile, in which μ(-0.141)>μ(-0.143), indicates that the global electron density transfer (GEDT) will take place from diene (isoselenazole 1) to dienophile (acetylenic 2). Interestingly, the global electrophilic and nucleophilic indices show that the isoselenazole moiety behaves as nucleophile and electrophile in the same time, such as 1.52eV(1)>1.32eV(2) and 2.87eV(1)>2.36eV(2), and this is not suitable in point of view chemically, and then, to overcome this complicated situation and to correctly predict the electrophilic and/or the nucleophilic character of the diene and dienophile for this HDA reaction, in other words to evaluate the withdrawing and releasing groups, that envisaged us to identify the nature of the reaction mechanism (NRM). For this purpose, we will need to determine the absolute value of the energy difference such as: $E1|\varepsilon_{HOMO(Diene)}-\varepsilon_{LUMO(Dienophile)}|//E2|\varepsilon_{HOMO(Dienophile)}-\varepsilon_{LUMO(Diene)}|$. Note that the reaction is: Normal electronic demand (NED) if E1 < E2, and Inverse electronic demand (IED) if E2 < E1. Herein, we have found that E1(0.192)<E2(0.196), and thus this HDA reaction takes

place as a normal electronic demand (NED) which meant that the diene (isoselenazole) plays the role of electron donor (nucleophile), whereas the dienophile (acetylenic) plays the role of electron attractor (electrophile). Consequently, the charge transfer will take place from the diene to the dienophile, these results will be confirmed next by the charge transfer in the transition states.

In order to predict the selectivity of the HDA reactions (region/chemo), we have used the polar model (Domingo et al., 2008) which states that the formation of the first new σ bond will take place by the most favorable interaction between two sites (the more nucleophilic site is characterized by *the maximum nucleophilic value of local nucleophilicity index* N_k, while the more electrophilic site that possessing *the maximum electrophilic value of local electrophilicity index* ω_k) and Houk rule (Fleming, 1976), in this latter, "small-small" and "large-large" type interactions are more favored by report interactions 'large-small' and 'small-large'. However, this Houk approach is based essentially on the coefficients of orbital molecular HOMO/LUMO for diene and dienophile substrates. The results are given in Figure 2.

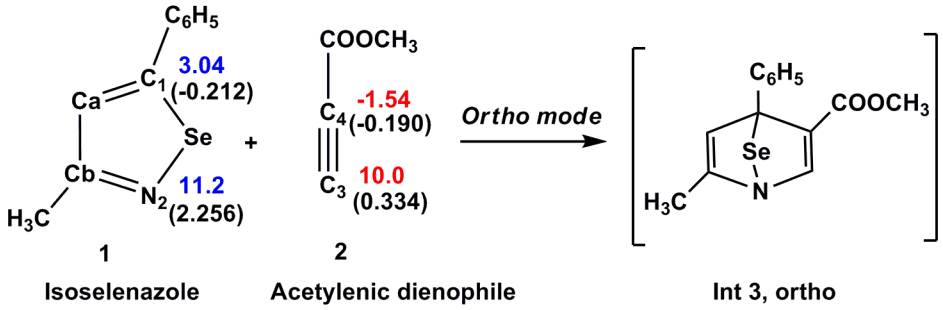

Fig. 2. Predict regioselectivity using the local nucleophilicity N_k (1, in blue) and local electrophilicity ω_k (2, in red) indices (eV) and Houk rule (in parentheses)

According to the results noted in Figure 2, we have established that the most favorable interactions are between N2 atom of the isoselenazole 1 and C3 atom of the acetylenic dienophile 2, so taking into account the polar model we have noted that; the local nucleophilic index *N* of N2 is 11.2eV, it is extremely superior to that of C1 carbon (3.04eV), while the local electrophilic index ω of C3, is 10.0eV, which very higher to compare with C4 atom (-1.54eV), therefore the most favorable interaction will take place between N2 and C3 centers that having the biggest nucleophilic N and electrophilic ω values, respectively. Subsequently, the ortho/endo adduct is the most stable product. Similarly, Houk rule shows that the large values and the small values of the coefficients of orbital molecular HOMO/LUMO are attributed consecutively to the atoms N2 (isoselenazole 1) vs C3(acetylenic dienophile 2) and {C1 vs C4}, respectively. Enabling us to deduce that the interaction is highly appreciated between N2 and C3 atoms, subsequently provide the ortho/endo adduct as majority product.

3.2. PES path study and analysis of the stationary points involved in the two regioisomeric pattern associated with the endo approach of isoselenazole 1 with unsymmetrical acetylenic dienophile 2

In Figure 3 and 4, we have shown that the activation energies of both regioisomeric patterns are generally very higher energy cost, 46(GP) /46 (ST)kcal/mol and 45 (GP) /44 (ST) kcal/mol in gas phase (GP) and in presence of solvent toluene (ST) at 298K of meta and ortho, respectively, similarly, we have remarked that an unappreciable amount of charge transfer in transition states 0.05e and 0.09e (see figure 2), strongly indicates this reaction is a non polar reaction, in good agreement with the chemical potential of both isomers that have a closer values (see Table 1). Thus, none of the reagents will have a tendency to exchange electron density with the other along of the reaction. So these reagents are not have evidently most important interactions, which induce a feeble change of electron density between so-called reagents, therefore the unsymmetrical substitution of the acetylenic dienophile does not has the sufficient effect for improving reactivity, in contrast to many (4+2) cycloaddition reactions. Whereas the calculations of Gibbs free energies ΔG of the reaction in gas phase show that theses mechanism processes are totally endergonic in which ΔG equal 14kcal/mol and 15kcal/mol of meta and ortho region-isomeric, respectively, indicate on the one hand, that these products not have the sufficient stability to compare with the

reagents, on the other hand, these mechanisms processes are not spontaneously possible. Subsequently, despite that the activation energy of ortho regioisomeric channel is somewhat lowest than meta regioisomeric, this reaction cannot occur efficiently because of the highest barrier activation and that can be related; firstly to the energy cost of the C1SeN2 fragment distort and secondly to the energy gain from bond formation (σ)/breaking (pi) processes, it is worthy to note that, a very similar reaction of selenadiazole with dimethyl actelenedicarboxylate (DMAD) is take place in the presence of solvent benzene (Takikawa et al., 1991). Some appealing conclusions can be drawn from this PES study, the closer values of chemical potential and the weak charge transfer of the reagent imply a very higher energy cost reaction. Taking into account these considerable results and furthermore to give a fundamental and basic explanation of not reactivity of such reaction between isoselenazole 1 and the unsymmetrical acetylenic dienophile 2 a complete investigation by molecular electron density (MED) theory will be performed.

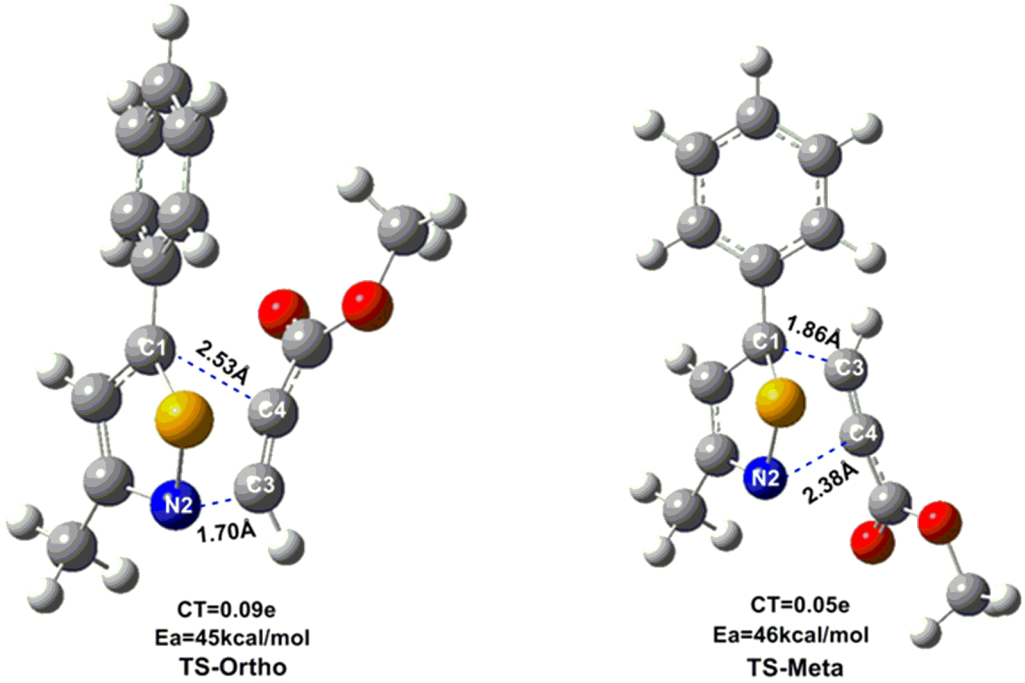

Fig. 3. Bond distances (Å), charge transfer in e and activation energy in kcal/mol of ortho and meta transition structures in the gas phase

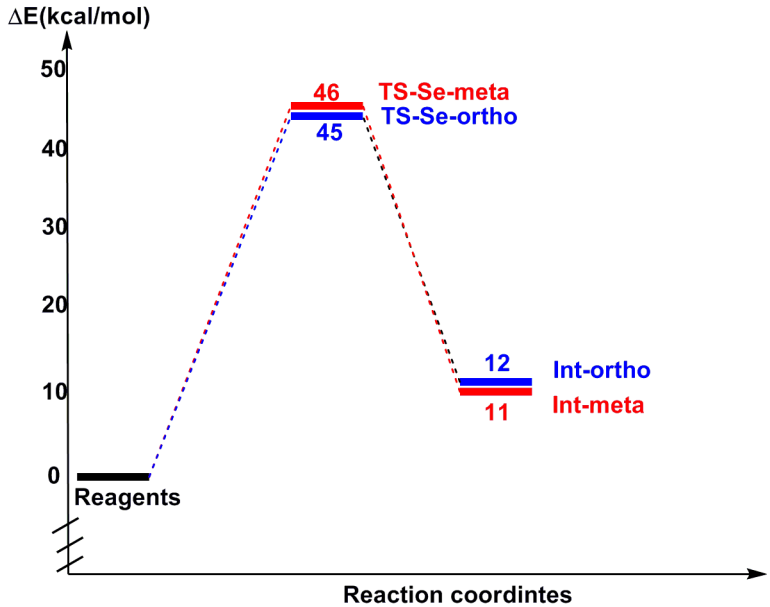

Fig. 4. Profile energetic, in gas phase, of HDA reaction between isoselenazole 1 and the unsymmetrical acetylenic dienophile 2

3.3. Analysis of bonding evolution in the HDA reaction using topological analysis of ELF function

In this study, we have shown previously that this reaction is highly energetic, 45kcal/mol for the most favorable channel, clearly indicates this reaction may not occur efficiently in the noted conditions, in good accordance with the reactivity experimentally observed (Shimada et al., 2009). Thus, a MED study of this HDA reaction will be carried out to interpret and understand the feeble reactivity. At this end, the topological analysis of the ELF along the reaction path associated with a cycloaddition is a valuable tool for understanding the bonding changes along the reaction path (Polo et al., 2004; Berski et al., 2006; Polo et al., 2008) and thus, to characterize the molecular mechanism (Silvi, 2002). Consequently, a topology analysis of the ELF along IRC of the most favorable *endo/ortho* channel associated with the HDA reaction between isoselenazole and acetylenic dienophile was performed to identify the distribution of electron density with the progress of the reaction along of bond breaking/formation. In this context, the total electronic populations of the more relevant ELF valence basins of selected structures along IRC (Figure 5) are listed in Table 2, the attractor positions for the most relevant points associated with the formation of the C1–C4 and N2-C3 single bond, are shown in Figure 5.

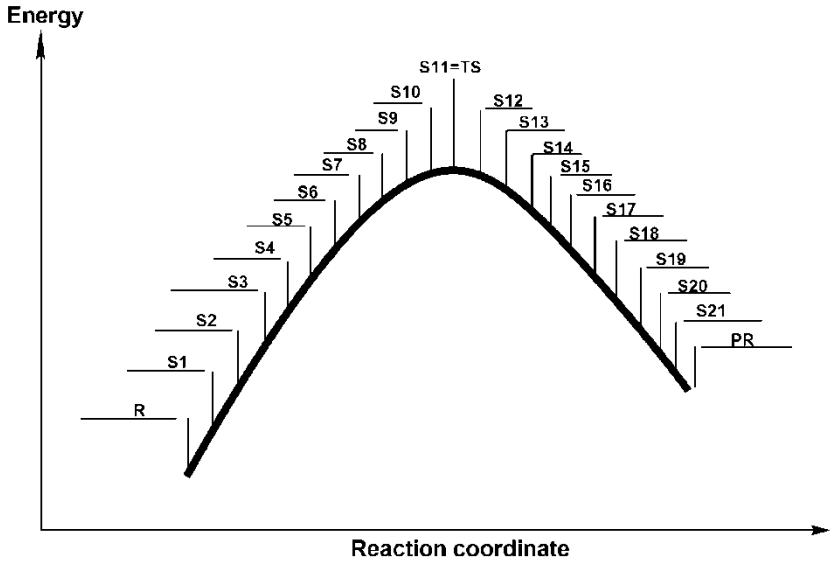

Fig. 5. Several analysis structures along IRC of Hetero-Diels-Alder reaction between isoselenazole with acetylenic dienophile

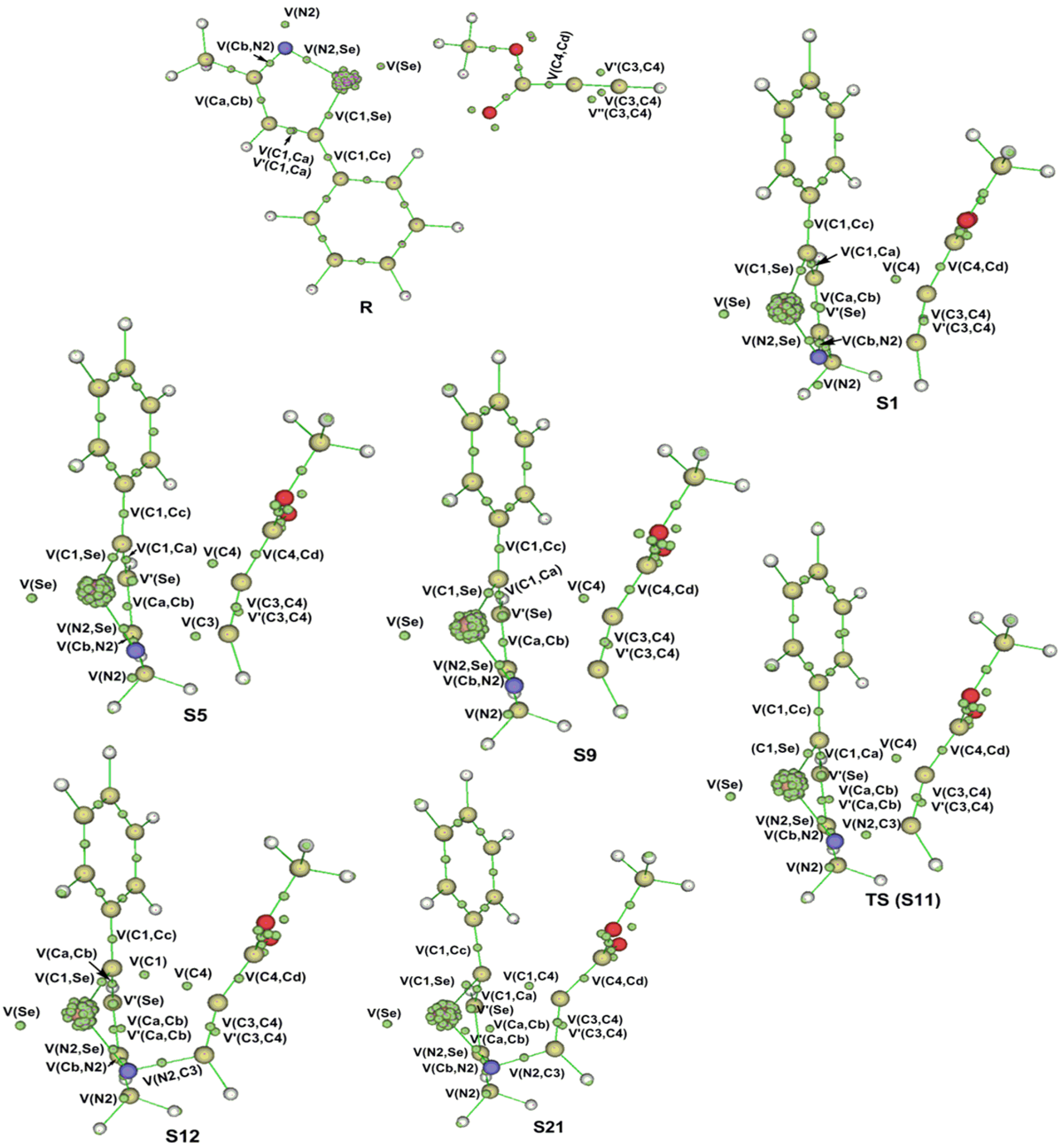

Fig. 6. ELF attractors of some selected points of the IRC associated with the formation of the new C–C and N-C single bond in the HDA reaction of isoselenazole 1 with acetylenic dienophile 2

Table 2. Valence basin populations of the most relevant points calculated from the ELF of HDA reaction of isoselenazole with acetylenic dienophile, associated with the C1–C4 and N2-C3 bonds formation step. Bond order (Wiberg index) and charge transfer in *e* (NBO)

Phase	R	S1	S2	S3	S4	S5	S6	S7	**S8**	**S9**	**S10**	S11 =TS	S12
d(C1-C4)	>2.83	2.83	2.81	2.78	2.76	2.73	2.71	2.68	2.65	2.61	2.57	2.53	2.48
d(N2-C3)	>2.19	2.19	2.13	2.08	2.03	1.98	1.93	1.88	1.83	1.78	1.74	1.70	1.67
V(C1)													0.20

V'(C1)													
V(N2)	3.25	3.19	3.18	3.18	3.18	3.18	3.19	3.19	3.23	3.57	2.71	2.67	2.64
V'(N2)													
V(C3)						0.06	0.14	0.21	0.27				
V(C4)		0.29	0.33	0.37	0.42	0.47	0.50	0.55	0.58	0.63	0.68	0.70	0.74
V(C1,Ca)	3.38	3.12	3.07	3.02	2.98	2.92	2.86	2.79	2.72	2.65	2.60	2.51	2.45
V'(C1,Ca)	3.38												
V(Ca,Cb)	2.43	2.68	2.75	2.81	2.88	2.96	3.05	3.14	3.22	3.27	3.32	3.38	3.41
V'(Ca,Cb)												3.38	3.41
V(Cb,N2)	2.76	2.56	2.51	2.47	2.42	2.36	2.30	2.25	2.18	2.14	2.09	2.05	2.00
V'(Cb,N2)													
V(N2,Se)	1.15	1.22	1.23	1.24	1.25	1.26	1.27	1.28	1.28	1.28	1.28	1.27	1.26
V(C1,Se)	1.81	1.86	1.86	1.87	1.88	1.88	1.89	1.90	1.90	1.93	1.96	2.02	1.85
V(C1,Cc)	2.22	2.27	2.27	2.28	2.28	2.28	2.29	2.30	2.30	2.30	2.30	2.30	2.29
V(C4,Cd)	2.38	2.50	2.51	2.51	2.52	2.52	2.54	2.55	2.56	2.57	2.60	2.57	2.56
V(C1,C4)													
V(N2,C3)											0.94	1.06	1.15
V(C3,C4)	2.75	2.53	2.50	2.48	2.45	2.41	2.38	2.32	2.19	2.20	2.15	2.10	2.07
V'(C3,C4)	2.49	2.46	2.44	2.42	2.41	2.37	2.28	2.23	2.16	2.15	2.12	2.09	2.06
V''(C3,C4)	0.13												
V(Se)	2.35	2.30	2.30	2.32	2.32	2.33	2.33	2.34	2.36	2.37	2.38	2.39	2.41
V'(Se)	2.39	2.46	2.47	2.47	2.46	2.46	2.46	2.47	2.47	2.47	2.47	2.47	2.47

Table 3 (Next)

Phase	S13	S14	S15	S16	S17	S18	S19	S20	S21	PR
d(C1-C4)	2.43	2.38	2.33	2.27	2.22	2.16	2.10	2.05	1.99	1.55
d(N2-C3)	1.64	1.62	1.60	1.58	1.57	1.56	1.55	1.54	1.54	1.48
V(C1)	0.27	0.33	0.44	0.46	0.49	0.53	0.54	0.56		
V'(C1)										
V(N2)	2.62	2.61	2.60	2.60	2.60	2.59	2.59	2.59	2.60	2.65

V'(N2)										
V(C3)										
V(C4)	0.76	0.80	0.85	0.86	0.87	0.89	0.93	0.98		
V(C1,Ca)	2.39	2.35	2.27	2.25	2.24	2.21	2.17	2.14	2.12	2.00
V′(C1,Ca)										
V(Ca,Cb)	3.45	3.48	3.54	3.51	1.83	1.82	1.85	1.87	1.86	1.87
V′(Ca,Cb)	3.45	3.48	3.54	3.51	1.74	1.77	1.77	1.77	1.79	1.88
V(Cb,N2)	1.97	1.95	1.93	1.90	1.88	1.86	1.84	1.83	1.82	1.72
V′(Cb,N2)										
V(N2,Se)	1.25	1.24	1.22	1.22	1.22	1.20	1.19	1.18	1.17	1.03
V(C1,Se)	1.82	1.79	1.74	1.73	1.71	1.70	1.68	1.65	1.63	1.32
V(C1,Cc)	2.28	2.27	2.24	2.25	2.22	2.21	2.18	2.17	2.17	2.15
V(C4,Cd)	2.54	2.52	2.46	2.50	2.44	2.41	2.39	2.37	2.35	2.39
V(C1,C4)									1.59	2.00
V(N2,C3)	1.23	1.28	1.39	1.40	1.42	1.46	1.49	1.52	1.54	1.78
V(C3,C4)	2.03	2.02	1.99	1.99	1.98	1.96	1.94	1.93	1.92	1.85
V'(C3,C4)	2.05	2.01	1.98	1.98	1.97	1.96	1.95	1.95	1.94	1.71
V''(C3,C4)										
V(Se)	2.41	2.43	2.45	2.45	2.45	2.47	2.47	2.47	2.48	2.54
V'(Se)	2.47	2.47	2.47	2.47	2.48	2.48	2.49	2.49	2.49	2.55

In order to explain the not feasibility of the Hetero-Diels-Alder reaction between isoselenazole and acetylenic dienophile we have commented 21 stationary points along IRC, also the structure of reagent and products are discussed. So, taking into account the results noted in table 2, relative to the most attractive centers. For isoselenazole, in distances d(C1-C4)>2.83Å and d(N2-C3)>2.19Å, ELF shows two {V(C1,Ca); V'(C1,Ca)} and only V(Cb,N2) disynaptic basins associated with C1-Ca and Cb-N2 double bonds, whose electronic population integrate 3,38e and 2,76e, respectively, the presence of a single disynaptic basin of Cb-N2 double bond reveals strongly that this bond is poor electronically and a part of electronic population has been absorbed by the lone pair of N2 atom, V(N2) monosynaptic basin, integrating 3.24e. However, in the same reagent the topology of the ELF relative of the Ca-Cb single bond shows an one V(Ca,Cb) disynaptic basin reaching 2.43e. Equally, for acetylenic dienophile, the ELF reveals that the presence of the three pairs V(C3,C4), V'(C3,C4) and V''(C3,C4) disynaptic basins associated with the C3-C4 triple bonds, whose electronic population 2.75e, 2.49e and 0.13e respectively. Therefore, the electronic population of the reagents is in good consistency with the molecular structure.

The bonding change (BC) theory along of the reaction mechanism gives us the opportunity to characterize the reorganization and the distribution of electron density between the reagents, and thus, the investigation of the reason of not feasibility of such reaction leads us to analysis exclusively the most significant attractors such as C1, N2, C3 and C4, because such atoms will react one of the other to yield poly-substituted pyridine. Although, in the most favorable ortho/endo adduct, C1 vs C4, while N2 must interact with C3 atom. In this context, in the structure 1 (S1) (Table 2), we have noted the appears of the first radical monosynaptic basin, V(C4) with an electronic population of 0.29e, this attractor will permit the creation of the new bond between C4 and C1 atoms, equally in this structure we have shown that a depopulation and reduction of the disynaptic basins relative to the C1-Ca, C3-C4 bonds. At this point, regarding the S2, S3, S4 and S5 structures, the second monosynaptic basin V(C3) positioned at C3 is appeared finally, integrates a very small electronic population to be 0.06e, note that these first appeared radicals are belonging to the acetylenic dienophile, whereas V(C1) and V(N2) basins of isoselenazole are not yet localized. In the structures S6 and S7, the noted basins do not have more changes throughout the progress of the reaction, at this long process the new monosynaptic basin of V(C1) and V(N2) are not yet appeared.

The most relevant changes in this reaction analysis take place in the structures S8, S9 and S10, while 2.57Å≤d(C1-C4)≤2.65Å, and 1.74Å≤d(N2-C3)≤1.83Å, herein in S8, we have remarked that V(N2) monosynaptic basin associated with the lone pair positioned at N2 nitrogen atom experience a slight increase to reach 3.23e, however, this basin experiences a feeble reduction from reagent to the structure S7, integrates 3.19e, it has a significant impact towards the reaction processes, equally in the same structure along IRC, the V(C3) monosynaptic basin profit to more electronic population, reaching 0.27e.

In S9, the V(N2) monosynaptic basin related to the lone pair has been increased to achieve a maximum electronic population, 3.57e, while V'(N2) monosynaptic basin is never going to likely take place. Surprisingly, the formation of the new N2-C3 bond is located in S10, and this is worth considering, because the formation of the new bond requires two adjacent pseudo-radicals under N2 and C3 atoms, however this process is not achieved. So in this case the formation of V'(N2) monosynaptic basin at N2 position involves high activation energy to occur efficiently, therefore three reasons should be responsible for the not formation of the N2 pseudoradical; (**1**): the observable amount of electronic density associated with the lone pair of N2 atom in S8 and S9 structures can be responsible for the not appearance of V'(N2) radical, in which an expect electron density presumed at V'(N2) has totally absorbed by the lone pair of the N2 atom, that can be explained by the high electronic population in the structure S9, (**2**): will N2 and C3 atoms near one to the other along IRC a noticeable amount of electron density has been shifted from the monosynaptic basin of V(C3) and V'(N2) to the monosynaptic basin of V(Se) and V(N2), (**3**) a very important energy is necessarily for distort C1SeN2 fragment. Consequently, the formation of the new bond of N2-C3 may not occur as a consequence of the absence of two radicals (basins) at the N2 and C3 atoms.

The analysis of the subsequent structures shows the split of the V(Ca,Cb) disynaptic basin in structure S11 (Transition State) to the pairs of V(Ca,Cb) and V'(Ca,Cb) disynaptic basins to reach 3.38e each one, indicates that this Ca-Cb sequence becomes double bonds, however the new monosynaptic basin of V(C1) has reached the sufficient electronic density to occur in structure S12, reaching 0.20e, and then, the analyses of the succeeding structures do not have any scientific significance considering the obvious reasons of the non reactivity found of this reaction.

Consequently, the feeble charge transfer involved in this reaction, an inequitable distribution of electron density and the huge energy cost to distort C1SeN2 fragment have unhelpfully influenced the reactivity and subsequently generate a great difficulty to form the pseudo-radical at the principle attractor, N2. So, when the reagents near one to the other, the formation of the N2 pseudo-radical has failed and due to the more reason (lone pair of the N2 attractor of electron, Se atom attractor of electron, C1SeN2 sequence distortion), therefore these factors are probably responsible for the high activation energy. However, the change of solvent or the substituent of both substrates of diene and dienophile could improve the reactivity through modifying the reorganization of the electron density and then to make a balance between the bond formation (energy gain)/breaking (energy loss) and the C1SeN2 sequence distortion energy cost within the molecule.

In conclusion, a schematic picture of the bonding changes along the selected points involved in this HDA reaction is given in Figure 7, and then; a clear representation of the not feasibility of this reaction has been depicted in Figure 8.

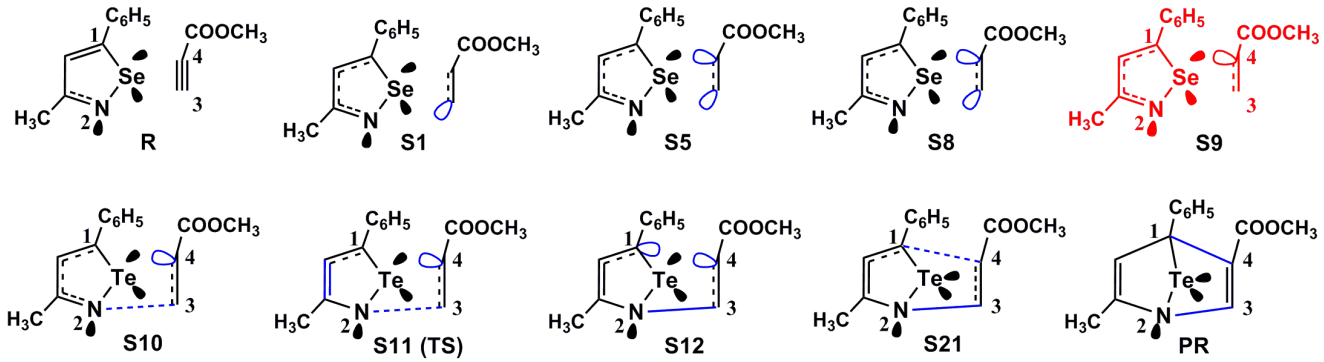

Fig. 7. Schematic picture of the bonding changes at the selected points involved in the HDA reaction of isoselenazole 1 with acetylenic dienophile 2. Lines represent bonding V(M,N) disynaptic basins, and ellipses represent non-bonding V(M) monosynaptic basins. Filled lines (in blue) indicate new V(M,N) disynaptic basins formation

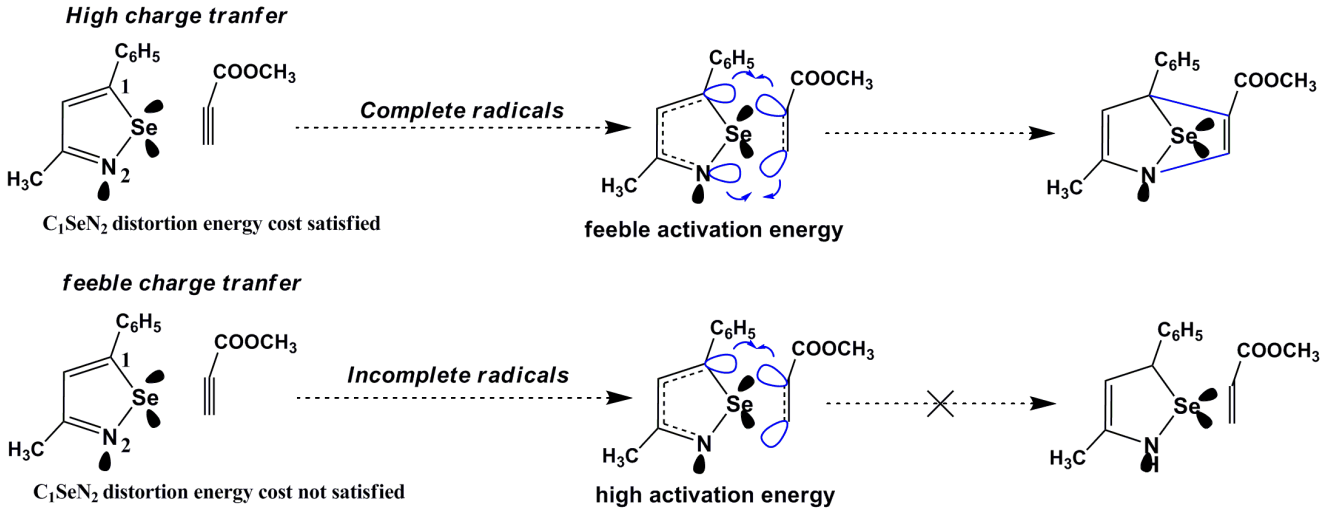

Fig. 8. Demonstration of not formation of the new N–C bond in the Hetero-Diels–Alder reaction of isoselenazole 1 with acetylenic dienophile 2

4. Conclusion

The reason responsible of the not feasibility of Hetero-Diels-Alder (HDA) reaction of isoselenazole with unsymmetrical acetylenic dienophile has been performed in this study using DFT, and ELF topological analysis methods at B3LYP/6-311++g(d,p) basis set level. And thus, this study shows that the formation of both isomers, necessities high activation energy, 45 (44) kcal/mol and 46(46) kcal/mol, in the gas phase and in the presence of the solvent toluene, for ortho and meta regioisomeric respectively. Equally, the ELF study of the most probably endo/ortho cycloadduct predicts that the electron density reorganization of the pseudo-radical centers of the most electrophilic site (C3 carbon) of acetylenic dienophile 2 and the most nucleophilic site (N2 nitrogen) of isoselenazole 1 are not appeared completely by the reason of the feeble charge transfer in the transition state, energy cost for distort C1SeN2 fragment, and electronic attractor of lone pair, they make it impossible the occur of N2 pseudo-radical. Therefore, the formation of the monosynaptic basin at N2 requires high energy contribution. Consequently, the formation of the pseudo-radical at the most attractive atoms is very significant for the formation of the new bond, however that can be solved by the use of another appropriate solvent or by the change of the substituent to make a balance between energy gain/energy loss relative to the bond formation/breaking and geometry reorganization energy cost due to distort of the C1SeN2 fragment.

References

Soto-Delgado et al., 2010 – *Soto-Delgado J., Domingo L.R., Contreras R.* (2010). Quantitative characterization of group electrophilicity and nucleophilicity for intramolecular Diels–Alder reactions, *Org. Biomol. Chem.* 8, 3678-3683.

Paton et al., 2011 – *Paton R.S., Steinhardt S.E., Vanderwal C.D., Houk K.N.* (2011). Unraveling the mechanism of cascade reactions of zincke aldehydes. *J. Am. Chem. Soc.* 133, 3895-3905.

Benallou et al., 2014 – *Benallou A., Garmes H., El Alaoui El Abdallaoui H.* (2014). Theoretical study of the regioselectivity in the intramolecular Diels–Alder reaction of the molecule triene amide. *Mor. J. Chem.* 2, 181-193.

Benallou et al., 2014 – *Benallou A., Garmes H., Knouzi N., El Alaoui El Abdallaoui H.* (2014). Elucidation of the regioselectivity in hetero diels-alder reaction by utilization of theoretical approaches; *Phys. Chem. News.* 72, 85-93.

Domingo, Saez, 2009 – *Domingo L.R., Saez J.A.* (2009). Understanding the mechanism of polar Diels-Alder reactions. *Org. Biomol. Chem.* 7, 3576-3583.

Berski et al., 2006 – *Berski S., Andres J., Silvi B., Domingo L.R.* (2006). New findings on the Diels-Alder reactions. An analysis based on the bonding evolution theory. *J. Phys. Chem. A* 110, 13939-13947.

Krokidis et al., 1998 – *Krokidis X., Silvi B., Alikhani M.E.* (1998). Topological characterization of the isomerization mechanisms in XNO (X=H, Cl). *Chem. Phys. Lett.* 292, 35.

Krokidis et al., 1999 – *Krokidis X., Vuilleumier R., Borgis D., Silvi B.* (1999). A topological analysis of the proton transfer in $H_5O^+_2$. *Mol. Phys.* 96, 265.

Mahdieh et al., 2017 – *Mahdieh D., Yaghoub S., Mahshid H.* (2017). Theoretical exploration of mechanism of carbapenam formation in catalytic Kinugasa reaction. *Tetrahedron* 73, 1673-1681.

Domingo et al., 2013 – *Domingo L. R., Pérez P., Sáez J. A.* (2013). Understanding the regioselectivity in hetero Diels–Alder reactions. An ELF analysis of the reaction between nitrosoethylene and 1-vinylpyrrolidine. *Tetrahedron.* 69, 107-114.

Mierzwa et al., 2015 – *Mierzwa G., Gordon A J., Latajka Z., Berski S.* (2015). On the multiple BO bonding using the topological analysis of Electron Localisation Function (ELF). *Comp. Theor. Chem.* 1053, 130-141.

Benallou et al., 2016 – *Benallou A., El Alaoui El Abdallaoui H., Garmes H.* (2016). Effect of hydrogen bonding on the intramolecular cycloaddition Diels-Alder reaction of triene-amide in an aqueous solution (case of a single molecule of water). *Tetrahedron.* 72, 76-83.

Benallou et al., 2016 – *Benallou A., El Alaoui El Abdallaoui H., Garmes H.* (2016). A conceptual DFT approach towards analysing feasibility of the intramolecular cycloaddition Diels-Alder reaction of triene amide in Lewis acid catalyst. *J. Chem. Sci.* 128, 1489-1496.

Diels, Alder, 1928 – *Diels O., Alder K.* (1928). Syntheses in hydroaromatic series. I. Addition of diene hydrocarbons. *Justus. Liebigs. Ann. Chem.* 460, 98.

Woodward et al., 1969 – *Woodward R.B., Hoffmann R.* (1969). The conservation of orbital symmetry**.** *Angew. Chem. Int. Ed. Engl.* 8,781.

Winkler, 1996 – *Winkler J.D.* (1996). Tandem Diels–Alder cycloadditions in organic synthesis**.** *Chem. Rev.* 96, 167.

Carruthers, 1990 – *Carruthers W.* (1990). Cycloaddition reactions in organic synthesis, Pergamon, Oxford, U.K.

Chen, Trudell, 1996 – *Chen Z., Trudell M.L.* (1996). Chemistry of 7-Azabicyclo[2.2.1]hepta-2,5-dienes, 7-Azabicyclo[2.2.1]hept-2-enes, and 7-Azabicyclo[2.2.1]heptanes. *Chem. Rev.* 96, 1179.

Finguelli, Tatichi, 2002 – *Finguelli F., Tatichi A.* (2002). The Diels-Alder reaction. Selected practical methods. Wiley; New York.

Shimada et al., 2009 – *Shimada K., Takata Y., Osaki Y., et al.,* (2009) regioselective synthesis of polysubstituted pyridines via hetero-diels–alder reaction of isotellurazoles with acetylenic dienophile. *Tetrahedron. Letters.* 50, 6651–6653.

Gonzalez, Schlegel, 1990 – *Gonzalez C., Schlegel H.B.* (1990). Reaction path following in mass-weighted internal coordinates. *J. Phys. Chem.* 94, 5523.

Lee et al., 1988 – *Lee C., Yang W., Parr R.G.* (1988). Development of the Colle-Salvetti correlation-energy formula into a functional of the electron density. *Phys. Rev. B* 37, 785.

Hehre et al., 1986 – *Hehre W.J., Radom L., Schleyer P.v.R., Pople J.A.* (1986). Ab initio molecular orbital theory, Wiley, New York.

Schlegel, 1994 – *Schlegel H.B.* (1994). In modern electronic structure theory. Ed, World Scientific Publishing, Singapore.

Fukui, 1970 – *Fukui K.* (1970). Formulation of the reaction coordinate. *J. Phys. Chem.* 74, 4161.

Gonzalez, Schlegel, 1991 – *Gonzalez C., Schlegel H.B.* (1991). Improved algorithms for reaction path following: Higher-order implicit algorithms. *J. Chem. Phys.* 95, 5853.

Reed et al., 1988 – *Reed A.E., Curtiss L.A., Weinhold F.* (1988). Intermolecular interactions from a natural bond orbital, donor-acceptor viewpoint. *Chem. Rev.* 88, 899.

Tian, Feiwu, 2012 – *Tian L, Feiwu C.* (2012). Multiwfn: A multifunctional Wavefunction analyzer. *J. Comp. Chem.* 3, 580-592.

Frisch et al., 2009 – *Frisch M.J., et al.* (2009). Gaussian 09, Revision A.02, Gaussian, Inc., Wallingford, CT.

Parr et al., 1999 – *Parr R.G., Szentpaly L.V., Liu S.* (1999). Electrophilicity Index. *J. Am. Chem. Soc.* 121, 1922.

Parr, Yang, 1989 – *Parr R.G., Yang W.* (1989). Density functional theory of atoms and molecule; Oxford University Press; New York, 1989.

Domingo et al., 2002 – *Domingo L.R., Aurell M.J., Perez P., Contreras R.* (2002). Quantitative characterization of the local electrophilicity of organic molecules. Understanding the regioselectivity on Diels-Alder reactions. *J. Phys. Chem. A* 106, 6871, 6875.

Domingo, Pérez, 2011 – *Domingo L.R, Pérez P.* (2011). The nucleophilicity N index in organic chemistry. *Org. Biomol. Chem.* 9, 7168.

Kohn et al., 1965 – *Kohn W, Sham L.* (1965). Self-consistent equations including exchange and correlation effects. *J. Phys. Rev.* 140, 1133.

Perez et al., 2009 – *Perez P., Domingo L.R., Duque-Noreña M., Chamorro E.* (2009). A condensed to-atom nucleophilicity index. An application to the director effects on the electrophilic aromatic substitutions. *J. Mol. Struct. (Theochem)* 895, 86-91.

Contreras et al., 1999 – *Contreras R., Fuentealba P., Galván M., Perez P.* (1999). A direct evaluation of regional Fukui functions in molecules. *Chem. Phys. Lett.* 304, 405-413.

Domingo et al., 2008 – *Domingo L.R, Chamorro E., Perez P.* (2008). Understanding the reactivity of captodative ethylenes in polar cycloaddition reactions. A theoretical study. *J. Org. Chem.* 73, 4615.

Fleming, 1976 – *Fleming I.* (1976). Frontier orbitals and organic chemical reactions, Wiley, New York.

Takikawa et al., 1991 – *Takikawa Y, Hikage S, Matsuda Y, Higashiyama K, Takeishi Y, Shimada K.* (1991). Novel conversion of selenium-containing five-membered aromatics to nitrogen-containing six-membered aromatics via Hetero Diels–Alder Reaction with acetylenic dienophiles. *Chem. Lett.* 20, 2043-2046.

Polo et al., 2004 – *Polo V., Andres J., Castillo R., Berski S., Silvi B.* (2004). Understanding the molecular mechanism of the 1,3-dipolar cycloaddition between fulminic acid and acetylene in terms of the electron localization function and catastrophe theory. *Chem. Eur. J.* 10, 5165-5172.

Berski et al., 2006 – *Berski S., Andres J., Silvi B., Domingo L.R.* (2006). New findings on the Diels-Alder reactions. An analysis based on the bonding evolution theory. *J. Phys. Chem. A* 110, 13939-13947.

Polo et al., 2008 – *Polo V., Andres J., Berski S., Domingo L.R., Silvi B.* (2008). Understanding reaction mechanisms in organic chemistry from catastrophe theory applied to the electron localization function topology. *J. Phys. Chem. A* 112, 7128-7136.

Silvi, 2002 – *Silvi B.* (2002). The synaptic order: a key concept to understand multicenter bonding. *J. Mol. Struct.* 614, 3.

Published in the Slovak Republic
European Journal of Molecular Biotechnology
Has been issued since 2013.
E-ISSN: 2409-1332
2018, 6(1): 16-24

DOI: 10.13187/ejmb.2018.1.16
www.ejournal8.com

The Contribution to Bonding by Lone Pairs in the Hydrogen Transfer of Adenine Tautomerization (3H→9H) in the First Excited Electronic State: ELF Analysis

Abdelilah Benallou [a, *], Habib El Alaoui El Abdallaoui [a], Hocine Garmes [b]

[a] Team of Chemoinformatics Research and Spectroscopy and Quantum Chemistry, Physical and Chemistry Lab, Faculty of Science, University Chouaib Doukkali, El Jadida, Morocco
[b] Laboratory of Bio-organic Chemistry, Department of Chemistry, Faculty of Science, University Chouaib Doukkali, El Jadida, Morocco

Abstract

The hydrogen transfer of adenine tautomerization (3H→9H) is performed by using ELF topological analysis, this study has been carried out at TD-DFT method with B3LYP and 6-311G++(d,p) basis set. Our investigation leads us to conclude that lone pairs electrons of nucleophilic nitrogen atom are not a non bonding electrons, although the lone pairs may contribute to the covalently bond with an electrophile (H atom) behind TS (second phase), whereas excited electrons are highly contributed to the first phase before TS location, the contribution to bonding by lone pairs is depending generally on the evolution of chemical structure along IRC. Therefore, lone pairs electron are considerably helped for hydrogen transfer of adenine tautomerization in the first electronic state. Subsequently, lone pairs and non bonding electrons are not strictly equivalent to each other.

Keywords: Adenine tautomers; H-transfer; Electronic state; ELF; Lone pairs; TD-DFT.

1. Introduction

The tautomerization reaction constitutes a very successful example of photochemistry reaction (Nir et al., 2001), this process received considerable attention, since thermal energy may easily transform one conformer to another, a number of lower energy conformer may coexist in same time. In addition, hydrogen transfer reaction is considered to be a first step in the mutation of DNA (Salter, Chaban, 2002). Interestingly, the contribution of lone pairs or non-bonding electrons in the reactivity between the reagents through participating in the covalent bond and others chemical bonding is a very significant subject, lone pairs entre the description of Lewis structure for simple and complex molecules to give explanation of the bonding interaction, bonding evolution is one of the most attractive topics of experimental and theoretical chemist (Berski et al., 2006; Benallou et al., 2018); where bonds are placed, how bonded type interaction and where lone pairs are located. For this instance, lone pairs are an essential element of the valence shell electron repulsion theory (Gillespie, 1972; Gillespie et al., 1991). The role of the lone pair in the molecular interaction between charged, radicals and ionic molecules are in very important interest. The contribution of lone pairs to the chemical bonding is fundamental to our work. In this sense, hydrogen bonded complexes exist as single species because of the stabilizing interaction between a donor lone pair (O, N…) and acceptor hydrogen on the other.

* Corresponding author
E-mail addresses: abdo_benallou@yahoo.fr (A. Benallou)

In our classical example to evaluating the role of lone pairs in the chemical bonding, we have reported the tautomerization reaction of adenine, H-proton transfer of the most stable and favorable monomer (3H-adenine) to the unstable monomer (9H-adenine), in gas phase situation, of the lowest excited state is evaluated.

Adenine an important product that represents a base in DNA and RNA, thus the role of hydrogen cyanide (HCN) in the prebiotic formation of adenine is taken a significant interest of by the experimental and theoretical chemists (Alfredsson et al., 1996; Heikkil, Lundell, 2000; Moser et al., 1976; Benallou, 2017; Wentrup et al., 1987; Evans et al., 1991; Jobst et al., 2008), Adenine is a molecule that in a quite abundant under primitive conditions in the universe and the early Earth, 5 HCN molecules in the primitive conditions, we can reproduce adenine as below, however this process is highly energetic (Benallou, 2016; Benallou, 2017).

HCN+HCN→H2C2N2(dimer)+HCN→H3C3N3(trimer)+HCN→H4C4H4(tetramer)+HCN→ H5C5N5 (adenine).

For that reason, quantum chemical studies of chemical reactions usually are restricted for determination of structures of reactants and transition state, very little attention is paid to the analysis of chemical bonds which are important during the chemical reaction. Lone pair in general do not enter directly into the atoms in molecules (AIM) theory (Bader, 1994), while, electron localization function (ELF) (Fuster, Silvi, 2000) theory takes into account the basin where electron pairs tend to exist, considering the bonding situation, to elaboration of the bonding evolution theory (BET) which merges the ELF.

In order to evaluate the contribution to bonding by lone pairs, the mechanism of H-transfer in the adenine tautomers is completely analysed from a point of view of the bonding evolution theory, we focus on a comparison of results achieved using the ELF analysis, then a characterization of the electron density redistribution following the hydrogen transfer along IRC is realized, finally a determination of lone pair or non-bonding electron contribution in the formation of N9-H and N3-H bonds. Note that this work will be performed in the first excited electronic state in which 3H adenine monomer is more stable to that of 9H adenine.

2. Computational methods

The geometry optimizations of such critical points were performed using the density functional formalism with the TD-DFT method and B3LYP exchange-correlation energy functional (Becke, 1993; Lee et al., 1988). All the calculations were realized with GAUSSIAN G09 program package (Frisch et al., 2009) and visualization of the output files is performed using the Gauss-View 5.0.8 software. The surface mapping was determined using a 6-311G** basis set level and the critical points (minima and transition states) were optimized and checked by calculating the intrinsic reaction coordinates (IRCs) with this basis set. All energies have been corrected for zero-point energy (ZPE) contributions calculated at the same level. For the BET analysis a reaction path was taken from an IRC calculation in mass-weighted Cartesian coordinates, the electronic structures of stationary points were analyzed by the natural bond orbital (NBO) method (Reed et al., 1988) and by ELF topological analysis. The ELF study was carried out with the Multiwfn program (Tian, Feiwu, 2012) using the corresponding mono determinant wave functions of the selected structures.

3. Results and discussion

The relative stability and abundance of adenine monomers are mostly studied in latter decade. 9H-adenine is well known more stable and has the lowest energy in the gas phase to compare with the other conformers such as 3H-, 7H-, and 1H-adenine of ground state situation. However, in the first excited electron 3H-adenine is relatively more stable and not much high in energy (Nowak et al., 1996). It is worthy to note that all adenine conformers have been found to coexist (Laxer et al., 2001; Chenon et al., 1975). So, hydrogen atom-transfer in the 3H, and 9H conformer, where the lone pairs are probably will contribute to covalent and other chemical bonds of hydrogen atom transfer in the first electronic state will be detailed step by step in this section.

3.1. Chemical structure of adenine tautomerization in the lowest electronic state

In the literature (Chenon et al., 1975), 3H-adenine is most stable to compare with 9H-adenine in the lowest excited electronic state. So, in order to investigate the transition state and reactants, we report all stationary points integrated into the tautomerization of adenine, lowest

electronic state is taken into consideration in this study, furthermore, TD-DFT method with 6-311++G(d,p) basis set are performed, and thus, the schematic pictures of adenine tautomerization (3H→9H) in the lowest electronic state is depicted in Figure 1.

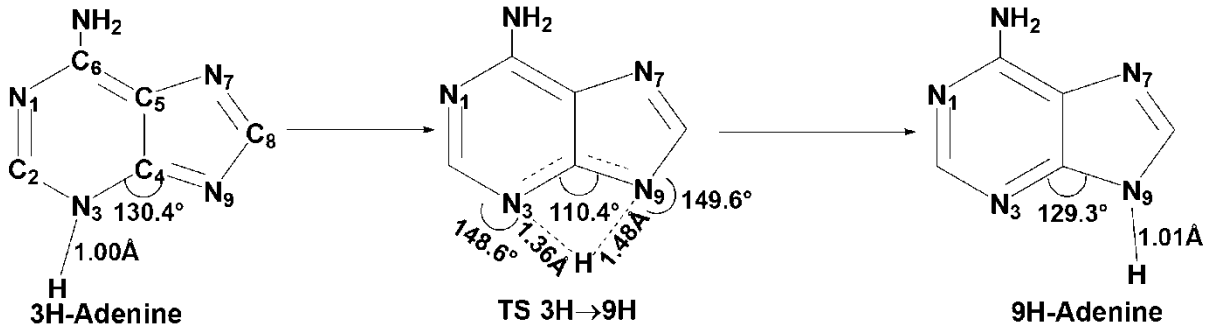

Fig.1. H-transfer of adenine tautomerization (3H→9H), in the lowest electronic state

The chemical structure of hydrogen atom transfer (3→9 tautomerization) for the first electronic state is analyzed, the results show that TS-structure is bent with two rings forming an angle of about 148.6° and 149.6° for C2N3Hα and C8N9Hα sequences respectively. Another observation is taken of this tautomerization reaction such as Hα atom transfer is somewhat closer to N3 instead of N9, 1.36Å. Whereas H-proton is almost positioned identically to both tautomers, 1.00Å for the N3-Hα bond and 1.01Å for the N9-Hα bond of 3H and 9H conformers of adenine respectively. However, this mechanism process is moderately energetic (Kim et al., 2007).

3.2. ELF bonding analysis of the IRC path of hydrogen atom transfer (3H→9H)

In this section, we will estimate the contribution of lone pairs electron to bonding in the hydrogen transfer, to this end, a characterization of the distribution of electronic density along the progress of the reaction is in very significant importance. For this purpose, an ELF analysis along IRC of the H-transfer will be performed. The electronic populations of the most relevant ELF valence basins of selected structures (points) along IRC are listed in Table 1, while the attractor positions for the most relevant points associated with the formation and breaking of the N3–Hα and N9-Hα bonds, are shown in Figure 2.

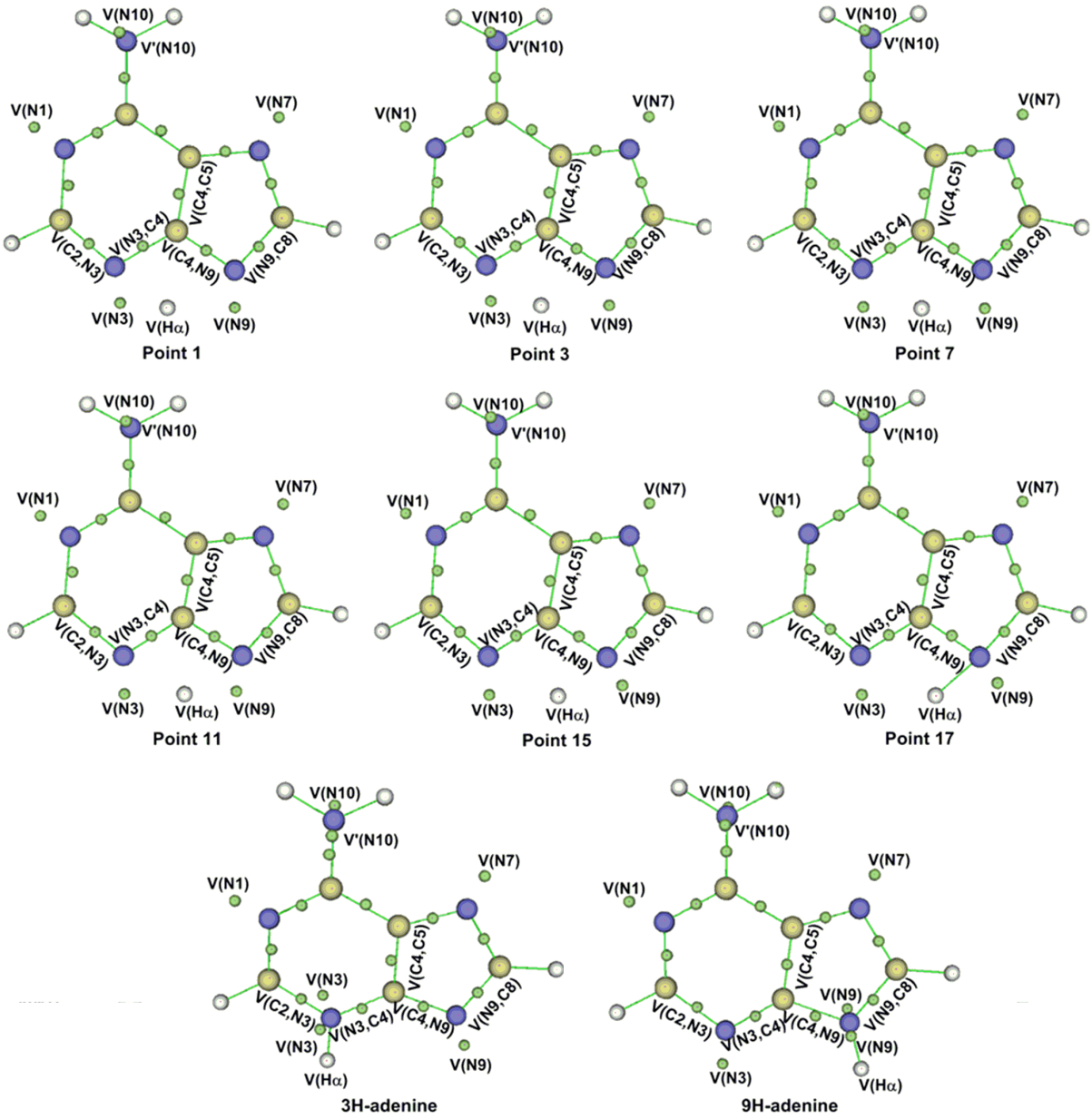

Fig.2. ELF attractors of some selected points of the IRC associated with the hydrogen transfer of adenine tautomerization (3H→9H)

Table 1. Valence basin populations of the hydrogen transfer calculated from the ELF of adenine tautomerization, associated with the N3–Hα and N9-Hα bonds formation/breaking step. Electron density in *e* (NBO) and bond distances in angstrom (Å)

Points	3H	P1	P2	P3	P4	P5	P6	P7	P8	P9	P10	P11 (TS)
d(N3-Hα)	1.00	1.34	1.36	1.37	1.39	1.40	1.41	1.42	1.43	1.44	1.44	1.45
d(N9-Hα)	2.75	1.49	1.48	1.46	1.45	1.43	1.42	1.40	1.39	1.37	1.37	1.36
V(N1)	2.77	2.88	2.87	2.86	2.85	2.83	2.80	2.79	2.76	2.75	2.75	2.75
V(N3)	0.56/ 0.56	2.87	2.90	2.93	2.86	2.98	3.02	3.04	3.06	3.08	3.09	3.09
V(N7)	3.00	2.95	2.94	2.94	2.95	2.95	2.95	2.94	2.95	2.95	2.95	2.95
V(N9)	2.96	3.10	3.10	3.09	3.08	3.07	3.06	3.05	3.04	3.02	3.02	3.02
V(N10)	0.89	1.46	1.47	1.48	1.49	1.50	1.50	1.50	1.50	1.52	1.52	1.52
V'(N10)	2.12	2.11	2.12	2.11	2.12	2.11	2.12	2.12	2.11	2.11	2.12	2.12
V(C2,N3)	2.16	2.32	2.28	2.26	2.24	2.20	2.17	2.13	2.11	2.06	2.06	2.06

V(N3,C4)	2.21	2.14	2.16	2.17	2.18	2.20	2.24	2.25	2.25	2.27	2.27	2.28
V(C4,N9)	2.42	2.20	2.18	2.18	2.17	2.16	2.15	2.13	2.11	2.10	2.10	2.09
V(N9,C8)	2.34	2.09	2.09	2.10	2.10	2.11	2.13	2.13	2.15	2.17	2.18	2.18
V(C4,C5)	2.73	2.95	2.95	2.95	2.95	2.95	2.94	2.94	2.94	2.94	2.94	2.94
V(Hα)	2.09	0.51	0.51	0.51	0.51	0.51	0.51	0.51	0.51	0.51	0.51	0.51

Table 1 (next).

Points	**P12**	**P13**	**P14**	**P15**	**P16**	**P17**	**P18**	**P19**	**P20**	**P21**	**9H**
d(N3-Hα)	1.48	1.51	1.55	1.59	1.63	1.67	1.72	1.77	1.81	1.86	2.78
d(N9-Hα)	1.33	1.30	1.27	1.23	1.20	1.16	1.13	1.10	1.08	1.06	1.01
V(N1)	2.77	2.77	2.78	2.79	2.80	2.82	2.82	2.83	2.83	2.84	2.79
V(N3)	3.07	3.07	3.06	3.05	3.04	3.02	3.01	3.00	2.99	2.98	2.95
V(N7)	2.94	2.93	2.92	2.95	2.92	2.90	2.90	2.89	2.88	2.87	2.94
V(N9)	1.48/1.50	1.32/1.57	1.58	1.59	1.59	1.59	1.58	1.57	1.57	1.56	0.63/0.63
V(N10)	1.51	1.51	1.51	1.51	1.51	1.51	1.52	1.52	1.52	1.52	0.93
V'(N10)	2.13	2.12	2.13	2.13	2.11	2.12	2.12	2.12	2.12	2.12	2.12
V(C2,N3)	2.09	2.16	2.20	2.24	2.28	2.32	2.94	2.36	2.38	2.40	2.21
V(N3,C4)	2.28	2.28	2.28	2.28	2.28	2.28	2.27	2.27	2.26	2.26	2.50
V(C4,N9)	2.10	2.10	2.09	2.07	2.08	2.05	2.05	2.05	2.05	2.05	2.16
V(N9,C8)	2.14	2.13	2.12	2.11	2.10	2.09	2.08	2.07	2.06	2.05	2.12
V(C4,C5)	2.94	2.94	2.95	2.97	2.97	2.97	2.97	2.97	2.98	2.98	2.84
V(Hα)	0.54	0.58	1.94	1.94	1.95	1.95	1.96	1.97	1.98	1.99	2.07

The results noted in Table 1 reveal that the most important changes of electron density are contributed exclusively to the lone pairs of the N3, N9 and Hα atom, these atoms are directly integrated into the hydrogen atom transfer of adenine tautomerization in the lowest excited state. However, the remaining attractors are not having more changes along IRC. So, in this case, we will focus especially on the basins relative to the V(N3), V(N9) and V(Hα) attractors. To this end, the electronic population associated with the basins of lone pairs and hydrogen atom transfer will be summarized, the results are given in Figure 3.

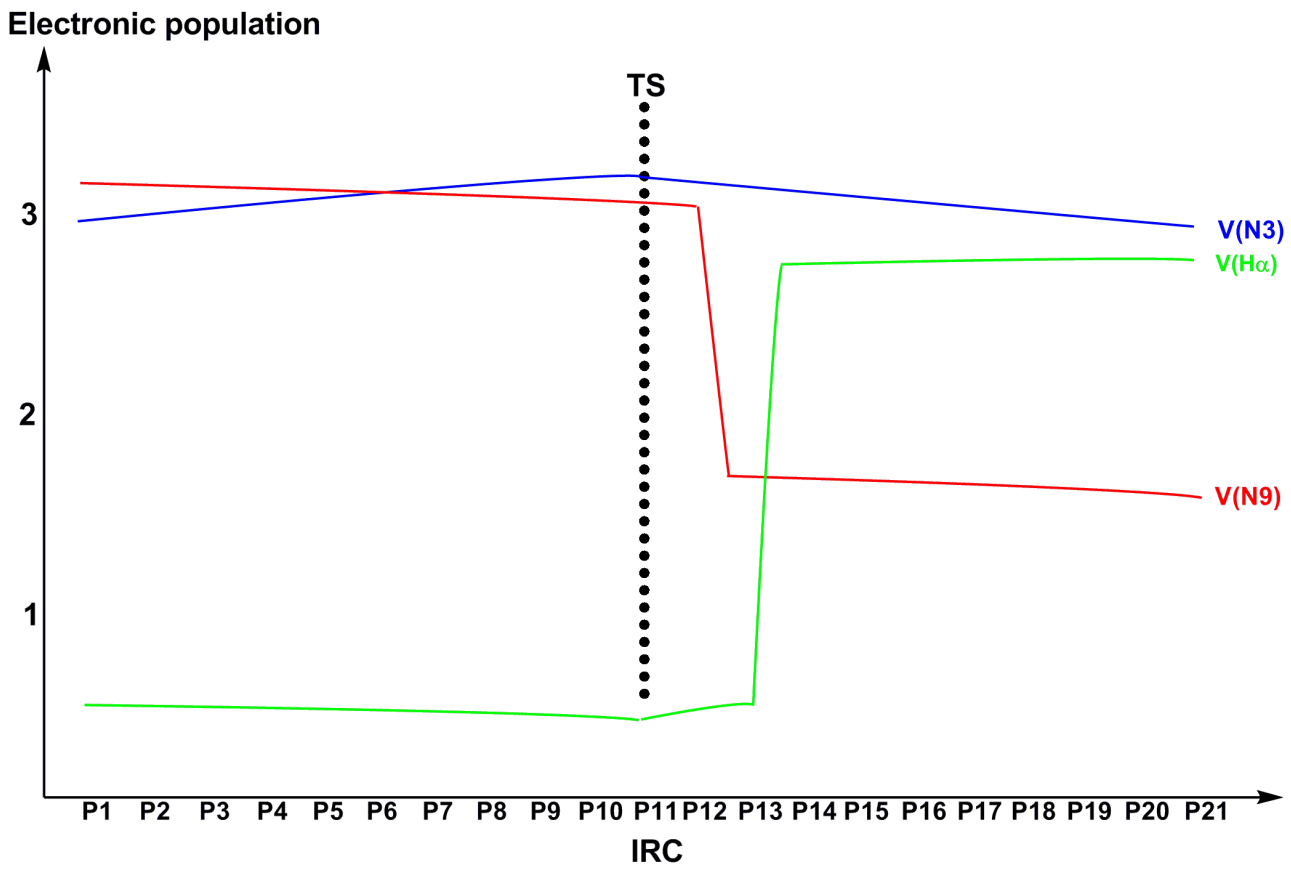

Fig.3. Electronic population in (e) along IRC of hydrogen transfer of the most significant atoms involved in the adenine tautomerization in the lowest electronic state

Showing the results given in Fig.3, we can separate the change of electron density of such attractor's (V(N3), V(N9) and V(Hα)) along IRC into two important phases:

First phase: is located between point 1 and TS. In this phase the electronic population of lone pairs N3 and N9 does not have more changes, the variation of electron density of both monosynaptic basin V(N3) and V(N9) relative to the lone pairs is generally stable along IRC. So, no contribution of lone pairs electron towards hydrogen atom can be stated. For this instance, the electronic population of the monosynaptic basin V(Hα) related to the hydrogen atom has not increased or decreased along IRC, this result is quite consistent with that found for V(N3) and V(N9) basins. Therefore, the contribution to bonding by lone pairs electron in the hydrogen transfer in the first phase is practically negligible; we suppose that lone pair of N3 atom is contributed to bonding in the hydrogen atom transfer, the electron density of such atom should increase along IRC, as long as N3 and Hα bond is broken at TS. So the electronic population of lone pairs of N3 must take a maximum value and that is never likely going to take place. Subsequently, taking into account the main role of valence shell electrons in the chemical bonding to compare with core electrons, furthermore Hα atom is very distant to N3 atom along this first phase (N3-Hα bond distances). Therefore, the excited electrons are evidently assisted by participating in the bonding of hydrogen atom transfer of adenine tautomerization.

Second phase; In this phase (TS to Points 21) the situation is completely different to that of the first phase, while Hα atom becomes very distant to N3 and closer to N9, N3-Hα bond is broken, at this point a new N9-Hα bond is begun to form, the electronic population of the monosynaptic basin of each attractors of lone pairs and hydrogen atom has been modified, principally to the N9 and Hα atom, whereas V(N3) basin is not varied. We have remarked the presence of a pseudo-horizontal symmetry axis between V(N9) and V(Hα) basins, as far as the electronic population related to the monosynaptic basin V(Hα) increases we have stated a decreases of V(N9) basin along the second phase of IRC (P11→P21). Therefore, the contribution to bonding by lone pairs of hydrogen atom transfer in the lowest excited electronic state is principal behind TS, in which N9-Hα covalently bond is formed.

Consequently, in the hydrogen atom transfer of adenine tautomerization in the lowest electronic state, two phases characterize the contribution to bonding by lone pairs; first phase (in the beginning of the reaction until TS; N3-Hα covalently bond), the contribution to bonding by lone pairs is negligible, and then the excited electrons play a significant role of hydrogen transfer by assisting to afford the necessary energy to breaking N3-Hα bond. However, in the second phase (TS until the formation of the N9-Hα bond), herein the contribution to bonding by lone pairs is more considerable, such as a very important part of electron density related to the N9 lone pair shifts regularly to the Hα atom to form the covalent bond of N9-Hα.

Subsequently, the lone pairs are not a non-bonding electron, but they are very useful for some system reactions. Lone pairs play a key in the hydrogen transfer by contributing to the covalently bond especially in the second phase behind TS between a good nucleophile (N9) and a hydrogen atom Hα (electrophile), while in the first phase the excited electrons are probably integrated into the transfer of hydrogen atom. A schematic picture of the lone pair contribution to the bonding is given in figure 4, while a representation of some significant point is depicted in figure 5.

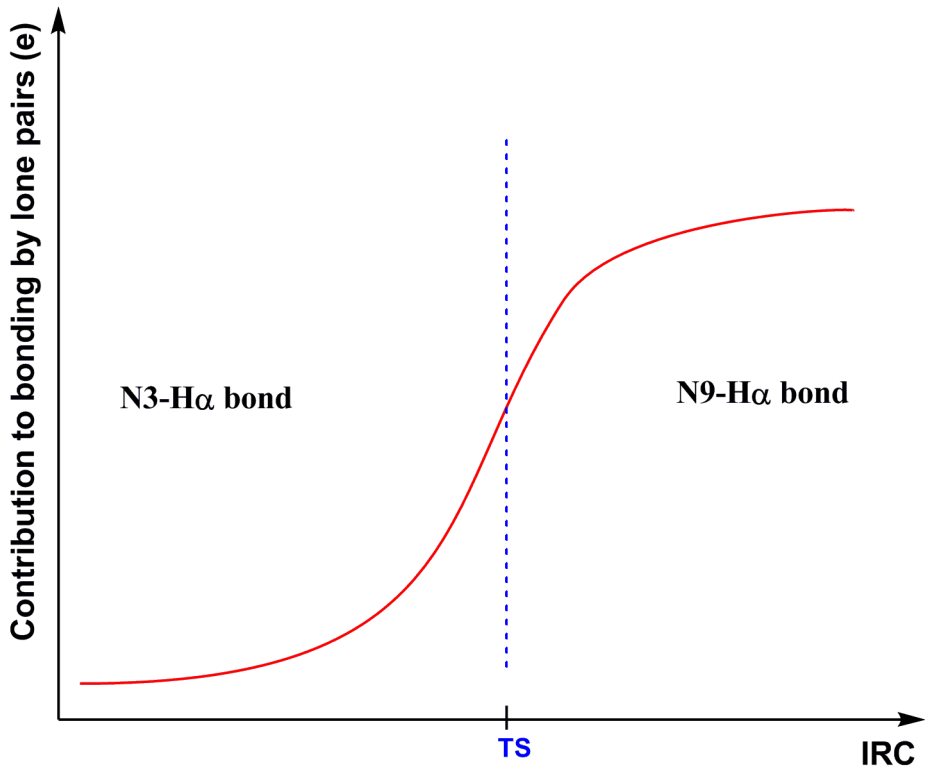

Fig. 4. Contribution to bonding by lone pairs of H-transfer (adenine tautomerization) along IRC

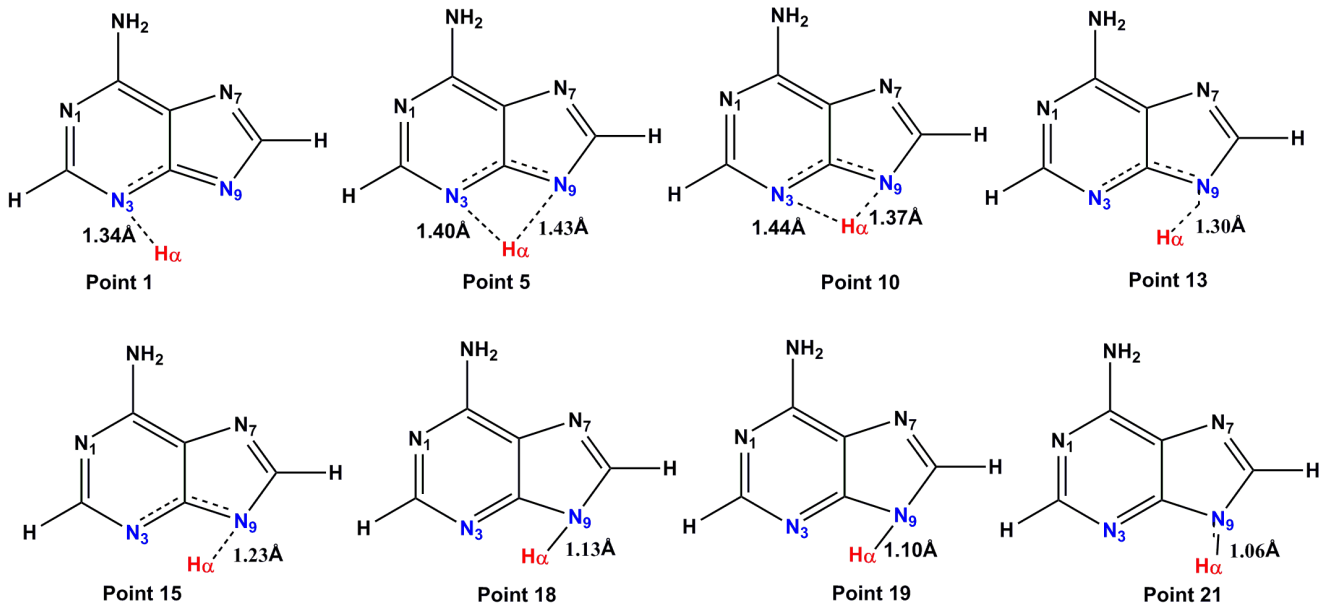

Fig. 5. Some significant points involved in the hydrogen transfer of adenine tautomerization. In brief, the contribution to bonding by lone pairs is depending generally on the evolution of chemical structure along IRC and the relative stability of each tautomers of adenine

4. Conclusion

ELF analysis of adenine tautomerization (H-transfer, 3H→9H) is performed in lowest electronic state at B3LYP and 6-311++G(d,p) basis set level. Two phases describe the contribution to bonding by lone pairs in the hydrogen transfer; the first phase (the beginning of reaction until TS along IRC), which H atom is closer to the N3 atom (N3-Hα covalently bond), the contribution of lone pairs is trivial, for this instance, 3H adenine conformer is very stable at the first electronic state, and then the excited electrons have been probably helped for the hydrogen atom transfer. However, in the second phase, the N3-Hα is broken wile a new bond of N9-Hα is formed (behind TS), the contribution of lone pairs is very important. Subsequently, the contribution to bonding by lone pairs is depending generally on the evolution of chemical structure along IRC and the relative stability of each adenine tautomers. So, lone pairs are not non-bonding electrons but are playing a very considerable role in the formation of chemical bonding.

References

Nir et al., 2001 – *Nir E., Kleinermanns k., Grace L., DeVries M.S.* (2001). On the photochemistry of purine nucleobases. *J. Phys. Chem. A* 105, 5106.

Salter, Chaban, 2002 – *Salter L.M., Chaban G.M.* (2002). Theoretical study of gas phase tautomerization reactions for the ground and first excited electronic states of adenine. *J. Phys. Chem. A* 106, 4251-4256.

Berski et al., 2006 – *Berski S., Andres J., Silvi B., Domingo L.R.* (2006). New findings on the Diels-Alder reactions. An analysis based on the bonding evolution theory. *J. Phys. Chem. A* 110, 13939.

Benallou et al., 2018 – *Benallou A., El Alaoui El Abdallaoui H., Garmes H.* (2018). C—C bond formation in the intramolecular Diels-Alder reaction of triene amides. *Heliyon*. 4, e00504.

Gillespie, 1972 – *Gillespie R.J.* (1972). Molecular Geometry, Van Nostrand Reinhold, London.

Gillespie et al., 1991 – *Gillespie R.J., Hargittai I.* (1991). VSEPR Model of Molecular Geometry, *Allyn and Bacon*, Boston.

Alfredsson et al., 1996 – *Alfredsson M., Ojame L., Hermansson K.G.* (1996). *Int. J. Quantum. Chem*. 60, 767.

Heikkil, Lundell, 2000 – *Heikkil A., Lundell J.* (2000). Strongly Bonded Bimolecular Complexes between HCN and HNC. *J. Phys. Chem. A* 104, 6637.

Moser et al., 1976 – *Moser R.E., Fritsch J.M., Westman T.L., Kliss R.M., Matthews C.N.* (1967). Hydrogen cyanide dimer. Aminocyanocarbene. *J. Am. Chem. Soc*. 89, 5673.

Benallou, 2017 – *Benallou A.* (2017). Understanding the temperature and pressure role of HCN→HNC isomerization as well as vibrational and rotational energies of these species. *Arab J. Phys. Chem.* 4, 1.

Wentrup et al., 1987 – *Wentrup C., Lorencak P., Maquestiau A., Flammang R.* (1987). C2H2N2 Isomers in the gas phase: Characterization of CH2N-CN and HNCH-CN by collisional activation mass spectrometry. *Chem. Phys. Lett.* 137, 241.

Evans et al., 1991 – *Evans R.A., Lorencak P., Ha T.K., Wentrup C.* (1991). HCN dimers: iminoacetonitrile and N-cyanomethanimine. *J. Am. Chem. Soc.* 113, 7261.

Jobst et al., 2008 – *Jobst K.J., Hanifa M.R., Terlouw J.K.* (2008). The covalently bound HCN dimer ions HCN^{-} NCH^{+} and HCN^{-} C (N) H^{+} are stable species in the gas-phase, but the neutral counterparts are not. *Chem. Phys. Lett.* 462, 152.

Benallou, 2016 – *Benallou A.* (2016). Understanding the most favourable dimer of HCN for the oligomerization process in the gas phase of interstellar clouds. *Comp. Theor. Chem.* 1097, 79-82.

Benallou, 2017 – *Benallou A.* (2017). The mechanism determination of trimer and tetramer HCN for adenine formation in the gas phase of interstellar space. *Comp. Theor. Chem.* 1101, 68-73.

Bader, 1994 – *Bader R.F.* (1994). Atoms in Molecules: A Quantum Theory, Oxford University Press, Oxford.

Fuster, Silvi, 2000 – *Fuster F., Silvi B.* (2000). Does the topological approach characterize the hydrogen bond. *Theor. Chem. Acc.* 104, 13.

Becke, 1993 – *Becke A.D.* (1993). Density functional thermochemistry. III. The role of exact exchange. *J. Chem. Phys.* 98, 1372-1377.

Lee et al., 1988 – *Lee C., Yang W., Parr R.G.* (1988). Development of the Colle-Salvetti correlation-energy formula into a functional of the electron density. *Phys. Rev. B.* 37, 785-789.

Frisch et al., 2009 – *Frisch M.J. et al.* (2009). GAUSSIAN 09, revision A. 02, GAUSSIAN Inc., Wallingford, CT.

Reed et al., 1988 – *Reed A.E., Curtiss L.A., Weinhold F.* (1988). Intermolecular interactions from a natural bond orbital, donor-acceptor viewpoint. *Chem. Rev.* 88, 899.

Tian, Feiwu, 2012 – *Tian L, Feiwu C.* (2012). Multiwfn: A multifunctional Wavefunction analyzer. *J. Comp. Chem.* 3, 580-592.

Nowak et al., 1996 – *Nowak M., Lapinski J., Kwiatkowski L., Leszczynski J.S.* (1996). Molecular structure and infrared spectra of adenine. Experimental matrix isolation and density functional theory study of adenine 15N isotopomers. *J. Phys. Chem.* 100, 3527.

Laxer et al., 2001 – *Laxer A., Major D.T., Gottlieb H.E., Fischer B.* (2001). (15N5)-Labeled Adenine Derivatives: Synthesis and Studies of Tautomerism by 15N NMR Spectroscopy and Theoretical Calculations. *J. Org. Chem.* 66, 5463.

Chenon et al., 1975 – *Chenon M.T., Pugmire R.J., Grant D.M., Panzica R.P., Townsend L.B.* (1975). Carbon-13 magnetic resonance. XXVI. Quantitative determination of the tautomeric populations of certain purines. *J. Am. Chem. Soc.* 97, 4636.

Kim et al., 2007 – *Kim H., Ahn D., Chung S.Y., Kim S.K, Lee S.* (2007). Tautomerization of Adenine Facilitated by Water: Computational Study of Microsolvation. *J. Phys. Chem. A* 111, 8007-8012.

Published in the Slovak Republic
European Journal of Molecular Biotechnology
Has been issued since 2013.
E-ISSN: 2409-1332
2018, 6(1): 25-40

DOI: 10.13187/ejmb.2018.1.25
www.ejournal8.com

Rhodopsin. Bacteriorhodopsin in Biotechnology. Electromagnetic Conception for the Eyesight

Ignat Ignatov [a,*], Yuliana Pesheva [a]

[a] Scientific Research Center of Medical Biophysics, Bulgaria

Abstract

This review article views predominately the structure and function of animal and bacterial photoreceptor pigments (rhodopsin, iodopsin, bacteriorhodopsin) and their aspects of nano- and biotechnological usage. On an example of bacteriorhodopsin is described the method of its isolation from purple membranes of photo-organotrophic halobacterium *Halobacterium halobium* by cellular autolysis by distilled water, processing of bacterial biomass by ultrasound at 22 KHz, alcohol extraction of low and high-weight molecular impurities, cellular RNA, carotenoids and lipids, the solubilization with 0,5 % (w/v) SDS-Na and subsequent fractionation by methanol and gel filtration chromatography on Sephadex G-200 Column balanced with 0.09 M Tris-borate buffer (pH = 8,35) with 0,1 % (w/v) SDS-Na and 2,5 mM EDTA.

Within the framework of the research the mechanism of color perception by the visual analyzer having the ability to analyze certain ranges of the optical spectrum, as colors was studied along with an analysis of the additive mixing of two colors. It was shown that at the mixing of electromagnetic waves with different wavelengths, the visual analyzer perceive them as separate or average wave length corresponding to mix colors (Marinov, Ignatov, 2008).

Keywords: vision, rhodopsin, iodopsin, bacteriorhodopsin, additive color mixing.

1. Introduction

Vision (visual perception) is a process of psycho-physiological processing of the images of surrounding objects, carried out by the visual system, which allows to get an idea of the size, shape and color of surrounding objects, their relative position and distance between them. By means of this animals can receive 90 % of all incoming information to the brain.

The function of the visual system is carried out through various interrelated complex structures designated as visual analyzer, consisting of a peripheral part (retina, optic nerve, optic tract) and the central department of combining stem and subcortical centers of the midbrain, as well as the visual cortex of the cerebral hemispheres. The human eye can perceive only light waves of a certain length – from 380 to 770 nm.

Light rays from treated subjects pass through the optical system of the eye (cornea, lens and vitreous body) and onto the retina, where the light-sensitive photoreceptor cells (rods and cones) are located. Light incidented on the photoreceptors, triggers a cascade of biochemical reactions of visual pigments (in particular, the most studied of them is rhodopsin responsible for the perception of electromagnetic radiation in the visible range), and in turn, – the occurrence of nerve impulses, which are transmitted through the following retinal neurons and further to the optic nerve.

* Corresponding author
E-mail addresses: mbioph@abv.bg (I. Ignatov)

The optic nerve carries the nerve impulses into the lateral geniculate body - subcortical center of vision, and thence to the cortical center, located in the occipital lobe of the brain, where the visual image is formed.

Over the last decade have been obtained new data revealing the molecular basis of visual perception. It were identified visual molecules of eucariotes (rhodopsin, iodopsin) and procariots (bacteriorhodopsin) involved in light perception and cleared up the mechanism of their action.

The structural research of rhodopsin and its affiliate chromophore proteins (iodopsin, bacteriorhodopsin) and the analysis of their functions have been carried out in the Scientific Research Center of Medical Biophysics (Bulgaria) throughout the last 20 years. The purpose of the research was the studying of basic biochemical mechanisms associated with visual perception and some nano- and biotechnological applications of visual phototransforming pigments as trans membrane chromo-protein bacteriorhodopsin (BR), isolated from purple membranes of halobacterium *Halobacterium halobium*.

2. Materials and Methods

2.1. Bacterial Objects

As a BR producer was used a carotenoid strain of extreme photo-organo-heterotrophic halobacterium *Halobacterium halobium* ET 1001, obtained from Moscow State University (Russia). The strain was modified by selection of individual colonies on solid (2 % (w/v) agarose) media with peptone and 4.3 M NaCl.

2.2. Growth Conditions

BR (yield 8–10 mg from 1 g biomass) was obtained in synthetic (SM) medium (g/l): D,L-alanine – 0.43; L-arginine – 0.4; D,L-aspartic acid – 0.45; L-cysteine – 0.05; L-glutamic acid – 1.3; L-lycine – 0.06; D, L-histidine – 0.3; D,L-isoleucine – 0.44; L-leucine – 0.8; L-lysine – 0.85; D,L-methionine – 0.37; D,L-phenylalanine – 0.26; L-proline – 0.05; D, L-serine – 0.61; D,L-threonine – 0.5; L-tyrosine – 0.2; D,L-tryptophan – 0.5; D,L-valine – 1.0, AMP – 0.1; UMP – 0.1; NaCl – 250; $MgSO_4$ $7H_2O$ – 20; KCl – 2; NH_4Cl – 0.5; KNO_3 – 0.1; KH_2PO_4 – 0.05; K_2HPO_4 – 0.05; Na^+-citrate – 0.5; $MnSO_4$ $2H_2O$ – 3 10^{-4}; $CaCl_2$ $6H_2O$ – 0.065; $ZnSO_4$ $7H_2O$ – $4{\cdot}10^{-5}$; $FeSO_4$ $7H_2O$ – $5{\cdot}10^{-4}$; $CuSO_4$ $5H_2O$ – $5{\cdot}10^{-5}$; glycerol – 1.0, biotin – $1{\cdot}10^{-4}$; folic acid – $1.5{\cdot}10^{-4}$, vitamin B_{12} – $2{\cdot}10^{-5}$. The growth medium was autoclaved for 30 min at 0.5 atm, the pH value was adjusted to 6.5–6.7 with 0.5 M KOH. Bacterial growth was performed in 500 ml Erlenmeyer flasks (volume of the reaction mixture 100 ml) for 4–5 days at 35 °C on Biorad shaker ("Birad Labs", Hungary) under intense aeration and monochromatic illumination (3 lamps × 1.5 lx). All further manipulations for BR isolation were carried out with the use of a photomask lamp equipped with an orange light filter.

2.3. Isolation of Purple Membranes (PM)

Biomass (1 g) was washed with distilled water and polluted by centrifugation on T-24 centrifuge ("Carl Zeiss", Germany) (1500 g, 20 min). The precipitate was suspended in 100 ml of dist. H_2O and kept for 3 h at 4 °C. The reaction mixture was centrifuged (1500 g, 15 min), the pellet was resuspended in 20 ml dist. H_2O and disintegrated by infrasound sanitation (22 kHz, 3 times × 5 min) in an ice bath (0 °C). The cell homogenate after washing with dist. H_2O was resuspended in 10 ml of buffer containing 125 mM NaCl, 20 mM $MgCl_2$, and 4 mM Tris-HCl (pH = 8.0), then 5 mg of RNA-ase (2–3 units of activity) was added . The mixture was incubated for 2 h at 37 °C. Then 10 ml of the same buffer was added and kept for 10–12 h at 4 °C. The aqueous fraction was separated by centrifugation (1500 g, 20 min), the PM precipitate was treated with 50% (v/v) ethanol (5 times × 7 ml) at 4 °C followed by separation of the solvent. This procedure was repeated 6 times to give colorless washings. The protein content in the samples was determined spectrophotometrically on DU-6 spectrophotometer ("Beckman Coulter", USA) by the ratio D_{280}/D_{568} ($\varepsilon_{280} = 1.1{\cdot}10^5$; $\varepsilon_{568} = 6.3{\cdot}10^4$ $M^{-1}{\cdot}cm^{-1}$) (Neugebauer *et al.*, 1978). PM regeneration is performed as described in (Rudiger et al., 1997). Yield of PM fraction – 120 mg (80–85 %).

2.4. Isolation of BR

Fraction PM (in H_2O) (1 mg/ml) was dissolved in 1 ml of 0.5% (w/v) sodium dodecyl sulfate (SDS-Na), and incubated for 5–7 h at 37 °C followed by centrifugation (1200 g, 15 min).

The precipitate was separated, than methanol was added to the supernatant in divided portions (3 times × 100 ml) at 0 °C. The reaction mixture was kept for 14–15 h in ice bath at 4 °C and then centrifuged (1200 g, 15 min). Fractionation procedure was performed three times, reducing the concentration of 0.5 % SDS-Na to 0.2 and 0.1 %. Crystal protein (output 8–10 mg) was washed with cold ^2H_2O (2 times × 1 ml) and centrifuged (1200 g, 15 min).

2.5. Purification of BR

Protein sample (5 mg) was dissolved in 100 ml of buffer solution and placed on a column (150 × 10 mm), stationary phase – Sephadex G-200 ("Pharmasia", USA) (specific volume packed beads – 30–40 units per 1 g dry. Sephadex) equilibrated with buffer containing 0.1 % (w/v) SDS-Na and 2.5 mM ETDA. Elution proceeded by 0.09 M Tris-borate buffer containing 0.5 M NaCl, pH = 8.35 at a flow rate of 10 ml/cm^2 · h. Combined protein fraction was subjected to freeze-drying, in sealed glass ampoules (10 × 50 mm) and stored in frost camera at -10 °C.

2.6. Quantitative Aanalysis of Protein

The procedure was performed in 12.5% (w/v) polyacrylamide gel (PAAG) containing 0.1 % (w/v) SDS-Na. The samples were prepared for electrophoresis by standard procedures (LKB protocol, Sweden). Electrophoretic gel stained with Coomassie blue R-250 was scanned on a CDS-200 laser densitometer (Beckman, USA) for quantitative analysis of the protein.

2.7. Absorption Spectra

Absorption spectra of pigments were recorded on programmed DU-6 spectrophotometer (“Beckman Coulter”, USA) at 280 nm and 750 nm.

2.8. IR-Spectrospopy

IR-spectra were registered on Brucker Vertex IR spectrometer (“Brucker”, Germany) (a spectral range: average IR – 370–7800 cm^{-1}; visible – 2500–8000 cm^{-1}; the permission – 0.5 cm^{-1}; accuracy of wave number – 0.1 cm^{-1} on 2000 cm^{-1}) and Thermo Nicolet Avatar 360 Fourier-transform IR.

2.9. Color Analyzing

Colors were analyzed by using color analyzer “Tsvetan” (“Photopribor”, Cherkassk, Ukraine). Operating relative absorbance, % from -80 to 70. Measurement error, ±5 %. Response time from 0.4 to 63 sec. Overall dimensions, 300 mm.

3. Results and Discussion

3.1. Theoretical Aspects of Molecular Basis of Vision

The process of perception of light has a definite localization in photoreceptor light-sensitive cells of the retina. The retina in its structure is a multilayer layer of nervous tissue that is sensitive to light, which lines the inside of the back of the eyeball. Pigmented retina located at the membrane referred to as retinal pigmented epithelium (RPE), which absorbs light passing through the retina. This prevents the reverse reflection of the light through the retina and does not allow the vision to disperse.

Light enters through the eye and creates a complex biochemical reaction in the photoreceptor cells of the retina. Photoreceptor cells are divided into two types that due to their characteristic form are designated as rods and cones (Hubel, 1995). Rods are receptors of light of low intensity; they arranged in a colored layer of the retina, in which is synthesized photochromic protein rhodopsin, responsible for color perception. Cones on the contrary contain a group of visual pigments (iodopsin), and adapted to distinguish different colors. Rods can pensive black and white images in the dim light, cones – to carry out color vision in bright light. Human retina contains approximately 3 million of cones and 100 million of rods. Their dimensions are very small – the length of about 50 mm, the diameter from 1 to 4 μm. Electrical signals generated by the rods and cones, are handled by other retinal cells – bipolar and ganglion cells before they are transmitted to the brain via the optic nerve (Hogan et al., 1971). Additionally, there are two intermediate layers of neurons. Horizontal cells transmit messages back and forth between the photoreceptor cells, bipolar cells and each other. Amacrine cells of the retina are linked to bipolar cells, ganglion cells,

as well as with each other. Both types of these intermediate neurons play a major role in the processing of visual information at the level of the retina before it is transmitted to the brain for final processing.

Cones are approximately 100 times less sensitive to light than rods, but much better perceive the rapid movement. The wand can be stimulated by a single photon. Cascade of molecular interactions enhances this "quantum" of information into a chemical signal, which is then perceived by the nervous system. The degree of enhancement signal varies depending on ambient light: rods are more sensitive under low than inder bright light. As a result, they operate effectively in a wide range of ambient light. Sensory system of rods is packed up in clearly distinguishable cellular substructure that can be easily selected and investigated *in vitro* in isolated state. This property makes them as indispensable object for further structural-functional studies as well as studies of photoreceptor pigments (rhodopsin, iodopsin). These animal photoreceptor pigments are used as models for studying of bacterial photoreceptor pigment bacteriorhodopsin (BR) from purple membranes of halobacterium *Halobacterium halobium*.

3.2 Rhodopsin and its Structural and Functional Pproperties

Rhodopsin (*Nathans et al., 1986*) is one of the most important integral photoreceptor proteins of rod cells, which absorbs a photon and creates a biochemical response constituting a first step in a chain of events that provide vision. Rhodopsin consists of two components – a colorless protein opsin and a chromophore component 11-*cis*-retinal residue, acted as the light acceptor (Figure 1). The absorption of a light photon by 11-*cis*-retinal "turns on" the enzymatic activity of opsin and further photosensitive biochemical cascade of reactions that are responsible for vision (Liang et al., 2004).

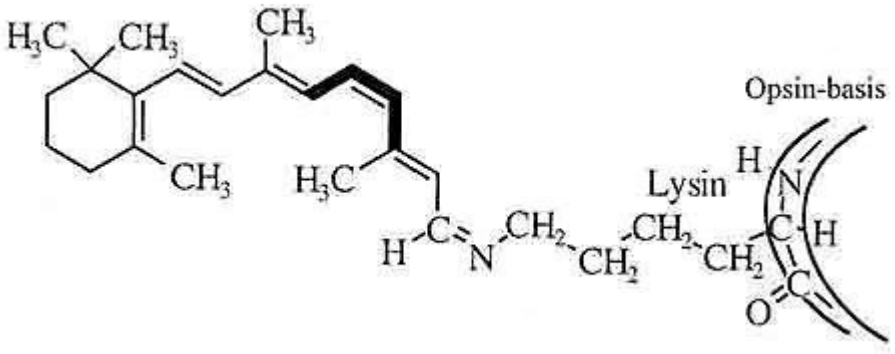

Fig. 1. Configuration of photosensitive chromophore of rhodopsin in the basic (unexcited) phase (at the double bond is marked 11-*cis*-configuration)

Rhodopsin belongs to the group of the G-protein-coupled receptors (GPCR-receptors) of the retibylidene protein family responsible for transmembrane signaling mechanism based on the interaction with intracellular membrane G-proteins – universal intermediaries in the transmission of hormonal signals from the cell membrane receptors to effect or proteins, causing the final cellular response. The establishment of the spatial structure of rhodopsin is so important because rhodopsin as the "originator" of the family of GPCR-receptors is a "model" for the structure and function of other receptors that it is extremely important from fundamental scientific and practical points of view (Palczewski, 2006).

Spatial structure of rhodopsin was long defied by the study of "direct" methods – X-ray diffraction and NMR spectroscopy, while the molecular structure of related to rhodopsin transmembrane chromoprotein bacteriorhodopsin (Henderson et al., 1990) having a similar structure, performing the functions of ATP-dependent translocase in the cell membranes of halophilic microorganisms pumped protons across the cytoplasmic membrane of the cell and is involved in the anaerobic photosynthetic phosphorylation (non-green synthesis), was determined as early as 1990. On the contrary the structure of rhodopsin remained unknown until 2003

(Palczewski et al., 2000). The opsin fragment of the rhodopsin molecule has 348 amino acid residues in a polypeptide chain that is formed by seven transmembrane α-helix segments situated across the membrane and joined with short non-helix sections (Ovchinnikov et al., 1983). The N-terminus of α-helix is located in the extracellular region, while the C-terminus – in the cytoplasmic region. The 11-*cis*-retinal residue is connected to one of the α-helixes, located near the middle of the membrane, so that its long axis is parallel to the membrane surface (Figure 2). It was also determined the dislocation of 11-*cis*-retinal aldimine bond with ε-amino group of Lys-296 residue located in the seventh α-helix. Thus, 11-*cis*-retinal is mounted in the center of a complex highly organized protein in the cellular membrane comprising rods. This structure provides a photochemical "adjustment" of retinal residue, affecting its absorption spectrum. The free 11-*cis*-retinal in a dissolved form has an absorption maximum in the ultraviolet region - at a wavelength of 380 nm, while rhodopsin absorbs green light at 500 nm (Hargrave et al., 1983). This shift in the wavelength of light is important from a functional point of view; it is aligned with the spectrum of light that enters the retina.

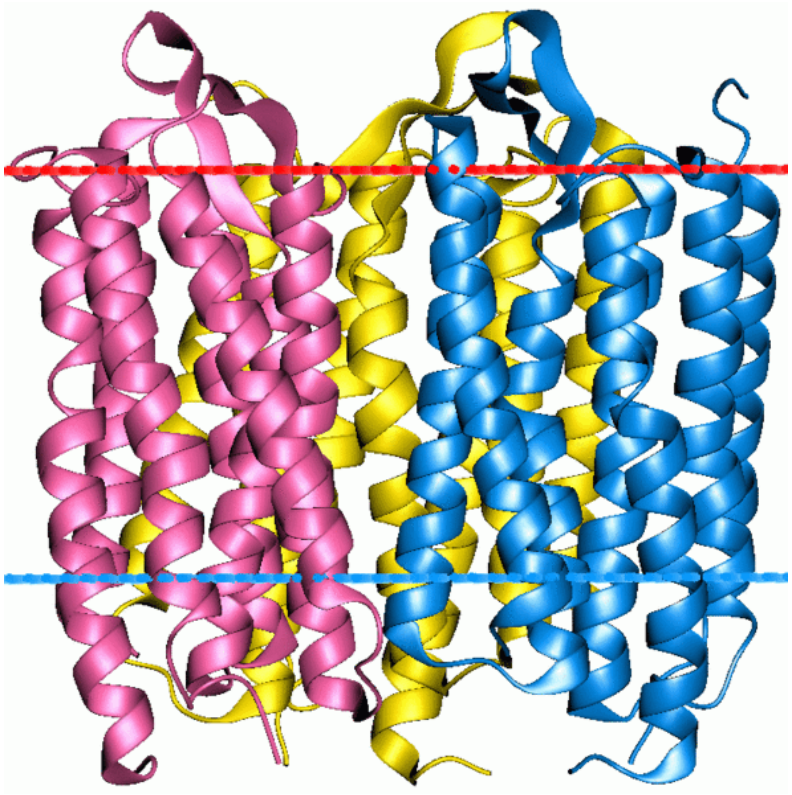

Fig. 2. The structure of rhodopsin according to computer modeling data

The absorption spectrum of rhodopsin is defined by properties of the chromophore - 11-*cis*-retinal residue and opsin fragment. This range in vertebrates has two characteristic peaks – one in the ultraviolet (278 nm) due to the opsin fragment, and the other – in the visible region (500 nm) corresponds to absorption of the chromophore (Fig. 3). Further transformation of rhodopsin under the action of light to the final stable product consists of a series of very fast intermediate stages. Investigating intermediates absorption spectra of rhodopsin in extracts at low temperatures at which these products are stable, allows to describe in the detail the photochemical changes of rhodopsin (Schertler, Hargrave, 1995).

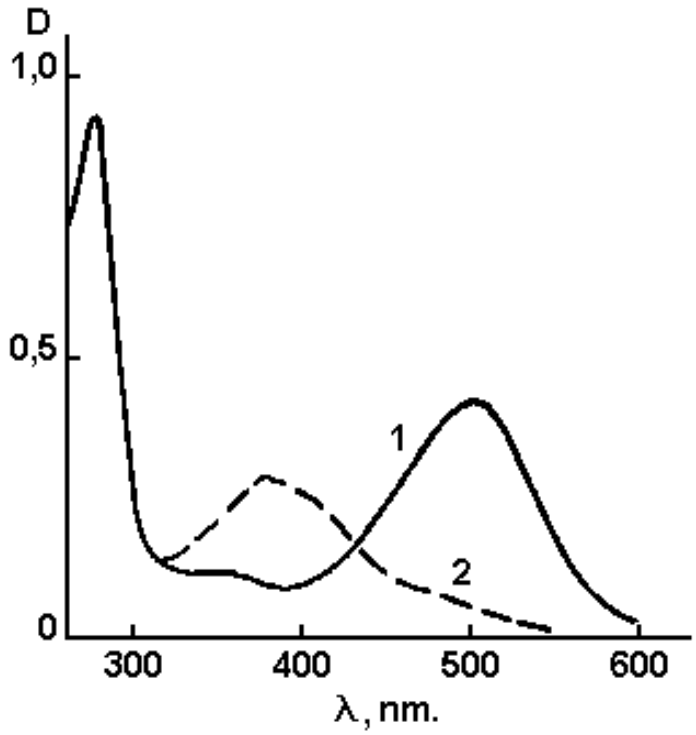

Fig. 3. Absorption spectrum of rhodopsin from the frog *Rana temporaria* (in water extract): 1 – rhodopsin (restored pigment); 2 – yellow indicator (discolored pigment)

Upon absorption of light photon it is occurred isomerization of 11-*cis*-retinal into 11-*trans*-retinal (quantum yield, 0.67), that induces a conformational change in the protein and activates photopsin and promotes its binding to G protein transducin, which triggers a second messenger cascade (Lipkin, 2001). Subsequent cycles of the photochemical reactions of rhodopsin lead to a local depolarization of the membrane and the stimulation of the nerve impulse propagates along the nerve fiber due to changes in ion transport in the photoreceptor (Figure 4). Subsequently rhodopsin restored (regenerated) with participation of retinal isomerase through steps: 11-*trans*-retinal → 11-*trans*-retinol → 11-*cis*-retinol → 11-*cis*-retinal, the latter is connected with opsin to form rhodopsin.

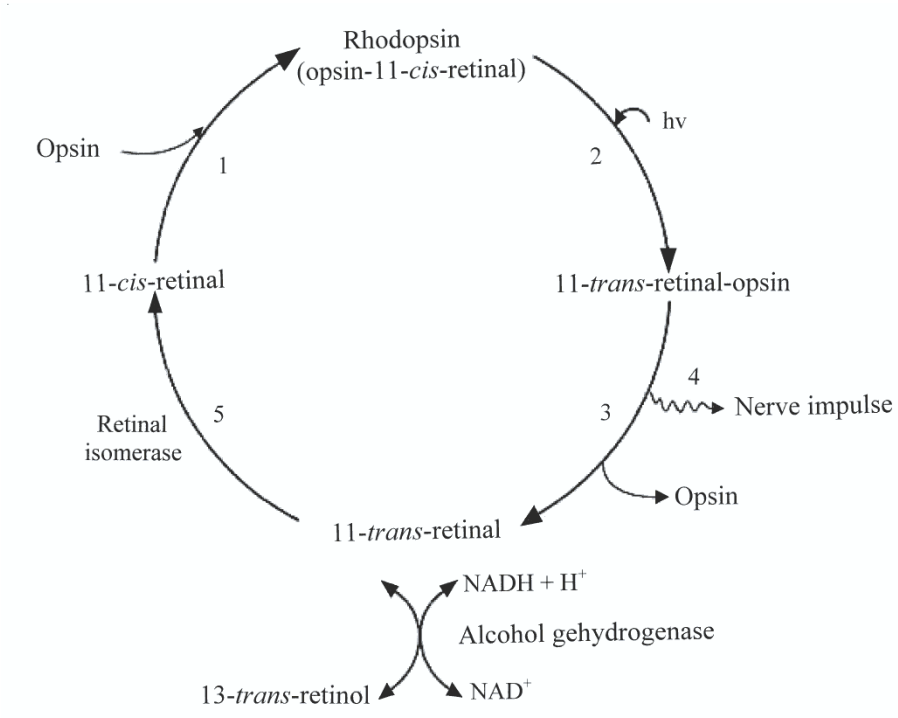

Fig. 4. Photocycle scheme of rhodopsin: 1 – 11-*cis*-retinal in the dark links with protein opsin to form rhodopsin; 2 – under light illumination occurs photoisomerization of 11-*cis*-retinal into 11-*trans*-retinal; 3 – 11-*trans*-retinal-opsin complex splits onto 11-*trans*-retinal and opsin; 4 – local depolarization of the membrane and the occurrence of a nerve impulse propagates along the nerve fiber; 5 – regeneration of the original pigment

3.3. Bacteriorhodopsin and its Applications

Bacteriorhodopsin (BR), named by analogy to the visual apparatus of mammalian chromoprotein rhodopsin, was isolated from the cell membrane of extreme photo-organo-heterotrophic halobacteria *Halobacterium halobium* in 1971 by D. Osterhelt and W. Stohenius (Oesterhelt, Stoeckenius, 1971). This photo-transforming trans-membrane chromo-protein with the molecular weight ~26.5 kDa is a chromoprotein determining the purple-red culour of halophilic bacteria, contained as chromophore group an equimolar mixture of 13-*cis*-and 13-*trans*-retinol C20-carotenoid, bound by Schiff base (as in the visual animal pigments) with Lys-216 residue of the protein.

In its structure and location in the cell membrane BR refers to integral transmembrane proteins, penetrating the cell membrane, which is divided into three fractions: yellow, red and purple. Purple fraction comprising on 75% (w/w) of cell membrane consists from carotenoids, phospholipids (mostly phosphoglycerol diesters with a small amount of nonpolar lipids and isoprenoids) forms a natural two-dimensional crystals which can be investigated using electron microscopy diffraction methods as X-ray scattering (Lanyi, 2004). These methods have established the existence in the BR molecule seven α-helical protein segments, while in the middle are symmetrically located a retinal residue (Figure 5).

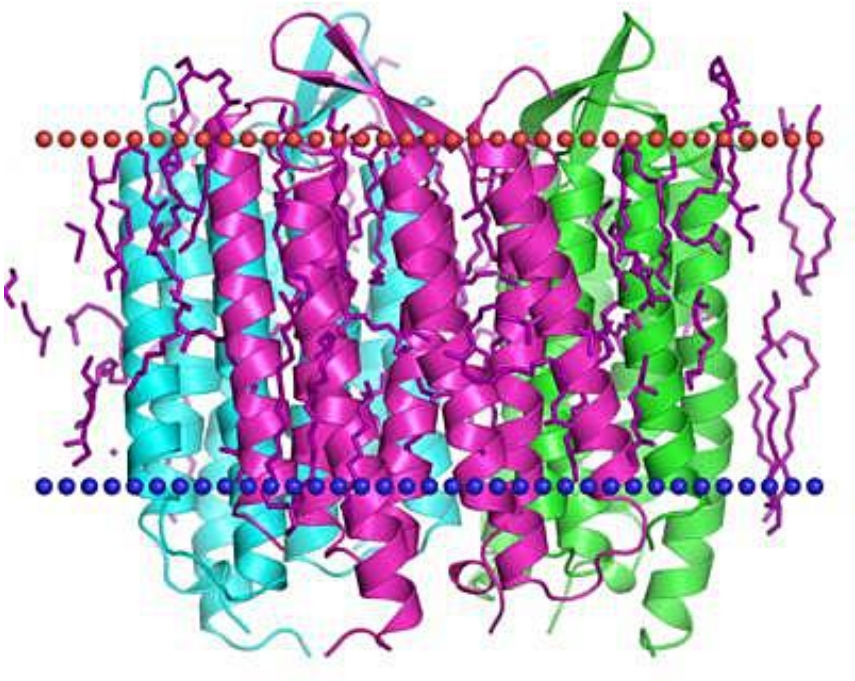

Fig. 5. The structure of BR from PM of halophilic bacterium *H. halobium* according to computer modeling data

Polypeptide chain of BR consists of 248 amino acid residues, 67 % of which are hydrophobic, formed with the aromatic amino acids, and 33 % – hydrophilic residues of aspartic and glutamic acids, arginine and lysine (Jap et al., 1983). These residues play important structural and functional role in the spatial orientation of the α-helical segments of the BR molecule, arranged in PM in an orderly manner forming trimers with an average diameter ~0.5 μm and a thickness 5–6 nm; each trimmer is surrounded by six others so that to form a regular hexagonal lattice (Nonella et al., 1991). The BR molecule arranged in a direction perpendicular to the plane of the membrane. Hydrophobic domains represent transmembrane segments and hydrophilic domains protruding from the membrane, connect the individual α-helical intramembranous segments of the BR molecules.

BR acts as a light-dependent proton pump, pumping protons across the cell membrane and generates an electrochemical gradient of H^+ on the surface of the cell membrane, which energy is used by the cell for the synthesis of ATP in the anaerobic photosynthetic phosphorylation. The mechanism of ATP synthesis is called “non-chlorophyll photosynthesis”, in contrast to the plant photosynthesis with the participation of chlorophyll. In this mechanism, at absorbtion of a light photon BR molecule became decolorized by entering into the cycle of photochemical reactions, resulting in the release of a proton to the outside of the membrane, and the absorption of proton from intracellular space. By the absorption of a light photon is occured reversible isomerization of 13-*tras*-BR (λ_{max} = 548 nm) (the quantum yield 0.03 at 20 °C) in the 13-*cis*-BR (λ_{max} = 568 nm) (Zimanyi *et al.*, 1993), initiating a cascade of photochemical reactions lasting from 3 ms to 1 ps with the formation of transitional intermediates J, K, L, M, N, and O, followed by separation of H^+ from the retinal residue of BR and its connection from the side of cytoplasm (Fig. 6). As a result, between the internal and external surface of the membrane forms a concentration gradient of H^+, which leads that illuminated halobacteria cells begin to synthesize ATP, i.e. convert light energy into energy of chemical bonds. This process is reversible and in the dark flows in the opposite direction. In this way the BR molecule behaves as a photochromic carrier

with a short relaxation time – the transition from the excited state to the ground state. Optical characteristics of BR vary depending on the method of preparation of PM and the polymer matrix.

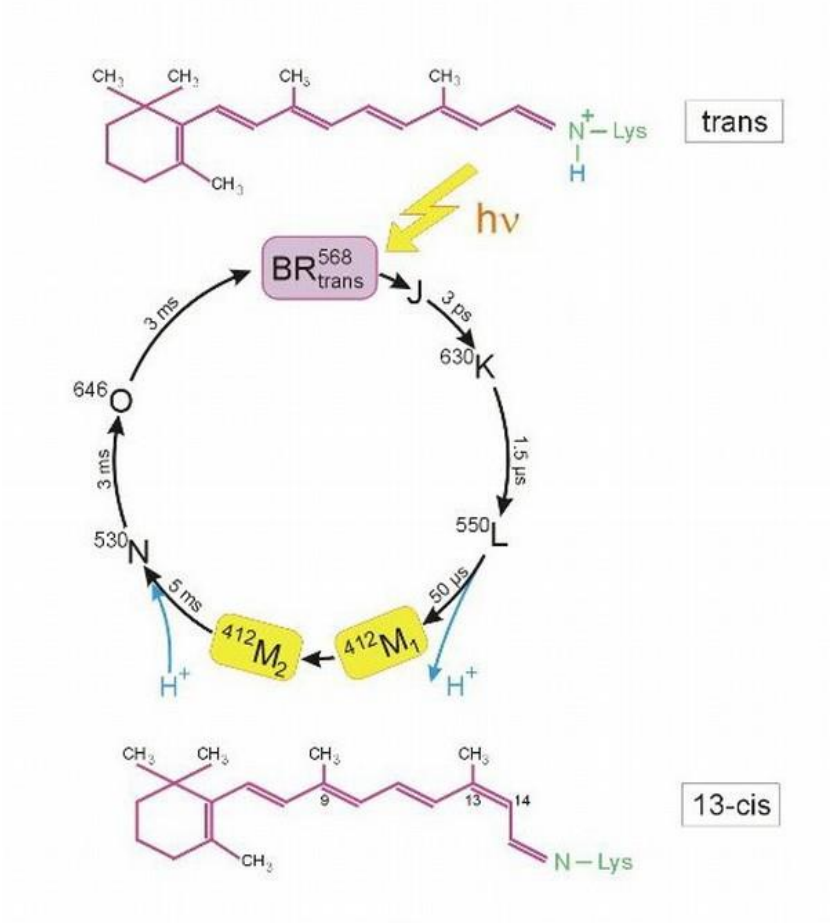

Fig. 6. Photocycle scheme of BR (aqueous solution, pH = 7.2, t = 20 °C). Latin numbers J, K, L, M, N, O denote the spectral intermediates of BR. M_1 and M_2 represent spectral intermediants of *meta*-bacteriorhodopsin with the protonated and deprotonated aldimine bond. The superscripts correspond to the position of the absorption maximum of the photocycle intermediates (nm)

BR is the focus of bio-and nanotechnology because of its high sensitivity and resolution, and is used in molecular bioelectronics as natural photochromic material for light-controlled electrical regulated computer modules and optical systems (Vought, Birge, 1999; Hampp, Oesterhelt, 2004). In addition, BR is very attractive as a model for studies related to the research of functional activity and structural properties of photo-transforming membrane proteins in the native and photo-converting membranes (Wang et al., 2008).

Nanofilms produced using the BR-containing purple membranes (PM) of halobacteria were first obtained and studied in this country in the framework of the project "Photochrome", when it was demonstrated effectiveness and prospects for the use of BR as photochromic material for holographic recording (Figure 7). The main task for the manufacture of BR-containing nanofilms is the orientation of PM between the hydrophobic and hydrophilic media. Typically, to improve the characteristics of the BR-containing films use multiple layers of PM that are applied to the surface of the polymeric carrier and dried up, preserving their natural structure. The best results are achieved in the manufacture of nanofilms based on gelatin matrix (Shuguang et al., 1993). This allows to achive high concentration of BR (up to 50 %) in nanofilms and avoid aggregation of membrane fragments and destruction of BR in the manufacturing process (Weetall, 1996). Embedded in a gelatin matrix PM fragments are durable (~10^4 h) and resistant to solar light, the effects of oxygen, temperatures greater than 80 °C (in water) and up to 140 °C (in air), pH = 1–12, and action of most proteases (Downie et al., 1998). Dried PM are stacked on top of each other, focusing in the plane of the matrix, so that a layer with 1 μm thickness contains about

200 monolayers (Korposh et al., 2005). When illuminated such nanofilms exert the electric potential 100–200 mV, which coincides with the membrane potential of living cells (Seitz, Hampp, 2000). These factors are of great practical importance for integration of PM into polymeric nanomatrix with keeping photochemical properties.

Technology for preparation of BR consists in growing of halobacteria on liquid synthetic growth media (with 15–20 % (w/w) NaCl) with amino acids, or on natural growth media with peptons – mixtures of polypeptides and amino acids derived from the partial hydrolysis product or powdered milk, animal meat by proteolytic enzymes (pepsin, trypsin, chymotrypsin), or protein-vitamin concentrate of yeast (Mosin et al., 1999). The subsequent isolation of BR from purple membranes is carried out by a combination of physical, chemical and enzymatic methods (Mosin et al., 2013). Under optimal growing conditions (incubation period 4–5 days, temperature 35 °C, illumination with monochromatic light at λ = 560 nm) in cells are synthesized the purple carotenoid pigment, characterized as BR by the spectral ratio of protein and chromophore fragments D_{280}/D_{568} = 1.5:1.0 in the molecule.

Within the framework of the research we described an effective method for isolation of BR from PM of photo-organo-heterotrophic halobacterium *H. halobium* consisted by cellular autolysis by distilled water, processing of bacterial biomass by ultrasound at 22 KHz, llocation of PM fraction, purification of PM from low and high-molecular weight impurities, cellular RNA, carotenoids and lipids, PM solubilization in 0.5 % (w/v) solution of the ionic detergent SDS-Na to form a microemulsion with the subsequent fractionation of the protein by methanol (Mosin, Ignatov, 2013a). The protein is localized in the PM; the release of low molecular weight impurities and intracellular contents is reached by osmotic shock of cells with distilled water in the cold after the removal of 4.3 M NaCl and the subsequent destruction of the cell membrane by ultrasound at 22 kHz. For the destruction of cellular RNA the cellular homogenate was treated with Rnase I. Fraction PM along with the desired protein in a complex with lipids and polysaccharides also contained impurity of related carotenoids and proteins. Therefore, it was necessary to use special methods of fractionation of the protein without damaging its native structure and dissociation.

BR being a transmembrane protein intricately penetrates bilipid layer in form of seven α-helices; the use of ammonium sulfate and other conventional agents to salting out did not give a positive result for isolation of the protein. The resolving was in the translation of the protein to a soluble form by the colloidal dissolution (solubilization) in an ionic detergent. Using as the ionic detergent SDS-Na was dictated by the need of solubilization of the protein in a native, biologically active form in complex with 13-*trans*-retinal, because BR solubilized in 0.5% (v/v) SDS-Na retains a native α-helical configuration (Mosin, Ignatov, 2013b). Therefore, there is no need the use organic solvents as acetone, methanol and chloroform for purification of lipids and protein, and precipitation and delipidization is combined in a single step, which significantly simplifies the further fractionation. A significant advantage of this method is that the isolated protein in complex with lipids and detergent molecules was distributed in the supernatant, and other high molecular weight impurities – in unreacted precipitate, easily separated by centrifugation. Fractionation of solubilized in 0.5 % (w/v) SDS-Na protein and its subsequent isolation in crystalline form was achieved at 4 °C in three steps precipitating procedure with methanol, reducing the concentration of detergent from 0.5, 0.25 and 0.1 % (w/v) respectively. The final stage of BR purification involved the separation of the protein from low-molecular-weight impurities by gel-permeation chromatography on dextran Sephadex G-200 Column balanced with 0.09 M Tris-borate buffer (pH = 8.35) with 0.1% (w/v) SDS-Na and 2.5 mM EDTA (output of the protein 8–10 mg).

Absorption spectrum of PM purified from carotenoids (4) and (5) (chromatographic purity 80–85 %) is shown in Figure 7 at various processing stages (*b*) and (*c*) relative to the native BR (*a*). Formation of retinal-protein complex in the BR molecule leads to a bathochromic shift in the absorption spectrum of PM (Fig. 7c) – the main band with (1) with the absorption maximum at λ = 568 nm caused by the light isomerization of the chromophore by the C13=C14 bond is determined by the presence of 13-*trans*-retinal residue in BR^{568}; additional low-intensity band with (2) at λ = 412 nm characterizes a minor impurity of a spectral form of *meta*-bacteriorhodopsin (M^{412}) (formed in the light) with deprotonated aldimine bond between 13-*trans*-retinal residue and protein; the total bandwith (3) with λ = 280 nm is determined by the absorption of aromatic amino acids in the polypeptide chain of the protein (for native BR D_{280}/D_{568} = 1.5 : 1.0).

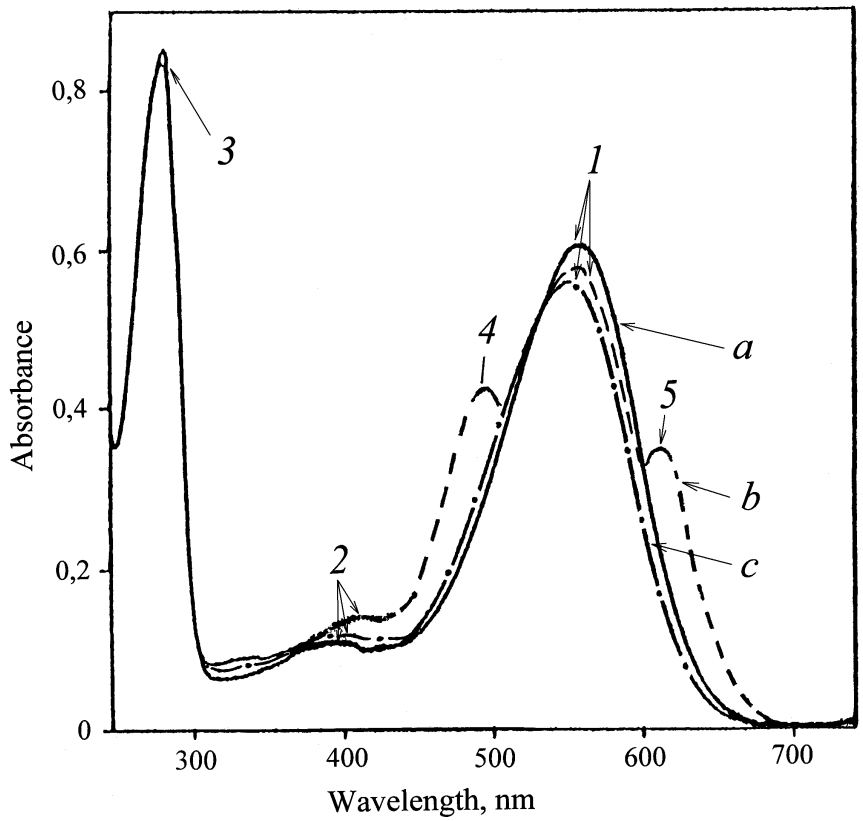

Fig. 7. The absorption spectra of the PM (50% (v/v) ethanol) at various stages of processing: (*a*) – natural BR; (*b*) – PM after intermediate treatment; (*c*) – PM purified from carotenoids. The bandwith (1) is the spectral form of BR^{568}, (2) – impurity of spectral form of *meta*-bacteriorhodopsin (M^{412}), (3) – the total absorption bandwith of aromatic amino acids, (4) and (5) – extraneous carotenoids. As a control used the native BR

3.4. Iodopsin

Iodopsin is a violet, light-sensitive pigment of the retinal cone cells, responsible for color vision, and close analogue of rhodopsin. This pigment consists of a protein photopsin linked with a chromophore, retinal residue. According to the three-component theory of vision, it is believed that there have to be three types of this pigment and accordingly three types of cones that are sensitive to blue, green and red light. Iodopsin consists of three pigments – hlorolab, eritrolab and tsianolab. With the densitometry method W. Rushton studied the coefficient of light absorption in the photo layers of the retina with different wavelengths (Rushton, 1958). The hlorolab pigment absorbs the rays corresponding to yellow-green (450–630 nm absorption band), the eritrolab – yellow and red (500-700 nm), and the tsianolab – blue-green (500–700 nm) parts of the visible spectrum (Wyszecki, Stiles, 1982). Not yet been found and the different types of cones.

3.5. The Mechanism of Color Vision

The retina has three types of cone cells – S, M and L cells, having a different sensitivity to different parts of the visible range of the spectrum (Figure 8). The cone cells of S type have a spectral range from 400 to 500 nm with a maximum peak at 420–440 nm, the cone cells of M type – from 450 to 630 nm with a maximum peak at 534–555 nm, while the cone cells of L type – from 500 nm to 700 nm with a maximum peak at 564–580 nm. As the curves of the sensitivity of the cone cells overlap, it is impossible for monochromatic light to stimulate only one type of cone cells. The other types of cone cells react though to a lesser degree. The set of all possible values of the color combinations causing a visual reaction determines the human color space. Human brain generally can discern approximately 10 million of different colors.

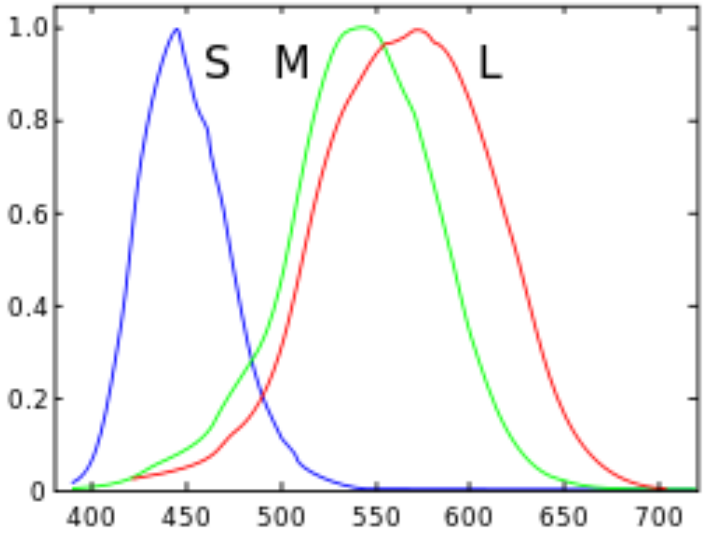

Fig. 8. Spectral sensitivity of the different types of receptor cells (cones) in the retina

The electromagnetic waves spectrum stimulates the different types of cone cells from the three types S, L and M to a different degree. The red light stimulates the L cone cells more than the M cone cells. The blue light stimulates the S cone cells in the strongest way. The yellow-green light provides a strong stimulation to the L and M cone cells, and a weaker stimulation to the S cone cells. The brain then combines the information from all types of cone cells for different wavelengths and analyzes them as different colors.

3.6. Studying of Additive Mixing of Colors

The analyses for the activity of the three types of cones – S, L and M in the perception of colors also show how the brain "deciphers" the colors. The foundation of this analysis, shown in Figure 9, was made by M. Marinov and I. Ignatov in 2008 (Marinov, Ignatov, 2008). However, it is not clear whether the green color we perceive is a combined effect of yellow and blue, or whether it corresponds to a wavelength of the green color from the visible spectrum. Our brain can register the colors, i.e. the green color as a spectrometer, with certain lengths of the electromagnetic waves. It can also register the green color as a mixture of yellow and blue. The full perception of colors by the visual analyzer cannot be defined by a spectrometer (Hunt, 2004).

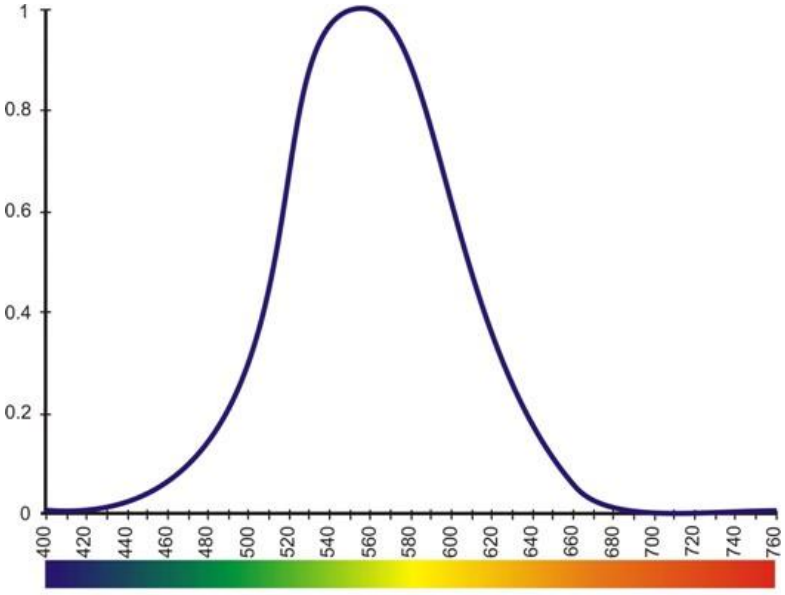

Fig. 9. Spectral sensitivity of the visual analyzer

As an example in the mixing of electromagnetic waves that correspond to green and red color, yellow color is obtained. In the mixing of green and red, no medium color is obtained; the brain therefore perceives it as yellow color (Ignatov, Mosin, 2013). When there is an emission of electromagnetic waves that correspond to green and red color, the brain adopts an "average decision" – yellow (Figure 10a). Analogously, for the yellow and blue color, the brain adopts an "average decision" – green. This means that a spectral mixing of colors is observed between the blue-yellow and green-red pairs (Ignatov, Marinov, 2008). In its turn, green and blue color is perceived as cyan. Vision sensitivity is at its lowest for the violet, blue and red color. The mixing of electromagnetic waves that correspond to blue and red color is perceived as violet. In the mixing of electromagnetic waves that correspond to more colors, the brain does not perceive them as separate or average, but as a white color. Thus the notion of color is not determined solely by the wavelength. The analysis is performed by brain, and the notion of color is at its essence a product of our consciousness.

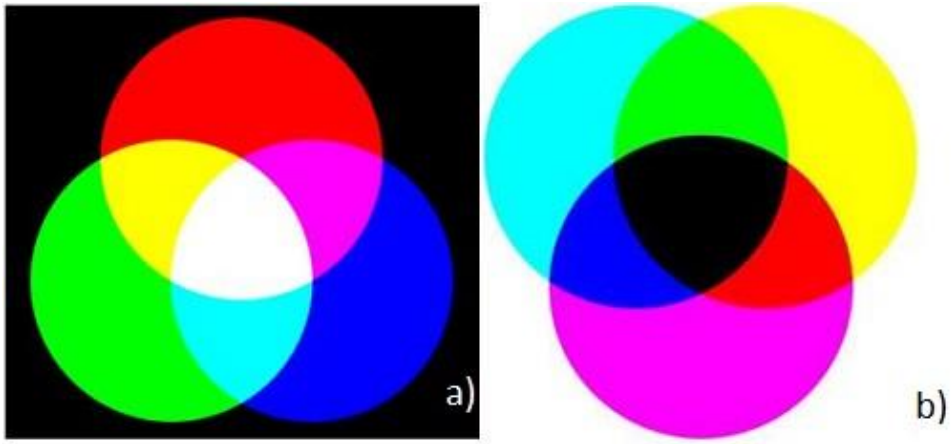

Figure 10 a, b. Additive mixing of colors

The authors have practice with improvement of vision functions with aronia, blueberry, VITA intense and catholyte water.

4. Conclusion

The mechanism of color perception by the visual analyzer have been carried out by the authors using photoreceptive chromo-protein rhodopsin as a model. A further research into the function of rhodopsin and other retina affiliated chromo-proteins as iodopsin will allow investigate in detail the mechanism of visual perception of light for better treatment of functional eye diseases in ophthalmology. It should be noted that rhodopsin up till now remains to be the most studied model chromoprotein of all GPCR-receptor family. This allowed us to better analyze the functional properties of another analogous trans membrane bacterial chromoprotein – bacteriorhodopsin isolated from purple membrane of halobacterium *H. halobium* in semi-preparative quantities, and study its application in nanotechnologies.

Within the framework of the research the mechanism of color perception by the visual analyzer having the ability to analyze certain ranges of the optical spectrum, as colors was studied along with an analysis of the additive mixing of two colors. It was shown that at the mixing of electromagnetic waves with different wavelengths, the visual analyzer perceive them as separate or average wave length corresponding to mix colors.

5. Acknowledgements

The authors wish to thank Vitaly Shvetz, Dmitry Skladnev and Parashkeva Tzaneva for their cooperation in the research. Also authors would like to commemorate the memory of Prof. Marin Marinov (1928–2009) – the initiator of the research of color vision in Bulgaria.

References

Downie et al., 1998 – *Downie, J., Timucin, D.A., Smithey, D.T., Crew, M.* (1998). Long Holographic Lifetimes in Bacteriorhodopsin Films, *Optics Letters*, 23(9), 730–732.

Gluhchev et al., 2015 – *Gluhchev, G., Ignatov, I., Karadzhov, S., Miloshev, G., Ivanov, I., Mosin, O.V.* (2015). Biocidal Effects of Electrochemically Activated Water, *Journal of Health, Medicine and Nursing*, 11, 67-83.

Gluhchev et al., 2015a – *Gluhchev, G., Ignatov, I., Karadzhov, S., Miloshev, G., Ivanov, I., Mosin, O.V.* (2015). Electrochemically Activated Water. Biophysical and Biological Effects of Anolyte and Catholyte as Types of Water, *Journal of Medicine, Physiology and Biophysics*, 10, 1-17.

Gluhchev et al., 2015b – *Gluhchev, G., Ignatov, I., Karadzhov, S., Miloshev, G., Ivanov, N., Mosin, O.V.* (2015). Electrochemically Activited Water: Biophysical and Biological Effects of Anolyte and Catholyte Types of Water, *European Journal of Molecular Biotechnology*,1, 12-26.

Gluhchev et al., 2015c – Gluhchev, G., Ignatov, I., Karadzhov, S., Miloshev, G., Ivanov, N., Mosin, O.V. (2015). Studying the Antimicrobial and Antiviral Effects of Electrochemically Activated Nacl Solutions of Anolyte and Catholyte on a Strain of E. Coli DH5 and Classical Swine Fever (CSF) Virus, *European Journal of Medicine*, 9 (3), 124-138.

Hampp, Oesterhelt, 2004 – *Hampp, N., Oesterhelt, D.* (2004). Bacteriorhodopsin and its Potential in Technical Applications. *Nanobiotechnology*, Ch. Niemeyer, C. Mirkin (eds.). Weinheim: Wiley-VCH-Verlag, 167.

Hargrave et al., 1983 – *Hargrave, P.A., McDowell, J.H., Curtis, D.R. et al.* (1983). The structure of bovine rhodopsin, *Biophys. Struct. Mech.*, 9, 235–244.

Henderson et al., 1990 – *Henderson, R., Baldwin, J., Ceska, T. et al.* (1990). Model for the Structure of Bacteriorhodopsin based on high-resolution electron cryo-microscopy, *J. Mol. Biol.*, 213(4), 899–929.

Hogan et al., 1971 – *Hogan, M. J., Alvarado, J. A.,Weddell, J. E.* (1971). Histology of the Human Eye, *Philadelphia: WB Saunders Co.*, 115.

Hubel, 1995 – *H*ubel, D. (1995). Eye, Brain and Vision**,** *Scientific American Library Series (Book 22), 2nd edition, New York: W.H. Freeman Publ.*, 256.

Hunt, 2004 – *Hunt, R.W.G.* (2004). The Reproduction of Colour (6th ed.), *Chichester: Wiley–IS&T Series in Imaging Science and Technology*, 724.

Ignatov et al., 2014 – *Ignatov, I., Karadzhov, S., Atanasov, A., Ivanova, E., Mosin, O.V.* (2014). Electrochemical Aqueous Sodium Chloride Solution (Anolyte and Catholyte) as Types of Water. Mathematical Models. Study of Effects of Anolyte on the Virus of Classical Swine Fever Virus, *Journal of Health, Medicine and Nursing*, 8, 1-28.

Ignatov et al., 2015 – *Ignatov, I, Gluhchev, G., Karadzhov, S., Ivanov, N., Mosin, O.V.* (2015).Preparation of Electrochemically Activated Water Solutions (Catholyte/Anolyte) and Studying Their Physical-Chemical Properties, *Journal of Medicine, Physiology and Biophysics*, 16, 1-14.

Ignatov et al., 2015 – *Ignatov, I., Gluhchev, G., Karadzhov, S., Miloshev, G., Ivanov, I., Mosin, O.V.* (2015). Preparation of Electrochemically Activated Water Solutions (Catholyte/Anolyte) and Studying of their Physical-Chemical Properties, *Journal of Health, Medicine and Nursing*, 13, 64-78.

Ignatov et al., 2015 – *Ignatov, I., Mosin, O. V. , Gluhchev, G., Karadzhov, S., Miloshev, G., Ivanov, I.* (2015). Studying Electrochemically Activated NaCl Solutions of Anolyte and Catholyte by Methods of Non-Equilibrium Energy Spectrum (NES) and Differential Non-Equilibrium Energy Spectrum (DNES), *Journal of Medicine, Physiology and Biophysics*, 14, 6-18.

Ignatov et al., 2015 – *Ignatov, I., Gluhchev, G., Karadzhov, S., Miloshev, G., Ivanov, I., Mosin, O.V.* (2015). Preparation of Electrochemically Activated Water Solutions (Catholyte/Anolyte) and Studying Their Physical-Chemical Properties, *Journal of Medicine, Physiology and Biophysics*, 11, pp. 1-21.

Ignatov et al., 2015 – *Ignatov, I., Gluhchev, G., Karadzhov, S., Miloshev, G., Ivanov, I., Mosin, O.V.* (2015). Preparation of Electrochemically Activated Water Solutions (Catholyte/Anolyte) and Studying of their Physical-Chemical Properties, *Journal of Medicine, Physiology and Biophysics*, 13, 18-38.

Ignatov et al., 2015 –*Ignatov, I., Mosin, O.V., Gluhchev, G., Karadzhov, S., Miloshev, G., Ivanov, N.* (2015). The Evaluation of Mathematical Model of Interaction of Electrochemically Activated Water Solutions (Anolyte and Catholyte) with Water, *European Reviews of Chemical Research*, 2 (4|),72-86.

Ignatov et al., 2016 –*Ignatov, I., Mosin, O.V., Gluhchev, G., Karadzhov, S., Miloshev, G., Ivanov, I.* (2016). Studying Electrochemically Activated NaCl Solutions of Anolyte and Catholyte by

Methods of Non-Equilibrium Energy Spectrum (NES) and Differential Non-Equilibrium Energy Spectrum (DNES), *Journal of Medicine, Physiology and Biophysics*, 20, 13-23.

Ignatov, 2016 – *Ignatov, I.* (2016). VITA intense – Proofs for Anti-inflammatory, Antioxidant and Inhibition Growth of Tumor Cells Effects. Relaxing Effect of Nervous System, Anti Aging Influence, *Journal of Medicine, Physiology and Biophysics*, 27, 43-61.

Ignatov, Pesheva, 2018 – *Ignatov, I., Pesheva, Y.* (2018). VITA Intense – Product with Negative Oxidation-reduction Potential (ORP) as Important Quality for Antioxidant and Inhibition Growth of Tumor Cells Effects. Anti Aging Effects, *European Journal of Medicine*, 6(1): 20-42.

Ignatov, Mosin, 2014 – *Ignatov, I., Mosin, O.V.* (2014). Electromagnetic Conception for the Eyesight in Additive Mixing of Colors, Colors, *Journal of Health, Medicine and Nursing*, 10, 65-83.

Ignatov, Mosin, 2014 – *Ignatov, I., Mosin, O.V.* (2014). Photoreceptors in Visual Perception and Additive Color Mixing. Bacteriorhodopsin in Nano- and Biotechnologies, *Advances in Physics Theories and Applications*, 27, 20-37.

Ignatov, Marinov, 2008 – *Ignatov, I., Marinov, M.* (2008). Color (Kirlian) Spectral Analysis. Color Observation with Visual Analyzer, *Euromedica*, 32.

Ignatov, Mosin, 2014 – *Ignatov, I., Mosin, O.V.* (2014). Visual Perception and Electromagnetic Conception for the Eyesight. Rhodopsin and Bacteriorhodopsin in Nano- and Biotechnologies, *Journal of Health, Medicine and Nursing*, 4, 1-20.

Ignatov, Mosin, 2013 – *Ignatov, I., Mosin, O.V.* (2013). Process of Perception of Light and Evolution of Sight at the Higher Animals and Humans. *Naukovedenie*, 3, 1–19. [in Russian]

Ignatov, Mosin, 2015 – *Ignatov, I., Mosin,O.V.* (2015). Physiology of Rhodopsin and Iodopsin. Electromagnetic Conception for the Eyesight in Additive Colors, *Journal of Health, Medicine and Nursing*, 9, 15-33.

Ignatov, Mosin, 2014 – *Ignatov, I., Mosin,O.V.* (2014). Studying of Phototransformans of Light Signal by Photoreceptor Pigments – Rhodopsin, Iodopsin and Bacteriorhopsin and Additive Mixing of Colors, *Journal of Medicine, Physiology and Biophysics*, 3, 30-47.

Ignatov, Mosin, 2014 – *Ignatov, I., Mosin, O.V.* (2014). Visual Perception. Electromagnetic Conception for the Eyesight. Rhodopsin and Bacteriodopsin, *Journal of Medicine, Physiology and Biophysics*, 2, 1-19.

Ignatovet al., 2016 – *Ignatov, I., Mosin, O.V., Kirov, P.* (2016). Matematical Model of Kangen Water® Biophysical and Biochemical Effects of Catholyte, *Advances in Physics Theories and Applications*, 51, 33-55.

Jap, et al., 1983 – *Jap, B.K., Maestre M.F., Hayward, S.B., Glaeser, R.M.* (1983). Peptide-chain Secondary Structure of Bacteriorhodopsin, *Biophys J.*, 43(1), 81–89.

Korposh et al., 2005 – *Korposh, S.O., Sichka, M.Y., Trikur, I.I. et al.* (2005). Films Based on Bacteriorhodopsin in Sol-gel Matrices, *Proc. of SPIE*, 5956, Paper Number 595616, 312–320.

Lanyi, 2004 – *Lanyi, J.K.* (2004). X-ray Diffraction of Bacteriorhodopsin Photocycle Intermediates, *Molecular Membrane Biology*, 21(3), 143–150.

Liang et al., 2004 – *Liang, Y., Fotiadis, D., Maeda, T. et al.* (2004). Rhodopsin Signaling and Organization in Heterozygote Rhodopsin Knockout Mice. *J. Biol. Chem.*, 279, 48189–48196.

Lipkin, 2001 – *Lipkin, V.M.* (2001). Visual System. Mechanisms of Transmission and Amplification of the Visual Signal in Eye Retina, *Soros Educational Journal*, 7(9), 2–8. [in Russian]

Mosin et al., 1999 – *Mosin, O.V , Skladnev, D.A., Shvets, V.I.* (1999). The Inclusion of Deuterated Aromatic Amino Acids in the Molecule of Bacteriorhodopsin *Halobacterium halobium*, *Applied Biochemistry and Microbiology*, 35(1), 34–42.

Mosin, Ignatov, 2013a – Mosin, O.V., Ignatov, I. (2013). The Photo-transforming Photochrome protein Bacteriorhodopsin derived from Photoorganoheterotrophic halobacterium *Halobacterium halobium*. *Nanoengineering*, 1, 14–21. [in Russian]

Mosin, Ignatov, 2013b – *Mosin, O.V., Ignatov, I.* (2013). The Natural Photo-transforming Photochrome Transmembrane Protein Nanomaterial Bacteriorhodopsin from Purple Membranes of Halobacterium *Halobacterium halobium*, *Journal of Nano and Microsystem Technique*, 7, 47–54. [in Russian]

Mosin et al., 2013 – *Mosin, O.V., Shvez, V.I., Skladnev, D.A., Ignatov, I.* (2013). Biosynthesis of Transmembrane Photo transforming Protein Bacteriorhodopsin Labeled with Deuterium on Residues of Aromatic Acids [2,3,4,5,6-$^{2}H_5$]Phe, [3,5-$^{2}H_2$]Tyr and [2,4,5,6,7-$^{2}H_5$]. *Nauchnoe priborostroenie*, 23(2), 14–26. [in Russian]

Nathans et al., 1986 – *Nathans, J., Thomas, D., Hogness, D.S. (1986) Molecular Genetics of Human Color Vision: the Genes Encoding Blue, Green, and Red Pigments. Science, 232(47), 193–202.*

Neugebauer et al., 1978 – *Neugebauer, D.Ch., Zingsheim, H.P., Oesterhelt, D.* (1978). Recrystallization of the Purple Membrane *in vivo* and *in vitro*, *Journal Molecular Biology*, 123, 247–257.

Nonella et al., 1991 – *Nonella, M., Windemuth, A., Schulten K.* (1991). Structure of Bacteriorhodopsin and *in situ* Isomerization of Retinal: A Molecular Dynamics Study, *Journal Photochem. Photobiol.*, 54(6), 937–948.

Oesterhelt, Stoeckenius, 1971 – *Oesterhelt, D., Stoeckenius, W.* (1971). Rhodopsin – like Protein from the Purple Membrane of *Halobacterium halobium*, *Nature*, 233(89), 149–160.

Ovchinnikov et al., 1983 – *Ovchinnikov, Yu.A., Abdulaev, N.G., Feigina, M.Yu., Artamonov, I.D., Bogachuk, A.S.* (1983). Visual rhodopsin: Whole amino acid sequence and topology in membrane. *Bioorganic. chemistry*, 10, 1331–1340.

Palczewski, 2006 – *Palczewski, K.* (2006). G-protein-coupled Receptor Rhodopsin. *Annu. Rev. Biochem.*, 75, 743–767.

Palczewski et al., 2000 – *Palczewski, K., Kumasaka, T., Hori, T. et al.* (2000). Crystal Structure of Rhodopsin: a G-protein-coupled Receptor. *Science*, 289, 739–745.

Rudiger et al., 1997 – *Rudiger, M., Tittor, J., Gerwert, K., Oesterhelt, D.* (1997). Reconstitution of Bacteriorhodopsin from the Apoprotein and Retinal Studied by Fourier-transformed Infrared Spectroscopy, *Biochemistry*, **36**, 4867–4874.

Rushton, 1958 – *Rushton, W.A.H.* (1958). In: *Visual problems of colour*. N.P.L. Sump. (Ed.) London: Her Majesty's Stationary Office, 1, 71–101.

Schertler, Hargrave, 1995 – *Schertler, G.F., Hargrave, P.A.* (1995) Projection Structure of Frog Rhodopsin in Two Crystal Forms, *Proc. Natl. Acad. Sci. U.S.A.*, 92, 11578–11582.

Seitz, Hampp, 2000 – *Seitz, A., Hampp, N.* (2000). Kinetic Optimization of Bacteriorhodopsin Films for Holographic Interferometry. *J. Phys. Chem. B*, *104*(30), 7183–7192.

Shuguang et al., 1993 – *Shuguang, W.U., Ellerby, L.M., Cohan, J.S. et al.* (1993). Bacteriorhodopsin Encapsulated in Transparent sol-gel Glass: a New Biomaterial, *Chem. Mater*, 5, 115–120.

Vought, Birge, 1999 – *Vought, B.W., Birge, R.R.* (Eds.) (1999). Molecular Electronics and Hybrid Computers. in: *Wiley Encyclopedia of Electrical and Electronics Engineering*. NY: Wiley-Interscience, 490.

Wang et al., 2008 – *Wang, W.W., Knopf, G.K., Bassi, A.S.* (2008). Bioelectronic Imaging Array Based on Bacteriorhodopsin film. *IEEE Transactions on Nanobiosciences,* 7(4), 249–256.

Water Electrolysis-Processes in Catholyte and Anolyte Results with Differential Non-Equilibrium Water Spectrum, *European Journal of Medicine*, 6(1): 3-12.

Weetall, 1996 – *Weetall, H.* (1996). Retention of Bacteriorhodopsin Activity in Dried Sol-gel Glass, *Biosensors, Bioelectronics*, 11, 325–333.

Wyszecki et al., 1982 – Wyszecki, G., Stiles, W.S. (1982). *Color Science: Concepts and Methods, Quantitative Data and Formulae* (2nd ed.). New York: Wiley–IS&T Series in Pure and Applied Optics, 935.

Zimanyi et al., 1993 – *Zimanyi, L., Cao, Y., Needleman, R., Ottolenghi, M., Lanyi J.K.* (1993). Pathway of Poton Uptake in the Bacteriorhodopsin photocycle, *Biochemistry*, 32, 7669–7678.

Published in the Slovak Republic
European Journal of Molecular Biotechnology
Has been issued since 2013.
E-ISSN: 2409-1332
2018, 6(1): 41-52

DOI: 10.13187/ejmb.2018.1.41
www.ejournal8.com

ZEOLITH Detox for Detoxification of Human Body. Proofs for Anti Inflammatory Effects of Zeolite and Detoxification

Ignat Ignatov [a, *], Yuliana Pesheva [a]

[a] Scientific Research Center of Medical Biophysics, Sofia, Bulgaria

Abstract

We studied the mathematical model of interaction with water of natural mineral and microporous crystalline mineral ZEOLITH detox of LavaVitae Company (Austria). In this report are submitted data about the interaction of ZEOLITH detox with water, obtained by non-equilibrium (NES) and differential-equilibrium energy spectrum (DNES) of water. The average energy ($\Delta E_{H...O}$) of hydrogen H...O-bonds among individual molecules H_2O after treatment of ZEOLITH detox with water measured by NES- and DNES-methods is ΔE=-0.0034±0.0011 eV for ZEOLITH detox. The average energy ($\Delta E_{H...O}$) of hydrogen H...O-bonds among individual molecules H_2O after treatment of ZEOLITH detox with water measured by NES- and DNES-methods is ΔE=-0.0034±0.0011 eV for ZEOLITH detox. The average energy ($\Delta E_{H...O}$) of hydrogen H...O-bonds among individual molecules H_2O after treatment of ZEOLITH detox with water measured by NES- and DNES-methods. These results suggest the restructuring of $\Delta E_{H...O}$ values among H_2O molecules with a statistically reliable increase of local extremums in DNES-spectra. The research is performed for ZEOLITH detox with study of pH and oxidative reduction potential (ORP).

The report shows the effects of zeolite for the detoxification of human body. The inflammations are one of the basic reasons for aging process. In this research we show anti inflammatory effects from ZEOLITH detox.

Keywords: ZEOLITH detox, anti inflammatory effects, detoxification, mathematical model, NES, DNES.

1. Introduction

The ZEOLITH detox is mineral refers to new generation of natural mineral sorbents (NMS). Zeolites are the alumosilicate members of the family of microporous solids known as "molecular sieves", named by their ability to selectively sort molecules based primarily on a size exclusion process. Natural zeolites form when volcanic rocks and ash layers react with alkaline groundwater. Zeolites also crystallize in post-depositional environments over periods ranging from thousands to millions of years in shallow marine basins. Naturally occurring zeolites are rarely pure and are contaminated to varying degrees by other minerals, metals, quarts, or other zeolites. For this reason, naturally occurring zeolites are excluded from many important commercial applications where uniformity and purity are essentials.

As natural mineral zeolite has unusually broad scope of application in industry. Adsorption, catalytic, and reduction-oxidation Zeolites is widely used in industry as a desiccant of gases and liquids, for treatment of drinking and sewage water from heavy metals, ammonia, phosphorus, as

* Corresponding author
E-mail addresses: mbioph@dir.bg (I. Ignatov)

catalyst in petrochemical industry for benzene extraction, for production of detergents and for extracting of radionuclides in nuclear reprocessing. It is also used in medicine as nutritional supplements having antioxidant properties. Some authors make qualifications of zeolites as nano materials.

A wide range of properties of zeolite defines the search for new areas of industrial application of these minerals in science and nano technology that contributes to a deeper study the mechanism of interaction of these minerals with water. The company LavaVitae produces ZEOLITH detox with results for detoxification. This paper deals with evaluating of mathematical models of interaction of ZEOLITH detox with water with proofs for anti inflammatory effects and inhibition of development of tumor cells.

2. Materials and Methods

2.1. Materials

The study is performed with samples of ZEOLITH detox from LavaVitae Company (Austria).

There are valid the following methods for research of zeolite.

2.2. Analytical Methods

The analytical methods were accredited by the Institute of Geology of Ore Deposits. Petrography, Mineralogy, and Geochemistry (Russian Academy of Sciences). Samples were treated by various methods as ICP-OES, GC, and SEM.

2.3. Gas-Chromatography

Gas-chromatography (GC) is performed at Main Testing Centre of Drinking Water (Moscow, the Russian Federation) on Kristall 4000 LUX M using Chromaton AW-DMCS and Inerton-DMCS columns (stationary phases 5 % SE-30 and 5 % OV-17), equipped with flame ionization detector (FID) and using helium (He) as a carrier gas.

2.4. Inductively Coupled Plasma Optical Emission Spectrometry (ICP-OES)

The mineral composition is studied by inductively coupled plasma optical emission spectrometry (ICP-OES) on Agilent ICP 710-OES (Agilent Technologies, USA) spectrometer, equipped with plasma atomizer (under argon stream), MegaPixel CCD detector, and 40 MHz free-running, air-cooled RF generator, and Computer-optimized exhale system: the spectral range at 167–785 nm; plasma gas: 0–22.5 l/min in 1.5 l/min; power output: 700–1500 W in 50 W increments.

2.5. Transmission Electron Microscopy (TEM)

The structural studies were carried out with using JSM 35 CF (JEOL Ltd., Korea) device, equiped with X-ray microanalyzer "Tracor Northern TN", SE detector, thermomolecular pump, and tungsten electron gun (Harpin type W filament, DC heating); working pressure: 10^{-4} Pa (10^{-6} Torr); magnification: 300.000, resolution: 3.0 nm, accelerating voltage: 1–30 kV; sample size: 60–130 mm.

2.6. IR-Spectrospopy

IR-spectra of water samples, obtained after being contacted 3 days with shungite and zeolite, are registered on Fourier-IR spectrometer Brucker Vertex ("Brucker", Germany) (a spectral range: average IR – 370–7800 cm^{-1}; visible – 2500–8000 cm^{-1}; the permission – 0.5 cm^{-1}; accuracy of wave number – 0.1 cm^{-1} on 2000 cm^{-1});

For the research of ZEOLITH detox the methods are:

2.7. Non-equilibrium Spectrum (NES) and Differential Non-equilibrium Spectrum (DNES)

The energy spectrum of water is characterized by a non-equilibrium process of water droplets evaporation, therefore, the term non-equilibrium spectrum (NES) of water is used. The difference

Δf(E) = f (samples of water) – f (control sample of water) – is called the "differential non-equilibrium energy spectrum of water" (DNES).

2.8. Measurement of pH and ORP (oxidative-redox potential)

The research is performed from Georgi Gluhchev with device from Hanna Instruments.

3. Results and Discussion

In comparison with zeolite comprises a microporous crystalline aluminosilicate mineral commonly used as commercial adsorbents, three-dimensional framework of which is formed by linking via the vertices the tetrahedral $[AlO_4]^{2-}$ and $[SiO_4]^{2-}$ (Panayotova, Velikov, 2002). Each

tetrahedron $[AlO_4]^{2-}$ creates a negative charge of the carcasses compensated by cations (H^+, Na^+, K^+, Ca^{2+}, NH_4^+, etc.), in most cases, capable of cation exchange in solutions. Tetrahedrons formed the secondary structural units, such as six-membered rings, five-membered rings, truncated octahedra, etc. Zeolites framework comprise interacting channels and cavities forming a porous structure with a pore size of 0.3–1.0 nm. Average crystal size of the zeolites may range from 0.5 to 30 μm.

By the measurement of IR spectra in the range of vibrations in the crystal mineral framework one can obtain the information: a) on the structure of the framework, particularly type lattice ratio SiO_2/Al_2O_3, nature and location of cations and changes in the structure in the process of the thermal treatment; b) on the nature of the surface of the structural groups, which often serve as adsorption and catalytically active sites.

Other method for obtaining information about the average energy of hydrogen bonds in an aqueous sample is measuring of the spectrum of the water state. It was established experimentally that at evaporation of water droplet the contact angle θ decreases discretely to zero, whereas the diameter of the droplet changes insignificantly (Antonov, 1995). By measuring this angle within a regular time intervals a functional dependence f(θ) can be determined, which is designated by the spectrum of the water state (Ignatov, 2005; Ignatov, 2012; Ignatov, Mosin, 2013). For practical purposes by registering the spectrum of water state it is possible to obtain information about the averaged energy of hydrogen bonds in an aqueous sample. For this purpose the model of W. Luck was used, which consider water as an associated liquid, consisted of O–H...O–H groups (Luck et al., 1980). The major part of these groups is designated by the energy of hydrogen bonds (-E), while the others are free (E = 0). The energy distribution function f(E) is measured in electron-volts (eV^{-1}) and may be varied under the influence of various external factors on water as temperature and pressure.

For calculation of the function f(E) experimental dependence between the water surface tension measured by the wetting angle (θ) and the energy of hydrogen bonds (E) is established:

$$f(E) = b\, f(\theta) / 1 - (1 + b\, E)^2)^{1/2},$$
where $b = 14.33\ eV^{-1}$; $\theta = \arccos(-1 - b\, E)$

The energy of hydrogen bonds (E) measured in electron-volts (eV) is designated by the spectrum of energy distribution. This spectrum is characterized by non-equilibrium process of water droplets evaporation, thus the term “non-equilibrium energy spectrum of water” (NES) is applied.

The difference Δf(E) = f (samples of water) – f (control sample of water) – is designated the “differential non-equilibrium energy spectrum of water” (DNES).

DNES is calculated in milli-electron volts (0.001 eV or meV) is a measure of changes in the structure of water as a result of external factors. The cumulative effect of all other factors is the same for the control sample of water and the water sample, which is under the influence of this impact. The research with NES method of water drops received after 3 days stay with zeolite in deionized water may also give valuable information on the possible number of hydrogen bonds as percent of water molecules with different values of distribution of energies. These distributions are basically connected with restructuring of H_2O molecules with the same energies.

3.1. Results with spectral analysis of 1% solution of ZEOLITH detox

The average energy ($E_{H...O}$) of hydrogen H...O-bonds among individual H_2O molecules in 1 % solution of ZEOLITH detox is measured at E=-0.1219 eV. The result for the control sample (deionized water) is E=-0.1185 eV. The results obtained with the NES method are recalculated with the DNES method as a difference of the NES (1% solution of ZEOLITH detox) minus the NES (control sample with deionized water) equaled the DNES spectrum of 1% solution of ZEOLITH detox. Thus, the result for 1% solution of ZEOLITH detox recalculated with the DNES method is ΔE=-0.0034±0.0011 eV. The result shows the increasing of the values of the energy of hydrogen bonds in 1% solution of ZEOLITH detox regarding the deionized water. The result is effect of stimulation on human body. This shows restructuring of water molecules in configurations of clusters, which influence usefully on human health on molecular and cellular level. The effects are describing with mathematical model of 1% solution of ZEOLITH detox.

3.2. Mathematical model of ZEOLITH detox

The research with the NES method of water drops is received with 1% solution ZEOLITH detox, and deionized water as control sample. The mathematical models of 1% solution ZEOLITH detox gives the valuable information for the possible number of hydrogen bonds as percent of H_2O molecules with different values of distribution of energies (Table 1 and Figure 1). These distributions are basically connected with the restructuring of H_2O molecules having the same energies.

Table 1. The distribution (%, $(-E_{value})/(-E_{total\ value})$ of H_2O molecules in 1% water solution of ZEOLITH detox (product of LavaVitae, Austria) and control deionized water

-E(eV) x-axis	1 % water solution ZEOLITH detox (LavaVitae) y-axis (%((-E_{value}) */ (-$E_{total\ value}$)**	Control Sample Deionized water y-axis (%((-E_{value})*/ (-$E_{total\ value}$)**	-E(eV) x-axis	1 % water solution ZEOLITH detox (LavaVitae) y-axis (%((-E_{value}) */ (-$E_{total\ value}$)**	Control Sample Deionized water y-axis (%((-E_{value})*/ (-$E_{total\ value}$)**
0.0937	0	6.7	0.1187	0	15.5
0.0962	0	6.7	0.1212	**18.9**[2]	0
0.0987	0	6.7	0.1237	0	6.7
0.1012	6.0	15.5	0.1262	0	6.7
0.1037	12.5	6.7	0.1287	0	0
0.1062	0	6.7	0.1312	0	3.3
0.1087	3.1	0	0.1337	12.5	0
0.1112	**3.1**[1]	0	0.1362	12.5	3.3
0.1137	0	15.5	0.1387	**18.9**[3]	0
0.1162	12.5	0	–	–	–

Notes:
E=-0.1212 eV is the local extremum for anti inflammatory effect
E= -0.1387 eV is the local extremum for inhibition of development of tumor cells of molecular level
Notes:
* The result ($-E_{value}$) is the result of hydrogen bonds energy for one parameter of (-E)
** The result ($-E_{value}$) is the total result of hydrogen bonds energy

Figure 1 shows the distribution (%, $(-E_{value})/(-E_{total\ value})$ of H_2O molecules in and 1 % of water solution of ZEOLITH detox (product of LavaVitae, Austria) (red line) and control sample deionized water (blue line).

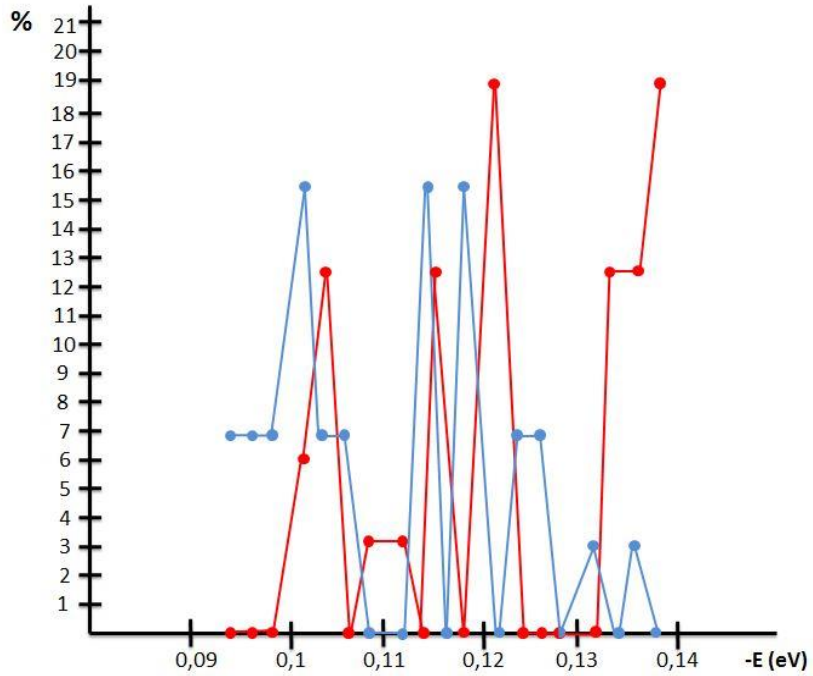

Notes:
E=-0.1212 eV is the local extremum for anti-inflammatory effect
E= -0.1387 eV is the local extremum for inhibition of development of tumor cells of molecular level

Fig. 1. Mathematical model (Ignatov, Mosin, 2013) of 1% water solution of ZEOLITH detox (product of LavaVitae, Austria).

The experimental data obtained testified the following conclusions from the mathematical model of in 1 % water solution of ZEOLITH detox (product of LavaVitae, Austria) and control deionized water. The distribution (%, $(-E_{value})/(-E_{total\ value})$ of water molecules in mathematical model of in 1 % water solution of ZEOLITH detox (product of LavaVitae, Austria) and control deionized water. The distribution (%, $(-E_{value})/(-E_{total\ value})$ of water molecules in ZEOLITH detox (product of LavaVitae, Austria) according control sample is different. However, for the value E = -0.1387 eV or λ = 8.95 μm there is the biggest local extremum (18.9 (%, $(-E_{value})/(-E_{total\ value})$) corresponding to the re-structuring of hydrogen bonds among H_2O molecules for inhibition of development of tumor cells of molecular level. This difference may indicate on the different number of hydrogen bonds in water samples, as well as their physical parameters (pH, ORP), resulting in different distribution of H_2O molecules and different values of H_2O molecules with ratios of $(-E_{value})/(-E_{total\ value})$. Particularly it was observed the statistical re-structuring of H_2O molecules in water samples according to the energies. The experimental data may prove that stipulates the restructuring of H_2O molecules on molecular level and may be used for the prophylaxis of development of tumor cells. For the value E=-0.1212 eV or λ=10.23 μm there is the bigger local extremum (18.9 (%, $(-E_{value})/(-E_{total\ value})$) corresponding to the re-structuring of hydrogen bonds among H_2O molecules for anti inflammatory effect. The experimental data for ZEOLITH detox may prove that stipulates the restructuring of H_2O molecules on molecular level and the biophysical effects are:

E=-0.1212 eV is the local extremum for anti inflammatory effect

E= -0.1387 eV is the local extremum for inhibition of development of tumor cells of molecular level

4. Results with pH and ORP

There are valid the following results of pH as indicator for acid alkaline medium of the products of Lava Vitae. There are the results also of ORP or Oxidation-reduction potential.

The results are for 1 % of solutions of products, which are made from deionized water. This research is performed with Georgi Gluhchev from Bulgarian Academy of Science. The results of pH of deionized water is 6.05 and of ORP is 119.7. Table 2 shows the results of pH and ORP.

Table 2. Results of products of company LavaVitae for pH and ORP

Product	pH	ORP (mV)	Coordinates Fig. 2
VITA intense	4.07±0.02	- 104.5	Point 1 (4,07; -104.5)
BOOST	3.60±0.02	+113.6	Point 2 (3,90;113.6)
ZEOLITH detox	8.01±0.02	+109.5	Point 3 (8,01;103.3)
Deionized water	6.05±0.02	+119.7	

Figure 2 shows the dependence between the acidity and basicity (pH) of electrochemically activated solutions and the oxidation-reduction potential (ORP). The pH value within the interval from 3 to 10 units and the ORP within the interval from -400 mV to +900 mV characterize the area of the biosphere of microorganisms. Outside these ranges of pH and ORP the microorganisms will hardly survive.

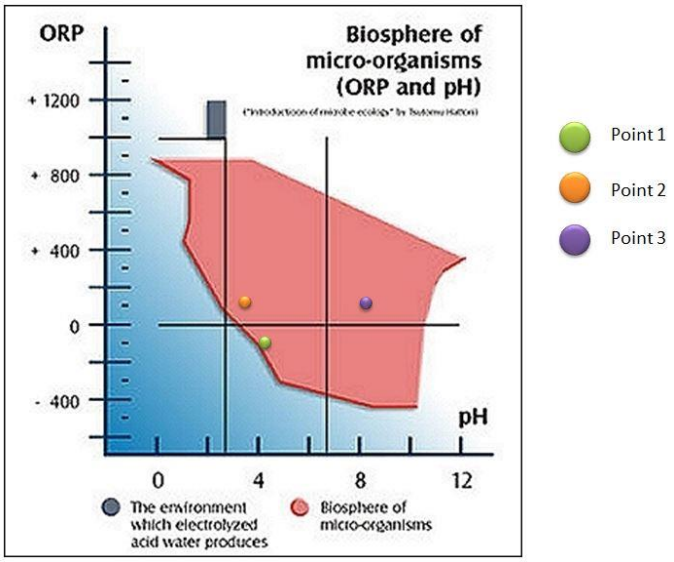

Fig. 3. The dependence between acidity and basicity (pH) of solutions and the ORP on the biosphere of micro-organisms (point 1; VITA intense), (point 2; BOOST), point 3; ZEOLITH detox)

Owing to the unique porous structure the mineral Zeolites are ideal absorbents and fillers (Gorshteyn *et al*., 1979), and as sorbents have a number of positive characteristics:

- High adsorption capacity, characterized by low resistance to water pressure;
- Mechanical strength and low abrasion resistance;
- Corrosion-resistance;
- Absorption capacity relatives to many substances, both organic (oil, benzene, phenol, pesticides, etc.) and inorganic (chlorine, ammonia, heavy metals);
- Catalytic activity;
- Relatively low cost;
- Environmental friendliness and ecological safety.
-

5. Detoxification of zeolite. Proofs for anti inflammatory effects as base for detoxification of zeolite.

There are proofs for anti inflammatory effects in process of detoxification.

Resolvin-E1 (RvE1) has been demonstrated to promote inflammatory resolution in numerous disease models. Given the importance of epithelial cells to coordination of mucosal inflammation, we hypothesized that RvE1 elicits an epithelial resolution signature. Notably, RvE1 induced intestinal alkaline phosphatase (ALPI) expression and significantly enhanced epithelial ALPI enzyme activity. One role recently attributed to ALPI is the detoxification of bacterial LPS. In studies, RvE1-exposed epithelia detoxified LPS (assessed by attenuation of NF-κB signaling). (Campbell et al., 2010).

The research shows hypothesize that susceptibility to persistent airway inflammation in atopic individuals is characterized by an inherited deficiency in the effectiveness of detoxification of inhaled irritants and products of oxidative stress such as reactive oxygen species (ROS). The case-control studies show that polymorphisms at the glutathione S-transferase, GSTP1, locus on chromosome 11q13 may account for variation in host response to oxidative stress, a key component of airway inflammation. Frequency of the GSTP1 Val/Val genotype is reduced in atopic subjects compared with nonatopic subjects. Trend analysis also shows a significant decrease of GSTP1 Val/Val (with parallel increase of GSTP1 Ile/Ile) genotype frequency with increasing severity of airflow obstruction/bronchial hyperresponsiveness. The implication of specific polymorphisms at the GSTP1 locus in airway inflammation is entirely novel: however, GST are recognized as a supergene family of enzymes critical in 1) cell protection from the toxic products of ROS-mediated reactions, 2) modulation of eicosanoid synthesis (Spiteri et al., 2000).

Severe hemolysis or myolysis occurring during pathological states, such as sickle cell disease, ischemia reperfusion, and malaria results in high levels of free heme, causing undesirable toxicity leading to organ, tissue, and cellular injury. Free heme catalyzes the oxidation, covalent cross-linking and aggregate formation of protein and its degradation to small peptides. It also catalyzes the formation of cytotoxic lipid peroxide via lipid peroxidation and damages DNA through oxidative stress. Heme being a lipophilic molecule intercalates in the membrane and impairs lipid bilayers and organelles, such as mitochondria and nuclei, and destabilizes the cytoskeleton. Heme is a potent hemolytic agent and alters the conformation of cytoskeletal protein in red cells. Free heme causes endothelial cell injury, leading to vascular inflammatory disorders and stimulates the expression of intracellular adhesion molecules. Heme acts as a pro-inflammatory molecule and heme-induced inflammation is involved in the pathology of diverse conditions; such as renal failure, arteriosclerosis, and complications after artificial blood transfusion, peritoneal endometriosis, and heart transplant failure. Heme offers severe toxic effects to kidney, liver, central nervous system and cardiac tissue. Although heme oxygenase is primarily responsible to detoxify free heme but other extra heme oxygenase systems also play a significant role to detoxify heme. A brief account of free heme toxicity and its detoxification systems along with mechanistic details are presented (Kumar, Bandyopadhyay, 2005).

Rheumatoid arthritis (RA) is characterised by migration of activated phagocytes and other leukocytes into synovial and periarticular tissue. Activated oxygen species and other mediating substances from triggered phagocytes appear to exacerbate and perpetuate the rheumatoid condition. Iron excesses are capable of aggravating the arthritic inflammation, probably through their pro-oxidant potentials. In contrast, therapeutically given gold salts, through a lysosomal loading of the metal, inhibit the triggered cells, thereby reducing the toxic oxygen production. Pharmacological doses of zinc also may immobilise macrophages. Furthermore, the copper–zinc-containing enzyme SOD (superoxide dismutase) can act as a scavenger of toxic oxygen in the tissues. Therapeutic remission of RA has been obtained following intraarticular administration of SOD. Intramuscular administration of copper complexes has induced remission in about 60 % of RA patients in open studies. Another drug, penicillamine, that protects cellular membranes against toxic oxygen in vitro, is presumed to act as an antirheumatic via the SOD mimetic activity of its copper complex. Thiomalate and other thiols may possess similar activities. Selenium compounds also may act as oxygen radical scavengers. A significant alleviation of articular pain and morning stiffness was obtained following selenium and vitamin E supplementation in a double-blind study on RA patients. The observations reviewed here indicate that metal compounds and other antioxidants can reduce the rheumatic inflammation by reducing the cellular production and/or concentration of toxic oxygen species (Aaseth et al., 1998).

Zeolite$^-$ creates a negative charge of the carcasses compensated by cations (H^+, Na^+, K^+, Ca^{2+}, NH_4^+, etc.), in most cases, capable of cations exchange in solutions. Efficiency of using zeolite is

stipulated by the high range of valuable properties (absorption, catalytic, antioxidant, regenerative, antibacterial). There is permanent antioxidant activity of zeolite on enzymes (Dogliotti et al., 2012; Ignatov, Mosin, 2015).

There has been no proven method thus far to accelerate the clearance of potentially toxic perfluorinated compounds (PFCs) in humans. PFCs are a family of commonly used synthetic compounds with many applications, including repelling oil and stains on furniture, clothing, carpets and food packaging, as well as in the manufacturing of polytetrafluoroethylene – a non-stick surfacing often used in cookware (e.g. Teflon(r)). Some PFCs remain persistent within the environment due to their inherent chemical stability, and are very slowly eliminated from the human body due, in part, to enterohepatic recirculation. Exposure to PFCs is widespread and some subpopulations, living in proximity to or working in fluorochemical manufacturing plants, are highly contaminated. PFC bioaccumulation has become an increasing public health concern as emerging evidence suggests reproductive toxicity, neurotoxicity and hepatotoxicity, and some PFCs are considered to be likely human carcinogens. A case history is presented where an individual with high concentrations of PFCs in serum provided: sweat samples after use of a sauna; and stool samples before and after oral administration of each of two bile acid sequestrants – cholestyramine (CSM) and saponin compounds (SPCs). Stool samples before and after use of a cation-exchange zeolite compound were also examined. PFCs found in serum were not detected in substantial quantities in sweat or in stool prior to treatment. Minimal amounts of perfluorooctanoic acid, but no other PFCs, were detected in stool after SPC use; minimal amounts of perfluorooctanesulfonate, but no other PFCs, were detected in stool after zeolite use. All PFC congeners found in serum were detected in stool after CSM use. Serum levels of all PFCs subsequently declined after regular use of CSM. Further study is required but this report suggests that CSM therapy may facilitate gastrointestinal elimination of some PFCs from the human body (Genuis et al., 2010).

As a result of different energies of hydrogen bonds, the surface tension 1 % water solution of ZEOLITH detox is increasing. The increasing of surface tension is regarding the control sample. This effect is connected with preservation of the energy in human body as result of biochemical process among water molecules and bio molecules. As effect of big increasing of surface tension and the spectrum is begging from E= -0.1162 eV and this shows effects with detoxification (Ignatov, 2016).

Our study shows anti inflammatory effect of zeolite. For the value E=-0.1212 eV or λ=10.23 μm. there is the bigger local extremum (18.9 (%, $(-E_{value})/(-E_{total\ value})$) corresponding to the re-structuring of hydrogen bonds among H_2O molecules for anti inflammatory effect of ZEOLITH detox. Anti inflammatory effect is part of process of detoxification of zeolite with the following effects - absorption, catalytic, antioxidant, regenerative, antibacterial. $Zeolite^-$ creates a negative charge by cations (H^+, Na^+, K^+, Ca^{2+}, NH_4^+, etc.), in most cases, capable of cations exchange in solutions. There is permanent antioxidant activity of zeolite on enzymes (Dogliotti et al., 2012; Ignatov, Mosin, 2015).

Our study shows connection between pH and ORP and that water solution of ZEOLITH detox has positive role for microorganisms. Inhibition of development of tumor cells is influenced from anti inflammatory effects. Our proofs are for the value E = -0.1387 eV or λ = 8.95 μm there is the biggest local extremum (18.9 (%, $(-E_{value})/(-E_{total\ value})$) corresponding to the re-structuring of hydrogen bonds among H_2O molecules for inhibition of development of tumor cells of molecular level.

6. Discussion and Conclusions

ZEOLITH detox (product of LavaVitae company)

The interaction of ZEOLITH detox with water is quiet complex and results the restructuring of energy values among H_2O molecules with a statistically reliable increase of local extremums in DNES-spectra after treatment of ZEOLITH detox with water. These values are measured at -0.1219 eV for ZEOLITH detox. The result for control sample (deionized water) is -0.1185 eV. The results with NES method were recalculated by the DNES method. The result of ZEOLITH detox with DNES method is 0.0034±0.0011 eV.

From the NES and DNES spectrum and mathematical model of 1 % solution of ZEOLITH detox and deionized water as control sample are valid the following conclusions for biophysical effects for ZEOLITH detox (LavaVitae Company)

- Anti-inflammatory effect;
- inhibition of development of tumor cells of molecular level;

Naturally occurring zeolites are rarely pure and are contaminated to varying degrees by other minerals, metals, quarts, or other zeolites. For this reason, naturally occurring zeolites are excluded from many important commercial applications where uniformity and purity are essential. In comparison with zeolite comprises a microporous crystalline aluminosilicate mineral commonly used as adsorbent.

Our study shows anti inflammatory effect of zeolite. For the value E=-0.1212 eV or λ=10.23 μm. there is the bigger local extremum (18.9 (%, $(-E_{value})/(-E_{total\ value})$) corresponding to the re-structuring of hydrogen bonds among H_2O molecules for anti inflammatory effect of ZEOLITH detox. Anti inflammatory effect is part of process of detoxification of zeolite with the following effects – absorption, catalytic, antioxidant, regenerative, antibacterial. Zeolite$^-$ creates a negative charge by cations (H^+, Na^+, K^+, Ca^{2+}, NH_4^+, etc.), in most cases, capable of cations exchange in solutions. There is permanent antioxidant activity of zeolite on enzymes (Dogliotti et al., 2012; Ignatov, Mosin, 2015).

Our study shows connection between pH and ORP and that water solution of ZEOLITH detox has positive role for microorganisms. Inhibition of development of tumor cells is influenced from anti inflammatory effects. Our proofs are for the value E = -0.1387 eV or λ = 8.95 μm there is the biggest local extremum (18.9 (%, $(-E_{value})/(-E_{total\ value})$) corresponding to the re-structuring of hydrogen bonds among H_2O molecules for inhibition of development of tumor cells of molecular level.

7. Acknowledgements

The author wish to thank to Georgi Gluhchev for the research of pH and ORP. The author express thankful to Teodora Todorova for the preparation of the figures.

References

Aaseth et al., 1998 – *Aaseth, J., Haugen, M., Førre, O.* (1998). Rheumatoid arthritis and metal compounds – perspectives on the role of oxygen radical detoxification, *Analyst*, 1.

Antonov, 1995 – *Antonov, A.* (1995). Research of the Nonequilibrium Processes in the Area in Allocated Systems., Diss. Thesis Doctor of Physical Sciences. Sofia: Blagoev.

Campbell et al., 2010 – *Campbell et al.* (2010). Resolvin E1-induced Intestinal Alkaline Phosphatase Promotes Resolution of Inflammation through LPS Detoxification. *Proceeding of National Academy of Sciences,* 107 (32) 14298-14303.

Genius et al., 2010 – Genius, S. et al. (2010). Human Detoxification of Perfluorinated Compounds. *Public Health*, 124 (7) 367–375.

Gluhchev et al., 2015 – *Gluhchev, G., Ignatov, I., Karadzhov, S., Miloshev, G., Ivanov, I., Mosin, O.V.* (2015). Biocidal Effects of Electrochemically Activated Water. *Journal of Health, Medicine and Nursing*, 11, 67-83.

Gluhchev et al., 2015 – *Gluhchev, G., Ignatov, I., Karadzhov, S., Miloshev, G., Ivanov, N., Mosin, O.V.* (2015). Electrochemically Activited Water: Biophysical and Biological Effects of Anolyte and Catholyte Types of Water. *European Journal of Molecular Biotechnology*, 1, 12-26.

Gluhchev et al., 2015 – *Gluhchev, G., Ignatov, I., Karadzhov, S., Miloshev, G., Ivanov, N., Mosin, O.V.* (2015). Studying the Antimicrobial and Antiviral Effects of Electrochemically Activated Nacl Solutions of Anolyte and Catholyte on a Strain of E. Coli DH5 and Classical Swine Fever (CSF) Virus. *European Journal of Medicine*, 9 (3), 124-138.

Gluhchev et al., 2015 – *Gluhchev, G., Ignatov, I., Karadzhov, S., Miloshev, G., Ivanov, I., Mosin, O.V.* (2015). Electrochemically Activated Water. Biophysical and Biological Effects of Anolyte and Catholyte as Types of Water. *Journal of Medicine, Physiology and Biophysics*, 10, 1-17.

Gluhchev et al., 2018 – *Gluhchev, G., Mehandjiev, D., Ignatov, I., Karadzhov, S., Pesheva, Y., Atanasov, A.* (2018). Water Electrolysis-Processes in Catholyte and Anolyte Results with Differential Non-Equilibrium Water Spectrum. *European Journal of Medicine*, 6(1): 3-12.

Ignatov, 2005 – *Ignatov, I.* (2005). Energy Biomedicine, *Gea-Libris*, Sofia, 1–88.

Ignatov, 2010 – *Ignatov, I.* (2010). Which Water is Optimal for the Origin (Generation) of Life?*Euromedica*, Hanover, 34-35.

Ignatov, 2011 – *Ignatov, I.* (2011). Entropy and Time in Living Matter, *Euromedica,* 74.

Ignatov, 2012 – *Ignatov, I.* (2012). Origin of Life and Living Matter in Hot Mineral Water, Conference on the Physics, Chemistry and Biology of Water. *Vermont Photonics*, USA.

Ignatov, Mosin, 2013 – *Ignatov I., Mosin O.V.* (2013). Possible Processes for Origin of Life and Living Matter with Modeling of Physiological Processes of Bacterium *Bacillus Subtilis* in Heavy

Water as Model System. *Journal of Natural Sciences Research*, 3(9), 65-76.

Ignatov, Mosin, 2013 – *Ignatov, I., Mosin, O. V.* (2013). Modeling of Possible Processes for Origin of Life and Living Matter in Hot Mineral and Seawater with Deuterium. *Journal of Environment and Earth Science*, 3(14), 103-118.

Ignatov, Mosin, 2013 – *Ignatov, I., Mosin, O.V.* (2013). Structural Mathematical Models Describing Water Clusters. *Journal of Mathematical Theory and Modeling*, 3 (11), 72-87.

Ignatov, Mosin, 2014 – *Ignatov, I., Mosin, O. V.* (2014). The Structure and Composition of Carbonaceous Fullerene Containing Mineral Shungite and Microporous Crystalline Aluminosilicate Mineral Zeolite. Mathematical Model of Interaction of Shungite and Zeolite with Water Molecules. *Advances in Physics Theories and Applications*, 28, 10-21.

Ignatov, Mosin, 2014 – *Ignatov, I., Mosin, O.V.* (2014). The Structure and Composition of Shungite and Zeolite.Mathematical Model of Distribution of Hydrogen Bonds of Water Molecules in Solution of Shungite and Zeolite. *Journal of Medicine, Physiology and Biophysics*, 2, 20-36.

Ignatov, Mosin, 2014 – *Ignatov, I., Mosin, O.V.* (2014). Mathematical Models of Distribution of Water Molecules Regarding Energies of Hydrogen Bonds. *Journal of Medicine, Physiology and Biophysics*, 2, 71-94.

Ignatov, Mosin, 2014 – *Ignatov, I., Mosin,O.V.* (2014). Mathematical Model of Interaction of Carbonaceous Fullerene Containing Mineral Shungite and Aluminosilicate Mineral Zeolite with Water. *Journal of Medicine, Physiology and Biophysics*, 3, 15-29.

Ignatov, Mosin, 2014 – *Ignatov, I., Mosin, O. V., Bauer, E.* (2014). Carbonaceous Fullerene Mineral Shungite and Aluminosilicate Mineral Zeolite. Mathematical Model ans Practical Application of Water Solution of Water Shungite and Zeolite. *Journal of Medicine, Physiology and Biophysics*, 4, 27-44.

Ignatov, Mosin, 2016 – *Ignatov, I., Mosin, O.V.* (2016). Water for Origin of Life. *Altaspera Publishing & Literary Agency Inc*, 1-616. [in Russian]

Ignatov, Mosin, 2016 – *Ignatov, I., Mosin, O.V.* (2016). Deuterium, Heavy Water and Origin of Life, *LAP LAMBERT Academic Publishing*, 1-500.

Ignatovet al., 2016– *Ignatov, I.et al.* (2016). Results of Biophysical and Nano Technological Research of ZEOLITH Detox of LavaVitae Company. *Journal of Health, Medicine and Nursing*, 30, 44-49.

Ignatovet al., 2016– *Ignatov, I.* (2016). Product of LavaVitae BOOST is Increasing of Energy of Hydrogen Bonds among Water Molecules in Human Body. *Journal of Medicine, Physiology and Biophysics*, 27, 30-42.

Ignatov, 2016 – *Ignatov, I.* (2016). VITA intense – Proofs for Anti-inflammatory, Antioxidant and Inhibition Growth of Tumor Cells Effects. Relaxing Effect of Nervous System, Anti Aging Influence. *Journal of Medicine, Physiology and Biophysics*, 27, 43-61.

Ignatov, 2017 – *Ignatov, I.* (2017). VITA intense and BOOST – Products with Natural Vitamins and Minerals for Health. *Journal of Medicine, Physiology and Biophysics*, 31, 58-78.

Ignatov, 2017 –*Ignatov, I.* (2017). ZEOLITH detox for Detoxification and ZELOLITH Creme for Skin Effects as Products of LavaVitae Company. *Journal of Medicine, Physiology and Biophysics*, 31, 79-86.

Ignatov, 2017 – *Ignatov, I.* (2017). Distribution of Molecules of ZEOLITH detox and ZEOLITH Creme in Water as Factor for Health. *European Journal of Molecular Biotechnology*, 5, (1), 11-22.

Ignatov, 2017 – *Ignatov, I.* (2017). Biophysical Research of ZEOLITH detox and ZEOLITH Crème. *European Journal of Medicine*, 5 (2), 31-42.

Ignatov, 2017 –*Ignatov, I.* (2017). VITA intense –Antioxidant and Inhibition Growth of Tumor Cells Effects. Anti Aging Influence. Negative Oxidation-reduction Potential (ORP) Has Important Role in These Effects. *Journal of Medicine, Physiology and Biophysics*, 39, 20-42.

Ignatov et al., 2014 – *Ignatov, I., Karadzhov, S., Atanasov, A., Ivanova, E., Mosin, O.V.* (2014). Electrochemical Aqueous Sodium Chloride Solution (Anolyte and Catholyte) as Types of Water. Mathematical Models. Study of Effects of Anolyte on the Virus of Classical Swine Fever Virus. *Journal of Health, Medicine and Nursing*, 8,1-28.

Ignatov et al., 2015 – *Ignatov, I., Gluhchev, G., Karadzhov, S., Miloshev, G., Ivanov, I., Mosin, O.V.* (2015). Preparation of Electrochemically Activated Water Solutions

(Catholyte/Anolyte) and Studying Their Physical-Chemical Properties. *Journal of Medicine, Physiology and Biophysics*, 11, pp. 1-21.

Ignatov et al., 2015 – *Ignatov, I., Gluhchev, G., Karadzhov, S., Miloshev, G., Ivanov, I., Mosin, O.V.* (2015). Preparation of Electrochemically Activated Water Solutions (Catholyte/Anolyte) and Studying of their Physical-Chemical Properties. *Journal of Medicine, Physiology and Biophysics*, 13, 18-38.

Ignatov et al., 2015 – *Ignatov, I., Gluhchev, G., Karadzhov, S., Miloshev, G., Ivanov, I., Mosin, O.V.* (2015). Preparation of Electrochemically Activated Water Solutions (Catholyte/Anolyte) and Studying of their Physical-Chemical Properties. *Journal of Health, Medicine and Nursing*, 13, 64-78.

Ignatov et al., 2015 – *Ignatov, I., Mosin, O. V. , Gluhchev, G., Karadzhov, S., Miloshev, G., Ivanov, I.* (2015). Studying Electrochemically Activated NaCl Solutions of Anolyte and Catholyte by Methods of Non-Equilibrium Energy Spectrum (NES) and Differential Non-Equilibrium Energy Spectrum (DNES). *Journal of Medicine, Physiology and Biophysics*, 14, 6-18.

Ignatov et al., 2015 – *Ignatov, I, Gluhchev, G., Karadzhov, S., Ivanov, N., Mosin, O.V.* (2015).Preparation of Electrochemically Activated Water Solutions (Catholyte/Anolyte) and Studying Their Physical-Chemical Properties. *Journal of Medicine, Physiology and Biophysics*, 16, 1-14.

Ignatov et al., 2016 – *Ignatov, I., Mosin, O.V., Gluhchev, G., Karadzhov, S., Miloshev, G., Ivanov, I.* (2016). Studying Electrochemically Activated NaCl Solutions of Anolyte and Catholyte by Methods of Non-Equilibrium Energy Spectrum (NES) and Differential Non-Equilibrium Energy Spectrum (DNES). *Journal of Medicine, Physiology and Biophysics*, 20, 13-23.

Ignatov et al., 2015 –*Ignatov, I., Mosin, O.V., Gluhchev, G., Karadzhov, S., Miloshev, G., Ivanov, N.* (2015). The Evaluation of Mathematical Model of Interaction of Electrochemically Activated Water Solutions (Anolyte and Catholyte) with Water. *European Reviews of Chemical Research*, 2 (4|),72-86.

Ignatovet al., 2016 – *Ignatov, I., Mosin, O.V., Kirov, P.* (2016). Matematical Model of Kangen Water® Biophysical and Biochemical Effects of Catholyte. *Advances in Physics Theories and Applications*, 51, 33-55.

Ignatov, 2017 – *Ignatov, I.* (2017) Aluminosilicate Mineral Zeolite. Interaction of Water Molecules in Zeolite Table and Mountain Water Sevtopolis from Bulgaria. *Journal of Medicine, Physiology and Biophysics*, 31, 41-45.

Ignatov, Mosin, 2014 – *Ignatov, I., Mosin, O.V.* (2014). Methods for Measurements of Water Spectrum. Differential Non-equilibrium Energy Spectrum Method (DNES). *Journal of Health, Medicine and Nursing,* 6, 50-72.

Ignatov, Mosin, 2015 – *Ignatov, I., O.V.Mosin.* (2015). Origin of Life and Living Matter in Hot Mineral Water. *Advances in Physics Theories and Applications*, 39, 1-22.

Ignatov, Mosin, 2014a – *Ignatov, I., Mosin, O.V.* (2014). Mathematical Models of Distribution of Water Molecules Regarding Energies of Hydrogen Bonds. *Journal of Medicine, Physiology and Biophysics,* 6, 50-72.

Ignatov, Mosin, 2014 – *Ignatov, I., Mosin, O.V.* (2014). Structural Models of Water and Ice Regarding the Energy of Hydrogen Bonding. *Nanotechnology Research and Practice*, 7 (3), 96-117.

Ignatov, Mosin, 2014 – *Ignatov, I., Mosin, O.V.* (2014). Nano Mix of Shungite and Zeolite for Cleaning of Toxins and Increasing of Energy of Hydrogen Bonds among Water Molecules in Human Body. *Journal of Medicine, Physiology and Biophysics,* 27, 1-10.

Ignatov, 2016 – *Ignatov, I.* (2016). VITA intense – Proofs for Anti-inflammatory, Antioxidant and Inhibition Growth of Tumor Cells Effects. Relaxing Effect of Nervous System, Anti Aging Influence. *Journal of Medicine, Physiology and Biophysics*, 27, 43-61.

Ignatov, Pesheva, 2018 – *Ignatov, I., Pesheva, Y.* (2018). VITA Intense – Product with Negative Oxidation-reduction Potential (ORP) as Important Quality for Antioxidant and Inhibition Growth of Tumor Cells Effects. Anti Aging Effects. *European Journal of Medicine*, 6(1): 20-42.

Kumar, Bandyopadhyay, 2005 – *Kumar, Bandyopadhyay* (2005). Free Heme Toxicity and its Detoxification Systems in Human. *Toxicology letters,* 157(3-4), 175-188.

Luck et al., 1980 – *Luck, W., Schiöberg, D., Ulrich, S.* (1980). Infrared Investigation of Water Structure in Desalination Membranes. *J. Chem. Soc. Faraday Trans.*, 2(76), 136–147.

Mehandjiev et al., 2017 – *Mehandjiev, D., Ignatov, I., Karadzhov, I., Gluhchev, G., Atanasov, A.* (2017) On the Mechanism of Water Electrolysis. *Journal of Medicine, Physiology and*

Biophysics, 31, 23-26.

Mosin, Ignatov, 2013 – *Mosin, O.V., Ignatov, I.* (2013). The Structure and Composition of Natural Carbonaceous Fullerene Containing Mineral Shungite. *International Journal of Advanced Scientific and Technical Research*, 6(11–12), 9–21.

Mosin, Ignatov, 2012 – *Mosin, O.V., Ignatov, I.* (2012). The Composition and Structural Properties of Fullerene Natural Mineral Shungite. *Nanoengineering*, 18 (12), 17–24. [in Russian]

Mosin, Ignatov, 2012 – *Mosin, O.V., Ignatov, I.* (2012). Composition and Structural Properties of Fullerene Natural Mineral Shungite. *Nanomaterials and Nanotechnologies,* 2, 25-36.

Mosin, Ignatov, 2015 – *Mosin, O.V., Ignatov, I.* (2015). An Overview of Methods and Approaches for Magnetic Treatment of Water. *Water: Hygiene and Ecology*, 3-4 (4), 113-130.

Panayotova, Velikov, 2002 – *Panayotova, M., Velikov, B.* (2002) Kinetics of Heavy Metal Ions Removal by Use of Natural Zeolite. *Journal of Environmental Science and Health*, *Vol.* 37(2), 139–147.

Parfen'eva, 1994 – *Parfen'eva, L.S.* (1994). Electrical Conductivity of Shungite Carbon. *Solid State Physics*, 36(1), 234–236.

Podchaynov, 2007 – *Podchaynov, S.F.* (2007). Mineral Zeolite – a Multiplier of Useful Properties Shungite. Shungites and human safety. *Proceedings of the First All-Russian scientific-practical conference* (3–5 October 2006), ed. J.K Kalinin (Petrozavodsk: Karelian Research Centre of Russian Academy of Sciences), 6–74. [in Russian]

Spiteri al., 2000 – *Spiteri, M., Bianco, A., Strange, R., Fryer, A.* (2000). Polymorphisms at the Glutathione S-transferase, GSTP1 locus: a Novel Mechanism for Susceptibility and Development of Atopic Airway Inflammation. *Allergy*, 55 (s61), 5-66.

Published in the Slovak Republic
European Journal of Molecular Biotechnology
Has been issued since 2013.
E-ISSN: 2409-1332
2018, 6(1): 53-60

DOI: 10.13187/ejmb.2018.1.53
www.ejournal8.com

Targered Changes in the Natural and Semi-Artificial Arid Phytocenoses in the Contact Zone with the Agrocenoses: A System Control Model-Based Approach

Elena A. Ivantsova [a, *], Nikolay V. Onistratenko [a], Nadezhda V. German [a], Pavel A. Krylov [a], Anna A. Tikhonova [a], Valery V. Novochadov [a]

[a] Volgograd State University, Russian Federation

Abstract

The article presents the results of the study to analyze the plant and microbial soil associations in the composition of agrocenoses, natural steppe biocenoses and territorially integral areas of grasses on the border or within agrocenoses, mainly anthropogenic origin, named in the article as 'intrusions'. We show the key relationships between the main participants (47 plant species and 24 species of soil microorganisms, ranked by number in the association) in concurrence for the assimilation of soil trace elements. On the basis of data on the number, main phenological characteristics of plants and microorganisms, as well as the content of manganese, nickel, copper and zinc in the soil, the main consort bonds in this biosystem were identified. The analysis of the general influence of concrete intrusions on the adjacent agrocenosis made it possible to identify trace elements and types of soil microorganisms, which increase helped to limit the negative impact of intrusions. The obtained data can be used to form biotechnologies for optimization of agrocenoses in the conditions of the arid zone.

Keywords: arid plant communities, plant phenology, plant traits, plant-associated bacteria, soil microbial communities, iron, manganese, nickel, copper, phenotypic plasticity, environmental stress, plant biotechnology,

1. Introduction

From systems biology perspective, plant communities created by humans during agricultural or other work actively interact with microflora, other plants, representatives of the animal world, forming complex systems known as artificial biocenoses (Liu et al., 2014; Hudson et al., 2017). The dependence of the material and energy dynamics in biocenoses on the influence of soil and climatic conditions is considered in a number of quite extensive studies (El-Sayed et al., 2014; He et al., 2014; Mushaeva, 2015). A special place in the dynamics of such biocenoses is occupied by interactions with adjacent living systems, which, in the case of active influence on artificial biocenoses, acquire the character of intrusions with a dense junction or partial replacement of the artificial biocenosis territory. Biosystems in such areas can be attributed to semi-artificial biocenoses (Ndiribe et al., 2013; Ivantsova et al., 2017a).

According to modern concepts, microbial soil communities (soil microbiota) are considered to be the main control and producing component of terrestrial biocenoses. All soil bacteria are divided into four functional groups. Most of them are decomposers that consume simple carbon compounds, such as root exudates and plant residues. This type includes bacteria of the genus

* Corresponding author
E-mail addresses: ivantsova@volsu.ru (E.A. Ivantsova), novochadov.valeriy@volsu.ru (V.V. Novochadov)

Actinobacteria, Proteobacteria and *Bacteroidetes* (Remans et al., 2012; Belogolova et al., 2013). The second group consists of symbionts, which form partnerships with plants. The most famous of them are nitrogen-fixing bacteria. The third group of bacteria are pathogens, including those of anthropogenic origin, capable of being causative agents of various diseases. The fourth group, called lithotrophs, such as sulfur bacteria, methanobacteria, iron bacteria, etc., receives energy from compounds of nitrogen, sulfur, iron or hydrogen instead of carbon compounds. Some of these species are important in nitrogen circulation and in the destruction of pollutants (Sarker et al., 2017). At the same time, the composition of bacterial communities may differ from plant to plant: some may be tied to different types of plants, others ones prefer only to certain (Ma et al., 2016).

Biotechnology can provide a meaningful change in the communities due to the introduction of biogenic components such as bacteria or fungi, and exposure to abiotic factors, for example acoustic and optical effects or chemical modifiers, using the basis of advanced achievements in biophysics, molecular biology, biological chemistry and bioengineering. General environmental laws are moving from the category of conditions for the functioning the agricultural production in one of the innovative scientifically based tools to ensure their effectiveness (Delmont et al., 2011; Veselý et al., 2012; Soussi et al., 2016; Tecon, Or, 2017).

However, at the moment the detailed studies on this subject, taking into account the natural and climatic specifics of agriculture in the arid zone, are not numerous. To develop a control system of agrobiocenosis with the application of biotechnological tools we need understanding the soil microbiota was designed to be a key point for the formation and therefore a key object of management the ecosystems (Pasternak et al., 2013; Ding et al., 2013).

The aim of the work was to substantiate and form the main ways of targeted impact on the soil microbiota to optimize the competitive relationship of semi-artificial biocenoses (intrusions) and artificial agrocenoses.

2. Materials and Methods

The study was carried out in 18 areas, which were a combination of natural steppe, artificial agrocenosis (barley field in the stage of technological maturity) and intrusion (Ipatov, 2015). Last ones represented the stable semi-artificial anthropogenically altered biocenoses with a predominantly negative impact on the contacting agrocenosis. According to the degree of intensity of negative impact on the basis of expert assessments of the results of environmental and botanical monitoring, the invasion was divided into three groups: high (1), moderate (2) and low (3) impact on the surrounding agrocenosis. Detailed characteristics of these communities were previously published (Ivantsova et al., 2017b).

Determination of trace elements in soil

Sample preparation included drying the samples to air-dry state, obtaining an average sample and preparation of an acid extract (Onistratenko et al., 2016). The analysis was performed by the precision method of atomic absorption spectrometry using the spectrometer "QUANTUM.Z" (production of KORTEK LLC, Russia). The results obtained during the measurement in μg/l were recalculated according to the established procedure and expressed in mg/kg of soil.

Isolation and analysis of soil microbial associations

To isolate the soil microorganisms the roots of the plants with surrounding rhizosphere soil were accurately separated. The samples of the root soil in the volume from 500 to 1000 mg were suspended in 100 ml of sterile 0.85 % sodium chloride solution and the working dilutions of the solution were prepared (1:100, 1:1000, 1:10 000). Incubation of seed produced at a temperature of 20-21 °C for 24-72 h. bacteria growth occurred on the agar with enzymatic beef hydrolysate. Then, we calculated the number of growing colonies and investigated morphological and cultural properties of the isolated microorganisms, identifying the dominant microorganisms (Pasternak et al., 2013; Ma et al., 2016).

Protein concentration in microbial biomass was determined by Bradford method at a wavelength of 595 nm against bovine serum albumin as an optical density control. The amount of lipids was determined by phosphoric-molybdenum reagent. Both indicators were expressed as percentage of biomass.

Quantitative data were processed using with the calculation of the indices adopted to characterize the parametric samples. Results were shown as M ± m. To prove the validity of differences between groups the Student criterion was applied with P values less than 0.05.

3. Results and discussion

General characteristics and ranking of flora

In the observed plant associations, 47 species were found and identified. Due to the rarity of detection and insignificant presence in plant associations, we excluded from the subsequent modeling the effects of 23 species: *Amaránthus retrofléxus, Centaurea diffusa, Centaurea ruthenica, Consolida regalis, Descurainia sophia L., Lycopsis arvensis, Lamium maculatum, Lepidium perfoliatum, Limonium gmelinii, Lolium perenne, Onobrychis arenaria, Poa praténsis, Polýgonum aviculáre, Raphanus raphanistrum, Rumex confertus Willd, Salvia aethiopis, Senecio jacobaea, Silene wolgensis, Stipa capillata, Tanacetum vulgaris, Thláspi arvénse, Turgenia latifolia* и *Vincetoxicum scandens*. Biodiversity of plant species, taking into account the conducted censorship for the construction of a prognostic model, is presented in the Table. 1.

Table 1. A frequency (F) and abundance (A) of identified participants in the studied plant communities*

Species	Agrocenosis		Intrusion		Steppe	
	F	A	F	A	F	A
Achillea micrantha or A. millefólium	-	-	-	-	4	2
Artemísia absínthium or A. lercheana	-	-	-	-	4	3
Atriplex tatarica	-	-	3	2	4	2
Brōmopsis inērmis	-	-	-	-	2	3
Ceratocephala orthoceras	-	-	1	2	1	1
Cichórium íntybus	2	2	2	2	3	3
Convōlvulus arvēnsis	3	2	2	1	-	-
Crepis tectorum	-	-	3	1	1	1
Delphínium dictyocárpum or D. consolida	2	1	1	1	2	1
Elytrigia repens	-	-	3	3	2	3
Euphórbia seguieriána or E. helioscopia	-	-	3	2	2	2
Filágo arvénsis	-	-	-	-	3	2
Hordeum vulgare	4	4	1	1	-	-
Lactuca tatarica	-	-	4	2	2	1
Medicago sativa	-	-	2	1	3	1
Melilótus officinális	2	1	1	2	3	2
Scorzonera mollis	-	-	-	-	4	3
Tragopógon dúbius	-	-	-	-	3	2
Tripleurospérmum inodórum	1	1	3	2	2	3
Xanthium albinum	-	-	3	2	-	-

* Only data on plants with the (F + A) > 4 are included

As can be seen from the presented data, the steppe phytocenoses were most often dominated by *Artemísia absínthium* and *Scorzonera mollis*, while *Atriplex tatarica* and *Lactuca tatarica* were typical dominants in the composition of intursions.

Results of determination of trace elements in soil

These data are presented in the Table 2.

Table 2. Content of mobile forms of soil microelements in studied biocenoses, mg/kg

Influence	Zone		
	Agrocenosis	Intrusion	Steppe
Manganese			
Low	154,1 ± 13,3	177,4 ± 19,2	90,5 ± 7,27 *
Moderate	373,1 ± 43,1 #	186,2 ± 13,3 *	250,2 ± 21,6 *#
High	315,9 ± 26,4 #	349,7 ± 33,7 #	305,6 ± 26,2 #
Nickel			
Low	8,1 ± 0,61	7,5 ± 0,65	2,3 ± 0,19 *
Moderate	14,1 ± 1,35 #	8,1 ± 0,32 *	4,4 ± 0,45 *#
High	14,2 ± 0,93 #	10,8 ± 1,55	9,9 ± 0,41 *#
Copper			
Low	11,6 ± 1,02	21,6 ± 1,76 *	11,8 ± 0,95
Moderate	31,2 ± 3,51 #	11,7 ± 0,22 *#	7,1 ± 0,53 *
High	35,3 ± 3,41 #	23,7 ± 1,95 *	25,2 ± 1,07 *#
Zinc			
Low	1,9 ± 0,16	3,9 ± 0,29 *	2,1 ± 0,18
Moderate	4,8 ± 0,29 #	2,2 ± 0,19 *	4,4 ± 0,50
High	9,2 ± 2,02 #	6,8 ± 0,43 #	5,8 ± 0,41 #

– differences between agrocenosis and two other zones
* – differences between low, moderate, and high influence to agrocenosis

Maximum concentration manganese was recorded at moderate influence of the intrusion in the territory of agrophytocenosis. The manganese concentration is 2.3 higher than the same value at low intrusion influence.

A strong nickel concentration was recorded at a moderate and high intrusion effect of 14.1 mg/kg and 14.2 mg/kg respectively, which is almost 2 times higher than at a low intrusion effect. The nickel concentration was at the same level of the intrusion values in the steppe.

The cuprum concentration in the intrusion is 2 times higher than the agrophytocenosis and plain. At moderate and high influence, the cuprum concentration is 3 and 1.5 times higher, compared with the irruption values, steppe and agrophytocenosis with low intrusion influence.

With the high intrusion influence on the agrophytocenosis, the zinc concentration was 9.2 mg/kg, which is almost 5 times higher than the low intrusion influence. The zinc concentration in the steppe, the intrusion had close values.

Results of the study of soil microbial communities

In the agrophytocenosis research was revealed the dominant plant *Hordeum vulgare*, in the intrusion *Atriplex tatarica, Lactuca tatarica* and the steppe *Artemísia absínthium*. The maximum value of microbial number was recorded in the intrusion territory and was 2.4, which is 1.5 times higher than in agrophytocenosis and 2.6 times in the steppe under conditions of low intrusion influence. With the increasing intrusion influence on the agrophytocenosis, there was an increase in microbial number in relation to the intrusion zone.

The following microorganisms species were found in the study areas of *Pseudomonas, Bac. Subtilis* (agrophytocenosis, Pseudomonas, Actinomyces albus (intrusion), Clostridium acetobutylicum, Actinomyces albus (steppe). Indicators of Microbial protein and Microbial lipids in agrophytocenosis remained at the same level, regardless of the degree of intrusion influence. Similar trends were observed in the intrusion and steppe. It should be noted that Microbial protein and Microbial lipids in agrophytocenosis were lower than in the territory of intrusion and steppe.

The significance of the obtained result requires clarification, which involves a seasonal research to form a representative sample within the framework of the analysis of relations in the "soil-microorganism" system.

Table 3. Properties of microbial communities in rhizosphere soil associated with dominant plants

Influence	Zone (plant dominants)		
	Agrocenosis (*Hordeum vulgare)*	Intrusion (*Atriplex tatarica, Lactuca tatarica)*	Steppe (*Artemísia absínthium)*
Microbial number, 10^6/g			
Low	1,6 ± 0,15	2,4 ± 0,18	0,9 ± 0,11
Moderate	1,4 ± 0,13	2,2 ± 0,17 #	0,8 ± 0,09
High	1,7 ± 0,12	3,0 ± 0,24 *#	0,8 ± 0,08 #
Microbial dominants			
Low	*Pseudomonas, Bac. subtilis*	*Pseudomonas, Actinomyces albus*	*Clostridium acetobutylicum, Actinomyces albus*
Moderate			
High			
Microbial protein, %			
Low	18,5 ± 1,33	24,9 ± 1,93 #	32,4 ± 2,76 #
Moderate	18,0 ± 1,30	32,5 ± 2,77 #	30,8 ± 2,56 #
High	16,2 ± 1,22	36,0 ± 3,04 *#	35,6 ± 2,98 #
Microbial lipids, %			
Low	3,4 ± 0,22	5,7 ± 0,37 #	6,1 ± 0,50 #
Moderate	3,6 ± 0,25	4,2 ± 0,31 *	5,8 ± 0,47 #
High	3,2 ± 0,19	4,0 ± 0,28 *#	5,5 ± 0,41 #

– differences between agrocenosis and two other zones
* – differences between low, moderate, and high influence to agrocenosis

Identification of relationships between soil microbiota and dominant plants

Two consort connections were established between the microbiota and plants: "the plant is the dominant representative of the microbial community" and "the soil is the dominant representative of the microbial community".

The relations nature between soil microorganisms groups, ranked by dominance to microbiocenosis, and plants, ranked in descending order of dominance in the community (Figure 1).

Primary linkage analysis for this phytocenosis showed that the strongest relationship is that between the group of aerobic bacteria (Pseudomonas) and such species as *Euphorbia helioscopia* and *Atriplex tatarica*. A similar situation applies to the anaerobic bacteria group (*Cl. Asetobutilicum*) and *Artemisia lercheana*.

The resulting arrow model allows not only to carry out the primary analysis of the connections, but also to compare microorganisms and plants with which they interact with each other, with subsequent reference to the agrophytocenosis.

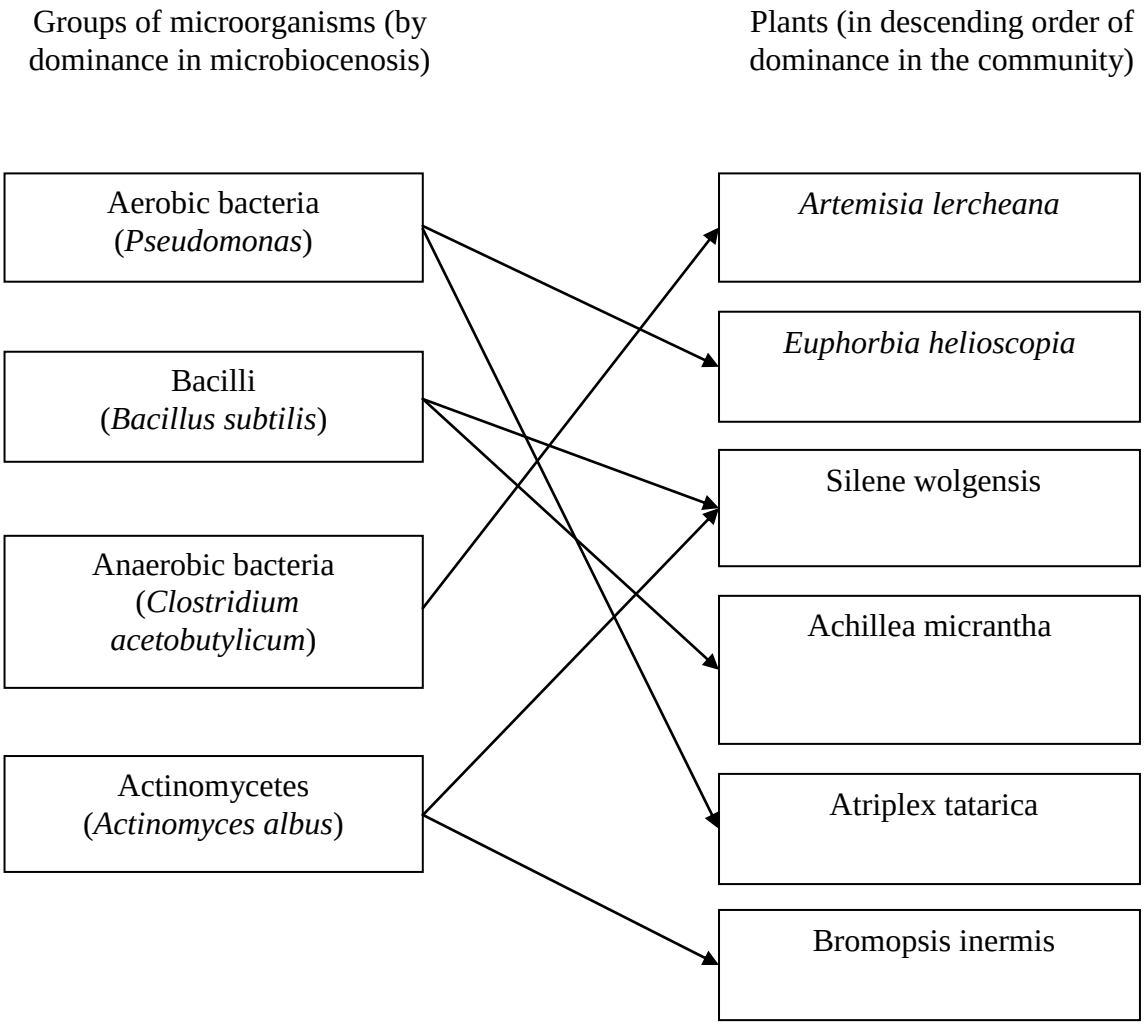

Fig. 1. The main consort relationships between different groups of soil microorganisms and plants (for example, plot № 3)

Discussion

The data obtained in studying the agrophytocenosis, the intrusion and the steppe is evidenced by the fact that with a high degree of intrusion there is a change in the trace elements composition, changes in the soil microflora. It is particularly noticeable that the presence of moderate or high intrusion influence leads to an increase in the trace elements concentration and their aggregates, which can have a negative influence on the agrophytocenosis (increasing soil toxicity to plants and microorganisms) (Totsche et al., 2018), and positively (by compensating for microelement deficiencies or stimulating growth) (Ma et al., 2016). It is important to note that such changes lead to the formation of "stress", which can both prevent the formation of agrophytocenosis, and protect agrophytocenosis from settling plants or microorganisms not peculiar to it (Drenovsky et al., 2012, Zefferman, 2015), it helps to reduce the probability of indirect competition between plants in the agrophytocenosis (Beck et al., 2010). All of the above is in good agreement with the experimental data, and in particular the increase in metal concentrations, has led to a decrease in the microbial number and species number in the agrophytocenosis.

This indicates that changes in the composition of the soil of trace elements, leads to a decrease in the microbial number communities, as well as prevents the growth of third-party plants and leads to the formation of new relationships between microorganisms groups (Drenovsky et al., 2012) and plants in agrophytocenosis.

4. Conclusion

The impact of intrusion on the agro-ecosystem is a complex, predominantly negative and is expressed in the following:

- on the periphery of the intrusion agrocenosis shows a decrease in projective cover and, as a consequence, a decrease in the biological productivity of the cultivated crop, which determines the yield as one of the economic indicators;
- the intrusion zone enhances the technogenic migration of elements, which determines the quality of agricultural products;
- technogenic intrusion is often associated with the formation of a special micro-relief of farmland, which affects the conditions of surface and underground runoff, changes the conditions of moisture and enhances the geochemical transfer of pollutants with their subsequent accumulation in the subsystem of agrocenosis " soil-plant»;
- the intrusion zone has a corrective effect on the trophic structure and the links between the main elements (soil, microbial communities, plants and fauna) in the surrounding agrocenosis.

Managing ecosystems as a whole is based on the assessment consortia connections between major structural elements: ecotope and biocoenosis.

As a result of the research two metals, such as manganese and copper, high concentrations of which contribute to the formation of biocenosis, to a minimum degree of competition to the adjacent agrocenosis, were identified. Similarly, three groups of microorganisms (Actinomycetes, Aerobic bacteria, Bacilli) were identified, whose dominance in microbial soil Association provides the same effect. These objects can be used to optimize the relationship between the agricultural lands and man-made intrusions in the conditions of arid zone.

5. Acknowledgments

This work was supported by the Ministry of Education and Science of the Russian Federation (Project no. 40.7534.2017/BC “Development of ecologically-oriented biotechnologies for the optimization of arid agrobiocenoses in the South of Russia based on the achievements of physic-chemical biology and bioinformatics”.

References

Beck et al., 2010 – *Beck M.J., Vander Wall S.B.* (2010). Seed dispersal by scatter-hoarding rodents in arid environments. *J. Ecol.* 98(6), 1300–1309. DOI: 10.1007/s00442-015-3490-4.

Belogolova et al., 2013 – *Belogolova G.A., Sokolova M.G., Gordeyeva O.K.* (2013). Migration and bio-accessibility of heavy metals, arsenic and phosphorus under the impact of rhizospheric bacteria in technogenic-polluted ecosystems. *Agricultural Chemistry (Msc).* (6), 69-77. [in Russian]

Ding et al., 2013 – *Ding G.-C., Piceno Y.M., Heuer H. Weinert N.* (2013) Changes of soil bacterial diversity as a consequence of agricultural land use in a semi-arid ecosystem. *PLoS ONE.* 8(3), e59497. DOI: 10.1371/journal.pone.0059497.

Delmont et al., 2011 – *Delmont T.O., Robe P., Cecillon, S., Clark I.M., Constancias F., Simonet P., Hirsch P.R., Vogel T.M.* (2011). Accessing the soil metagenome for studies of microbial diversity. *Appl. Environ. Microbiol.* 77(4), 1315–1324. DOI: 10.1128/AEM.01526-10.

Drenovsky et al., 2012 – *Drenovsky R.E., Grewell B.J., D'Antonio C.M., Funk J.L., James J.J., Molinari N., Parker I.M., Richards C.L.* (2012). A functional trait perspective on plant invasion. *Ann. Bot.* 110(1), 141–153. DOI: 10.1093/aob/mcs100.

El-Sayed et al., 2014 – *El-Sayed W.S., Akhkha A., El-Naggar M.Y., Elbadry M.* (2014). In vitro antagonistic activity, plant growth promoting traits and phylogenetic affiliation of rhizobacteria associated with wild plants grown in arid soil. *Front. Microbiol.* 5, e651. DOI: 10.3389/fmicb.2014.00651.

He et al., 2014 – *He M., Dijkstra F.A., Zhang K., Tan H., Zhao Y., Li X.* (2016). Influence of life form, taxonomy, climate, and soil properties on shoot and root concentrations of 11 elements in herbaceous plants in a temperate desert. *Plant and Soil.* 398(102), 339–350. DOI: 10.1007/s11104-015-2669-0

Hudson et al., 2017 – *Hudson L.N., Newbold T., Contu S., Hill S.L.L., Lysenko I., De Palma A., et al.* (2017). The database of the PREDICTS (Projecting Responses of Ecological Diversity In Changing Terrestrial Systems) project. *Ecol. Evol.* 7(1): 145–188). DOI: 10.1002/ece3.2579.

Ipatov, 2015 – *Ipatov V.S.* (2015). Using the projective cover to estimate the species role in the spatial structure of communities. *Botanicheskii Zhurnal.* 100(5), 508-512. [in Russian]

Ivantsova et al., 2017a – *Ivantsova E.A., Novochadov V.V., Onistratenko N.V., Postnova M.V.* (2017). Ecological aspects of phytosanitary optimization of arid agrobiocenoses of the south of Russia. *Bulgarian J. Agric. Sci.* 23(5), 834-842.

Ivantsova et al., 2017b – *Ivantsova E.A., Onistratenko N.V., Kholodenko A.V., Tikhonova A.A., Novochadov V.V.* (2017). Reduction of the negative impact on agrocenoses by managing adjacent natural and anthropogenic systems. *Sci. J. Volgograd St. Univ. Global Econ. Syst.* 19(4), 138-146. DOI: 10.15688/jvolsu3.2017.4.15 [in Russian]

Liu et al., 2014 – *Liu H., Zhang D., Yang X., Huang Z., Duan S., Wang X.* (2014). Seed dispersal and germination traits of 70 plant species inhabiting the Gurbantunggut desert in Northwest China. *Sci. World J. 2014.* e346405. DOI: 10.1155/2014/346405

Ma et al., 2016 – *Ma Y., Oliveira R.S., Freitas H., Zhang C.* (2016). Biochemical and molecular mechanisms of plant-microbe-metal interactions: relevance for phytoremediation. *Front Plant Sci.* Vol. 7, e918. DOI: 10.3389/fpls.2016.00918

Mushaeva, 2015 – *Mushaeva K.B.* (2015). Assessment of the current state of agropastoral landscapes in semi-arid areas of the Kalmykia republic with application of GIS-technologies. *Sci. J. Volgograd St. Univ. Natural Sci.* (1), 103-110. DOI: 10.15688/jvolsu11.2015.1.11 [in Russian]

Ndiribe et al., 2013 – *Ndiribe C., Pellissier L., Antonelli S., Dubuis A., Pottier J., Vittoz P., Salamin N., Guisanet A.* (2013). Phylogenetic plant community structure along elevation is lineage specific. *Ecol. Evol.* 3(15), 4925–4939. DOI: 10.1093/jpe/rtt064.

Onistratenko et al., 2016 – *Onistratenko N.V., Ivantsova E.A., Denysov A.A., Solodovnikov D.A.* (2016). Heavy metals in suburban ecosystems of industrial centres and ways of their reduction. *Ekologia Bratislava.* 35(3), 205-212. DOI: 10.1515/eko-2016-0016.

Pasternak et al., 2013 – *Pasternak Z., Al-Ashhab A., Gatica J., Gafny R., Avraham S., Minz D., Gillor O., Jurkevitch E.* (2013). Spatial and temporal biogeography of soil microbial communities in arid and semiarid regions. *PLoS One.* 8(7), e69705. DOI: 10.1371/journal.pone. 0069705.

Remans et al., 2012 – *Remans T., Thijs S., Truyens S., Weyens N., Schellingen K., Keunen E., Gielen H., Cuypers A., Vangronsveld J.* (2012). Understanding the development of roots exposed to contaminants and the potential of plant-associated bacteria for optimization of growth. *Ann. Bot.* 110(2), 239–252. DOI: 10.1093/aob/mcs105.

Sarker et al., 2017 – *Sarker J.R., Singh B.P., He X., Fang Y., Li G.D. et al.* (2017). Tillage and nitrogen fertilization enhanced belowground carbon allocation and plant nitrogen uptake in a semi-arid canola crop–soil system. *Sci. Rep.* 7, e10726. DOI: https:// doi.org/10.1038/s41598-017-11190-4.

Soussi et al., 2016 – *Soussi A., Ferjani R., Marasco R. Guesmi A., Cherif H., Rolli E., Mapelli F., Ouzari H.I., Daffonchio D., Cherif A.* (2016). Plant-associated microbiomes in arid lands: diversity, ecology and biotechnological potential. *Plant Soil.* 405(1-2), 357–370. DOI: 10.1007/s11104-015-2650-y.

Tecon, Or, 2017 – Teco*n R., Or D.* (2017). Biophysical processes supporting the diversity of microbial life in soil. *FEMS Microbiology Reviews.* 41(5), 599-623. DOI: 10.1093/femsre/fux039.

Totsche et al., 2018. – *Totsche K.U., Amelung W., Gerzabek M.H., Guggenberger G., Klumpp E., Knief C., Lehndorff E., Mikutta R., Peth S., Prechtel A., Ray N., Kögel-Knabner I.* (2018) Microaggregates in soils. *J. Plant Nutr. Soil Sci.* 18(1), 104-136. DOI: 10.1002/jpln.201600451.

Veselý et al., 2012 – *Veselý P., Bureš P., Šmarda P., Pavlíček T.* (2012). Genome size and DNA base composition of geophytes: the mirror of phenology and ecology? *Ann. Bot.* 109(1), 65–75. DOI: 10.1093/aob/mcr267.

Zefferman et al., 2015 – *Zefferman E., Stevens J.T., Charles G.K., Dunbar-Irwin M., Emam T., Fick S., Morales L.V., Wolf K.M., Young D.J., Young T.P.* (2015). Plant communities in harsh sites are less invaded: a summary of observations and proposed explanations. *AoB Plants.* 22(7), plv056. DOI: 10.1093/aobpla/plv056.

Published in the Slovak Republic
European Journal of Molecular Biotechnology
Has been issued since 2013.
E-ISSN: 2409-1332
2018, 6(1): 61-66

DOI: 10.13187/ejmb.2018.1.61
www.ejournal8.com

Bioactivity of Crude Extracts of Stem Bark of *Vetillaria Paradoxa*

I.A.A. Ibrahim [a, *], M.M. Mohammad [a], A. A. Faisal [a], H. Musa [b]

[a] Department of Science Laboratory Technology, School of Science and Technology, Abubakar Tatari Ali Polytechnic Bauchi, Nigeria
[b] Department of Microbiology, School of Science, Bauchi State University, Gadau, Bauchi, Nigeria

Abstract

This research aimed to study the bioactivity of crude extracts of stem bark of *Vetillaria paradoxa*"Shea-nut tree" as used in traditional medicine for treatment of stomach ache and control of diarrhea, using Hexane, Acetone and Ethanol as the extraction solvents. Phytochemical screening of stem bark of extracts of *Vitellaria paradoxa* revealed the presence of alkaloids, steroids, phenolic compounds, flavonoids, Saponins, tannins, and cardiac glycosides. Ethanol, acetone, and hexane extracts inhibited the growth of pathogenic *Escherichia coli, salmonella typhi,* and *stapilycoccus aureus* with varying degrees of activity with the ehanol extract demonstrating the highest activity against all the tested bacterial organisms.

Keywords: Phytochemiscals, antimicrobial, secondary metabolites, bioactivity, inhibition.

1. Introduction

Vitellaria paradoxa (Sapotaceae) is a plant that is locally abundant in Nigeria in the derived Savannah zones, particularly near towns and villages. It is rich in oil and replaces the oil palm as a source of edible oil in Northern Nigeria (Keay, 1989; Borokini, 2014). The plant species *(Vitellaria)* is easily distinguished by its very long leaf stalks, more widely spaced nerves and abundant white latex when slashed and in the petiole. Shea-butter is the fat extracted from the kernel of this plant. It is becoming increasingly popular as a component of cosmetic formulation in addition to its long standing use as a cocoa butter substitute in the chocolate industry (Hall et al, 1996;Omwirhiren, James, & Abass, 2016; Keay, 1989; Borokini, 2014)

Shea butter contains high level of uv-absorbing triterpenes esters which include cinnamic acid, tocopherols (vitamin A), and phytosterols (Leke, 2015). Badifu (1989) confirmed that shea butter contains a high level of unsaponifiables (5 – 15 %) which include: phytosterols ,campesterol, stigmasterol, sitosterol, spinosterol and triterpenes such as cinnamic acid ester and amyrin, parkeol, butyrospermol. lupeoland and a hydrocarbon called karitene. Analysis of the kernel reveals the presence of phenolic compounds such asgallic acid, catechin, epicatechin, epicateachingallate, gallocatechin, epigallocatechin, epigallocatehingallate, as well as quercetin and trans-cinnamic acid (Steven et al., 2001; Leke, 2015). Collinson and Zewdie-Bosuener (1999) and Bauer and Moll (1942) variously reported works on this plant which focused essentially on the fruit, kernel, seed and the fat from the seed.

* Corresponding author
E-mail addresses: iliyasuibrahim@gmail.com (I.A.A. Ibrahim)

V. paradoxa (formally *Butryspermumparadoxum*), *(Sa-potaceae)* is an immensely popular tree with many applications in folkloric medicine. It is commonly called Shea butter (English), Kareje (Fulfulde, Nigeria), Kadanya (Hausa, Nigeria) Koita (Gbagi, Nigeria), mameng (Cham, Nigeria). The tree grows naturally in the wild of the dry savanna belt of West Africa, from Senegal in the West to Sudan in the East and onto the foothills of the Ethiopian mountains. V. paradoxa is considered a sacred tree by many communities and ethnic groups and plays important roles in religious and cultural ceremonies. It is also believed to have some spiritual protective powers (Agbahungba and Depommier, 1989; Rajeshwar et al., 2016). Different parts of the plant including leaves, roots, seeds, fruit and stem bark have been used in the treatment of enteric infections such as diarrhea, dysentery, helminthes and other gastrointestinal tract infections, skin diseases and wound infections (Soladoye et al., 1989). The bark is used to suppress cough and also to treat leprosy (Ferry et al., 1974).

The research aims to assess the phytochemicals and antibacterial activities of the plant using three solvents and to compare same.

2. Materials and Methods

Preparation of reagents

Wagner's reagent

2.0 g iodine crystals and 3.0 g potassium iodide were dissolved in minimum amount of water and then made up to 100 ml with distilled water.

Mayer's reagent

13 g of mercuric chloride was dissolved in 50ml of distilled water. Also 50 g of potassium iodide was dissolved in 20ml of distilled water. The two solutions were mixed and the volume was made up to 100ml with distilled water.

Dragendroff's reagent

Bismuth (0.85 g) was dissolved in 100ml of glacial acetic acid and 40ml of water to give solution A. Another solution designated solution B was prepared by dissolving 8.0 g of potassium iodide in 20ml of distilled water. Both solutions were mixed to give a stock solution.

Ferric chloride solution

5.0g ferric chloride was dissolved in 100ml of distilled water.

Ethanol solution

45ml of absolute ethanol was mixed with 55ml of distilled water.

Dilute sulphuric acid

A 10.9ml aliquot of concentrated sulphuric acid was mixed with 5ml of distilled water and made up to 100ml.

Lead acetate solution

45ml of 15 % leads acetate (that is 15.0 g of lead acetate in 100ml of distilled water)
Was dissolve in 20ml of absolute ethanol and made up to 100ml with distilled water.

Dil. Hydrochloric acid

Measured volume, 2.0 ml concentrated hydrochloric acid was diluted with some distilled water and made up to 100ml.

Preparation of 0.3 % Sodium hydroxide

Sodium hydroxide (0.3 g) was dissolved in a little amount of water and made up to 100ml mark with distilled water.

Preparation of 2 % glacial acetic acid

2ml of glacial acetic acid was dissolved in distilled water and made up to 100ml.

Sample collection and preparation

Fresh stem bark of *Vitellaria paradoxa* (2.5 kg) were collected from Janligo village of Yana, Shira L.G.A in Bauchi State, Nigeria. The plant was identified by a local medical practitioner Mr. Kabiru Adamu (Dan-Chakwati) from Shira L.G.A Bauchi State and authenticated by a Botanist. The Sample was dried under (shade) room temperature for over 21 days and grinded using mortar and pestle, sieved in order to obtain a pure powdery form of the sample using 300mics sieve. The powdered material was stored in polythene bags at room temperature until needed.

Extraction

50 g of the dried and pulverized fiber-free stem bark of *Vitellaria paradoxa* was extracted exhaustively via maceration with 3*300cm^3 of Hexane (HE), acetone(ACE) and ethanol(EE), each

at room temperature for 24 hrs. Excess solvent was removed in to give crude extracts of HE, ACE, and EE, from Hexane, Acetone and Ethanol respectively.

Phytochemicals Screening

Crude Hexane extract (HE) was screened for phytochemicals using standard procedures (Harborne, 1984; Sofowora, 1984).

Phytochemicals screening methods

Detection for Alkaloids

Standard methods were used for the detection of alkaloids using Dragendroff's reagent (Harborne, 1984; Sofowora, 1984).

Detection for flavonoids

Standard methods were used for the detection of the presence of Ammonia (Harborne, 1984; Sofowora, 1984).

Detection for Tannins

Standard methods were used for the detection of Ferric chloride (Harborne, 1984; Sofowora, 1984).

Detection for Phenolic compounds

Standard methods were used for the detection of Phenols (Harborne, 1984; Sofowora, 1984).

Detection for Saponins Test

Standard methods were used for the detection of saponins (Harborne, 1984; Sofowora, 1984).

Detectionfor Terpenoids

Standard methods were used for the detection of Terpeniods (Harborne, 1984; Sofowora, 1984).

Detection of Glycosides

Standard methods were used for the detection Glycosides.

Detection for Sterols

Standard methods were used for the detection of sterols (Harborne, 1984; Sofowora, 1984).

Thin layer chromatography of *V. paradoxa Crude* Extract

Three chromatography papers of the same length (30cm) were used. Three different mixtures of solvent system varying polarities were also used to enhance ideal separation in different chromatography tanks: hexane/chloroform (1:1), chloroform, chloroform/ethyl acetate (1:1) and Ethyl acetate/Ethanol (1:1).

The solvent front and the separation were later calculated and the relation factor was obtained using the formula.

$R_f = m^1/m$

Were R_f=relation factor. M^1=separations (cm). M= solvent front (cm).

The disc diffusion method

The paper disc diffusion assay technique (Akpuaka et al., 2003 and Nuhu et al., 2000) was done.

Preparation of the medium

The nutrient agar medium was prepared by dissolving 7.0 g of agar in 250 ml of distilled water in a conical flask and heated to dissolve. The solution was sterilized in an autoclave at 121°C for 15 mins, cooled and poured into Petri dishes to set.

Preparation of culture media and inoculation

Culture of *Staphylococcus aureus*, *salmonella typhi*, and *Escherichia coli* were obtained from the microbiology laboratory of Abubakar Tafawa Balewa University, Bauchi, Nigeria. Pure isolates were obtained by sub-culturing unto fresh nutrient agar plates. The bacteria were separately used to inoculate the Petri dishes. The plates were incubated at 37 ± 2°C for 24 hours

Assay of extracts

Two different concentrations of each extract were obtained by suspending 250 mg of each extract in 6.0 ml of absolute ethanol and the volume was made up to 10.0 ml using sterile distilled water to give a concentration of 25 mg/ml (25,000 µg/ml). These also served as stock solutions. The second concentrations were obtained by diluting 2.0 ml each of the stock solutions with 2.0 ml of sterile distilled water giving a concentration of 12.5 mg/ml (12,500 µg/ml). Sterile 6 mm Whatman's filter paper discs were soaked in the extracts and placed on the plates and incubated for 24 h at 37 ± 2°C. The plates were examined for clear zones of activity. The zones of inhibition were measured using a transparent plastic meter ruler

Broth diffusion method

Equal volumes (1.0 ml) each of the extract solutions (25 and 12.5mg/ml) were mixed with same volume (1.0 ml) of an overnight broth culture of *S. aureus* and *E. coli* to give solutions of final concentrations of 12.5 and 6.25 mg/ml, respectively, in a test tube. These were then incubated at 37 ± 2°C for 24 h and observed for the presence of bacterial growth using a compound microscope

Inoculation and application of extracts

Bacterial strains were inoculated in 15ml of sterile nutrient broth an inoculated at 37°c for 24 hours. The concentration of inoculants was set to 0.5mc for loud standards after 24 hours the plate was removed from the oven and 3 different extracts 0.5ml was introduced to the plates and leaved for 24 hours.

Minimum Inhibitory Concentration (MIC)

This is the lowest drug concentration that prevents visible microorganisms' growth after overnight incubation, a plate of solid growth media. After a pure culture is isolated was examined and minimum inhibitory concentration was determined.

3. Results

Table 1. Weight of various macerated fractions of Vetillari aparadoxa

Fraction	Observation	Weight (g)
V. paradoxa + Ethanol	**Reddish brown**	**2.60**
V. paradoxa + Acetone	**Dark brown**	**3.70**
V. paradoxa + N-hexane	**Yellow brown**	**1.70**

Table 2. Result of phytochemical screening

Key:

Phytocompounds	Regents used	Extracts		
		ACE	HE	EE
Alkaloid	**Dragendroff's** **Mayer's**	+ +	+ +	- -
Flavonoids	**1 % ammonia,** **2 m NaOH, + HCl**	++ ++	+ +	- -
Tannins	**5 % FeCl**	+	-	+
Saponins	**Olive Oil**	+	+	-
Terpenoids	**Salkowski**	++	+	-
Glycosides	**Legal's** **Kelarkillani**	+ +	- -	+ +
Steroids	**Salkowski**	+	-	+
Phenols	**1 % gelatin solution** **10 % NaCl**	+	+	+

ACE = Acetone Extract
HE = Hexane Extract
EE = Ethanol Extract
+ = Slightly Present
++ = Moderately Present
+++ = Highly Present
- = Absent

Table 3. Antibacterial activity and zone of inhibition (mm) of V. paradoxa disc diffusion

Extracts	Concentration	E. coli	S. Typhi	S. aureous
EE	**25mg/ml** **12.5mg/ml**	**6** **-**	**8** **-**	**10** **-**
ACE	**25mg/ml** **12.5mg/ml**	7 -	7 -	**2** **-**
Hexane	**25mg/ml** **12.5mg/ml**	**1** **-**	**2** **-**	**3** **-**
Sreptomycin		**25**	**NT**	**NT**

NT = not tested/done: = no inhibition

Table 4. Various fractions from thin layer chromatography of stem bark of V.paradoxa

Extracts	Solvent System	Retention Faction (R.F)
Hexane	**hexane/Chloroform** **Chloroform/Ethyl acetate** **Ethyl acetone/Ethanol**	**0.6** **0.3** **0.5**
ACE	**hexane/Chloroform** **Chloroform/Ethyl acetate** **Ethyl acetone/Ethanol**	**0.7** **0.8** **0.8**
EE	**hexane/Chloroform** **Chloroform/Ethyl acetate** **Ethyl acetone/Ethanol**	**0.5** **0.4** **0.3**

HE =-Hexane Extract
ACE = Acetone Extract
E = Ethanol Extract

4. Conclusion

Phytochemical screening of Hexane, Acetone, and Ethanol, extracts revealed the presence of flavonoids, tannins, terpenoids, saponins, sterols, alkaloids and cardiac glycosides by positive reaction with the respective test reagents. Phytochemical screening showed that maximum presence of secondary metabolites was in Acetone extract than in the Hexane, and Ethanol, where almost all the phytocompounds appeared in the acetone extract (Table 1), whereas tannins, glycosides, and steroids where absent in hexane extract; alkaloids, flavonoids and Saponins, were absent in the Ethanol extract. Antimicrobial susceptibility of the extracts (50 mg/ml) against the test organisms showed that in all the three solvents used, the ethanol extracts demonstrated the highest activity, followed by Acetone, whereas hexane demonstrated the least activity on the tested bacteria as seen in (Table 3).

Preliminary phytochemical investigations of stem bark of *vitellaria paradoxa* revealed the presence of some/many secondary metabolites. These secondary metabolites are linked to microbial activity of the plant material and the extracts of this plant has antimicrobial effects on the tested enteric bacteria, hence serve as potential therapeutic agents against diarrhea and other microbial afflictions.

References

Agbahungba, Depommier, 1989 – *Agbahungba, G., Depommier, D.* (1989). Shea and African locust beans parklands aspects in southern Borgou. Bois et Forêts des Tropiques, 222, 41-54.

Badifu, 1989 – *Badifu, G.I.O.* (1989). Lipid composition of Nigerian Butyrospermum paradoxum. *Kernel Journal of Food Composition and Analysis*, 2(3), 238-244.

Bauer, Moll, 1942 – *Bauer K.H., Moll H.* (1942). The contents of the shea butter nut, the seed of Butryospermumparkii. Arch. Pharm. 280: 37-45.

Borokini, 2014 – *Borokini, T.* (2014). A Systematic Compilation of IUCN Red-listed Threatened Plant Species in Nigeria. *International Journal of Environmental Sciences*, 3(3), 104–133.

Collinson, Zewdie-Bosuener, 1999 – *Collinson C., Zewdie-Bosuener A.* (1999). Shea butter Markets: Their Implications for Ghanaian Shea butter Processors and Exporters; Project A0772, Report 2403; Natural Resources Institute, University of Greenwich, U.K. P. 20.

Ferry et al., 1974 – *Ferry M.P., Gessain M., Geeain R.* (1974). Vegetative Propagation of Shea, Kola and Pentadesma. Cocoa research institute, *Ghana Annual Report* (1987/88): 98-100.

Hall, 1996 – *Hall J.B., Aebischer D.P., Tomlison H.F., Osei-Amaning E., Hindle J.R.* (1996). Vitellaria paradox. A monograph: school of agricultural and forest sciences. University of wales. Bangor U.K.

Harborne, 1984 – *Harborne J.B.* (1984). Methods of Plant Analysis. In: Phytochemical Methods. Springer, Dordrecht.

Keay, 1989 – *Keay R.W.J.* (1989).Trees of Nigeria. A revised version of Nigerian trees (1960, 1964) by Keay RWJ, Onochie CFA, Stanfield DP. Clarendon press Oxford, pp. 389-390.

Leke, 2015 – *Leke, O.* (2015). Medical plants and natural products chemistry in Achebe' s" things fall apart": The metaphor of kola. *International Journal of Arts and Humanities*, 3(3), 70–76.

Omwirhiren et al., 2016 – Omwirhiren, E. M., James, S. A., Abass, A. O. (2016). Saudi Journal of Medical and Pharmaceutical Sciences The Phytochemical Properties and Antimicrobial Potentials of Aqueous and Methanolic seed Extract of Cola nitida (Vent.) and Cola acuminata (Beauvoir) grown in South West, Nigeria. *Saudi Journal of Nedical and Pharmaceutical Sciences*, 354–363. https://doi.org/10.21276/sjmps.2016.2.12.6

Rajeshwar et al., 2016 – *Rajeshwar, Y., Sreekanth, T., Kahsay, G., Hussen, D. A., Eticha, T.* (2016). Hepatoprotective activity of Anogeissus latifolia bark in ethanol intoxicated rats. The American Journal of Science and Medical Research, 1(2), 198–201. URL: https://doi.org/10.17812/ ajsmr1210.Published

Steven et al., 2003 – *Steven M., Zeev W., Nissim G.* (2003). Phenolic constituents of shea (Vitellriaparadoxa) kernel. *J. Agric. Food Chem*. 51: 6268-6273.

Sofowora, 1984 – *Sofowora A.* (1984). African Medicinal Plants, University of Ife Press, IIe-Ife, Nigeria, P. 104.

Soladoye et al., 1989 – *Soladoye M.O., Orhiere S.S., Ibimode B.M.* (1989). Ethanobotanical Study of two Indigenous Multipurpose Plants in the Guinea Savanna of Kwara State – Vitellariaparadoxa and Parkiabiglobosa Biennial Conference of Ecological Society of Nigeria, 14 August, Forestry Research Institute, Ibadan. P. 13.